Analysis of Non-Methane Hydrocarbons and Organic Nitrogen Compounds in the Atmosphere

Dissertation zur Erlangung des Grades “Doktor der Naturwissenschaften”
im Promotionsfach Chemie am Fachbereich 09 Chemie, Pharmazie und Geowissenschaften
der Johannes Gutenberg-Universität Mainz

von

Carina Sauvage

geb. in Worms

Mainz, 2019

Kurzfassung

Die vorliegende Arbeit befasst sich mit der Messung von flüchtigen Kohlenwasserstoffen und organischen Stickstoffverbindungen in der Atmosphäre und der Interpretation von Feldmessungen in Hinsicht auf atmosphärische Prozesse.

Nicht-Methan-Kohlenwasserstoffe (non-methane hydrocarbons, NMHC) wurden mit einem kommerziellen Gaschromatographen mit Flammenionisationsdetektor gemessen.

Für die Messung von stickstoffhaltigen, organischen Komponenten im Spurengasbereich wurde im Rahmen dieser Arbeit ein neues System aufgebaut und evaluiert. Es beinhaltet ein Gerät zur Anreicherung und Kryofokussierung der Gase, einen Gaschromatographen und einen Stickstoffchemielumineszenzdetektor (GC-NCD).

Es werden die Messergebnisse zweier Messkampagnen präsentiert. Im Sommer 2014 fand die CYPHEX-Kampagne (CYprus Photochemistry EXperiment) im Nordwesten Zyperns statt. Im Sommer 2015 kamen die Geräte bei der NOTOMO-Kampagne (NOcturnal chemistry at the Taunus Observatorium: insights into Mechanisms of Oxidation) auf dem *Kleinen Feldberg* im Taunus, Deutschland, zum Einsatz. Das GC-FID-System wurde dabei jeweils direkt vor Ort betrieben. Organische Stickstoffverbindungen wurden nach der Kampagne (CYPHEX) oder währenddessen (NOTOMO) offline aus gesammelten Kanisterproben (Whole air samples, WAS) im Labor analysiert.

Diese Arbeit präsentiert unserem Wissen nach die ersten Messungen von kurzkettigen Alkylnitraten (C_1-C_4) im Mediterranen Raum.

Ebenfalls wurde das GC-NCD-System zur Messung von WAS des CARIBIC-Projekts (Civil Aircraft for the Regular Investigation of the atmosphere Based on an Instrumented Container) über einen Zeitraum von einem Jahr genutzt und konnte somit das Konvolut an Analyten dieses Großprojekts um organische Nitrate erweitern.

Eine Laborstudie zur Messung von Pflanzenemissionen, in Ergänzung zur NOTOMO-Kampagne, lieferte neue Ergebnisse hinsichtlich des Einsatzgebietes und der Erweiterung der gemessen Komponenten des GC-NCD-Systems auch in Bezug auf quasi-online Messungen.

Nach einer Einführung in den theoretischen Hintergrund werden die Mess- und Probenahmetechniken in Kapitel 2 erläutert. Die Feldkampagnen werden in den Kapiteln 3-5 behandelt. Kapitel 6 gibt einen Überblick über die Ergebnisse dieser Doktorarbeit.

Abstract

This thesis deals with the measurement of volatile hydrocarbons and organic nitrogen compounds and the interpretation of field data with respect to atmospheric processes.

Non-methane hydrocarbons (NMHC) were measured with a commercial gas chromatograph with flame ionization detector.

For the measurement of nitrogen containing organic components in the trace gas range, a new system was set up and evaluated as part of this work. It includes a gas enrichment and cryofocusing device, a gas chromatograph and a nitrogen chemiluminescence detector (GC-NCD).

The results of two measurement campaigns are presented. The CYPHEX campaign (CYprus PHotochemistry EXperiment) took place in the northwest of Cyprus in the summer of 2014. In summer 2015, the devices were used in the NOTOMO campaign (NOcturnal chemistry at the Taunus Observatory: insights into Mechanisms of Oxidation) on the *Kleiner Feldberg*, Taunus, Germany. The GC-FID system was operated directly on site. Organic nitrogen compounds were analysed in the lab after the campaign (CYPHEX) or during the campaign (NOTOMO) from whole air samples (WAS).

As far as we are aware, this study presents the first measurements of short chained alkyl nitrates (C_1-C_4) in the Mediterranean region.

The GC-NCD-system was also regularly used to measure WAS of the CARIBIC project (Civil Aircraft for the Regular Investigation of the atmosphere Based on an instrumented Container) over a period of one year and was thus able to expand the pool of analytes by organic nitrates.

A laboratory study for the measurement of plant emissions, which was an extension of the NOTOMO campaign, provided new results regarding the field of application and the extension of the measured components of the GC-NCD system. In addition, the study also revealed new results on quasi-online measurements.

After an introduction to the theoretical background, the measurement and sampling techniques are explained in chapter 2. The field campaigns are addressed in the chapters 3-5. Chapter 6 summarizes the results of this doctoral thesis.

Table of contents

1 Introduction

The air we breathe is a complex mixture. The majority of it, 78%, is nitrogen, with 20% oxygen, and 1% argon. Based on their chemical inertness and high abundance small changes in the concentration of these species have little impact on the chemical properties of the air. Gases constituting less than 1% of the atmosphere are termed trace gases. Despite their low mixing ratios such species are extremely important to the chemistry of the atmosphere. Typical trace gas mixing ratios lie in the range of parts per million (ppm, 10^{-6}) down to sub parts per quadrillion (ppq, 10^{-15}). The low mixing ratios of trace gases impose special requirements on measurement techniques. The accurate determination of trace gases is essential to track the diverse sources and to follow multiple atmospheric oxidation reactions. The significance of trace gases to atmospheric chemistry, human health and radiative forcing is substantial.

1.1 Volatile Organic Compounds in the atmosphere

Volatile organic compounds (VOC) are carbon containing compounds with a vapor pressure higher than 10 Pa at 25 °C or a boiling point below 260 °C (Koppmann 2010, chapter 1: Volatile Organic compounds in the Atmosphere: An Overview, Jonathan Williams and Ralf Koppmann). VOCs are emitted from various sources, transported via meteorological processes and participate in many atmospheric chemical processes. The term VOC comprises a diversity of structures, from simple hydrocarbons (alkanes, alkenes, alkynes, aromatics) to more complex substances with functional groups containing different elements like oxygen, nitrogen or halogens (alcohols, aldehydes, acids, organohalogens, nitrates).

Sources of VOCs can be classified as natural or anthropogenic and differ in strength and species diversity of emitted substances. For example, plants are a source for reactive reduced VOCs such as isoprene or terpenes. Such compounds are involved in communication between individual plants, the attraction of pollinators or defense against pests (Greene and Gordon 2003; Krieger and Breer 1999; Kessler and Baldwin 2001; Cremer, Sledge, and Heinze 2002).

Vegetative emissions are extremely dependent on the surrounding environmental conditions like temperature, humidity, irradiation or oxidative stress. Isoprene emitting plants are better protected against ozone damage. Under high ozone burdens, even some algae have the ability to emit photolabile organohalogens which decompose ozone after photolysis (Carpenter, Liss, and Penkett 2003). Vegetation and oceans are also denoted as biogenic sources. Further natural sources of VOCs can be volcanoes, and forests or wildland fires (Andreae and Merlet 2001). Global model estimates suggest that about

760 Tg (C) yr^{-1} are released to the atmosphere as biogenic VOC (Sindelarova et al. 2014).

A major fraction of the anthropogenic sources stems from the use of fossil fuels. Coal and liquid fuels are burned in power plants, vehicles and households. Incomplete combustion of these fuels leads to the production of carbon monoxide (CO) and multiple partially oxidized products. Other industrial branches extend the variety of compounds. Solvents or cooling agents (e.g. chlorofluorocarbons, CFC) are released into the atmosphere daily and their fates can have influences on both, human health and the earth's climate.

Figure 1-1 shows a schematic overview of the sources and atmospheric chemical pathways of VOCs.

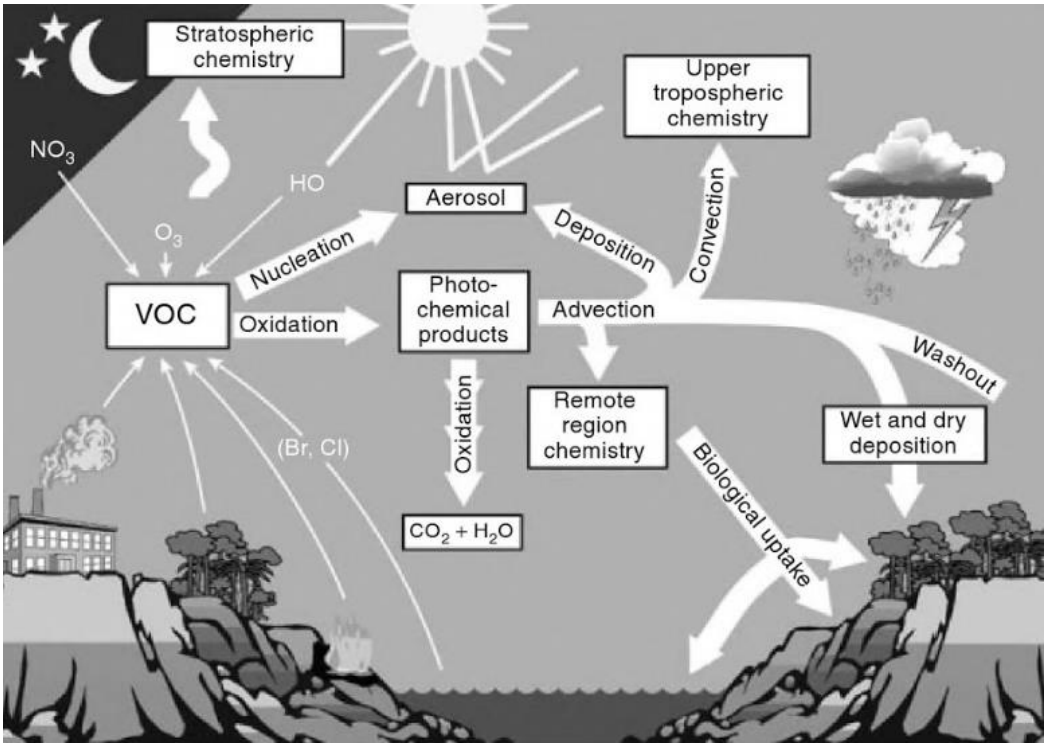

Figure 1-1: Schematic summary of sources and chemical and physical sinks of VOC from Koppmann 2010

VOC removal from the atmosphere can be via physical or chemical processes. Dry or wet deposition are physical sinks. This includes processes such as surface uptake or washing out by rain. Molecular weight, diffusion properties and the solubility of individual compounds have influence on this behavior.

Depending on the chemical structure of these compounds, the atmospheric lifetimes and transport pathways vary greatly. Hydrocarbons are involved in the formation of photochemical smog and surface ozone (O_3), isoprene and terpenes are part of nucleation pro-

cesses which lead to secondary organic aerosol with consequences for cloud formation, planetary albedo and the greenhouse effect. CFCs participate in the depletion of stratospheric ozone (Haagen-Smit 1952; O'Dowd et al. 2002; Molina and Rowland 1974).

1.1.1 Non-methane hydrocarbons

This doctoral thesis involves the measurement of non-methane hydrocarbons (NMHC) with GC-FID (gas chromatography-flame ionization detector) and organic nitrogen compounds with GC-NCD (gas chromatography-nitrogen chemiluminescence detector). NMHC are alkanes, alkenes, alkynes and aromatic hydrocarbons and are a subsection of volatile organic compounds containing only carbon and hydrogen atoms. NMHC sources are predominantly anthropogenic. Ethane is the smallest and atmospherically most abundant homologue of the NMHCs. It is released into the atmosphere through the use of natural gas and biomass burning. Natural sources include the emissions from soils and wetlands (Koppmann 2010). Natural gas is also the main source for propane. Higher homologues with $>C_4$ are entrained by evaporation from fossil fuels and solvents. With increasing carbon number the vapor pressures and consequently the atmospheric emission rates decrease. Larger molecules tend also to be more reactive and thus higher alkane homologues are generally found at lower mixing ratios. Aliphatic alkenes are formed mostly by incomplete combustion of fossil fuels and biomass. Similarly, aromatic compounds mainly derive from exhaust fumes and propellants. An important biogenic alkene is isoprene. The annual emission from plants is estimated at 500-700 Tg (Guenther et al. 2006).

The most important atmospheric removal process for NMHCs is the oxidation with the hydroxyl radical (OH), which is also sometimes called the detergent of the atmosphere (Finlayson-Pitts and Pitts 1999). Hydroxyl radicals are formed in the troposphere by photolysis of O_3 to electronically excited $O(^1D)$ at wavelengths below 336 nm and the subsequent reaction with water vapor. At the surface only around 10% of the formed $O(^1D)$ generates OH. The majority is deactivated to ground state $O(^3P)$ and re-forms O_3. Further sources for OH can be the photolysis of nitrous acid (HONO), formaldehyde (CH_2O) and hydrogen peroxide (H_2O_2). (Chemical reactions are consecutively numbered using roman numerals. Arabic numerals are used for mathematical equations.)

$$O_3 + hv\ (\lambda < 336\ nm) \rightarrow O(^1D) + O_2 \qquad [I]$$

$$O(^1D) + H_2O \rightarrow 2\ OH \qquad [II]$$

Without NMHCs present, ozone can react with NO to form NO_2 and O_2. Then, when NO_2 photolyzes it reforms the NO and generates an oxygen atom which goes on to form ozone. The ozone is destroyed in the first step of the cycle, but regenerated in the last.

The oxidation of NMHCs with OH begins with hydrogen abstraction and formation of thermodynamically stable water and a radical. Discussions on the removal of NMHCs from the atmosphere and on the rate of reaction (kinetics) in this thesis refer to this reaction [III]. The corresponding rate reaction coefficients are listed in Table 1-1. Additional oxidants can be chlorine (Cl) and nitrate radicals (NO_3), which are also included in Table 1-1. Alkyl radicals ($R\text{-}CH_2$) react with the abundant O_2 to form alkylperoxy radicals ($R\text{-}CH_2O_2$). Nitrogen (N_2) and oxygen (O_2) typically serve as collision partners to compensate excess energy.

$$OH + R\text{-}CH_3 \rightarrow RCH_2 + H_2O \qquad [III]$$

$$R\text{-}CH_2 + O_2 + M \rightarrow R\text{-}CH_2O_2 + M \qquad [IV]$$

In the presence of nitrogen oxide (NO) alkylperoxy radicals react to alkoxy radicals ($R\text{-}CH_2O$) and nitrogen dioxide (NO_2) in the major pathway.

A second pathway, which gets more important with increasing carbon number of alkylperoxides is the formation of alkyl nitrates. A mechanism via the intermediate (RCH_2OONO) and rearrangement to ($R\text{-}CH_2ONO_2$) was postulated by Darnall et al. 1976.

$$R\text{-}CH_2O_2 + NO \rightarrow R\text{-}CH_2O + NO_2 \qquad [Va]$$

$$R\text{-}CH_2O_2 + NO \rightarrow R\text{-}CH_2ONO_2 \qquad [Vb]$$

Further reactions of RCH_2O_2 can occur with HO_2 and other RCH_2O_2 to form carbonyl compounds and alcohols. Addition of NO_2 leads to the formation of peroxy nitrates ($RCH_2O_2NO_2$). Thermical depletion to aldehydes, isomerisation and further reaction with O_2 to ketones are additional fates of peroxy radicals.

These reactions are a substantial part of those leading to formation of surface ozone. These processes are depicted in Figure 1-2. Photolysis of NO_2 from reaction [Va] forms atomic oxygen which reacts with molecular oxygen.

As already described, alkylperoxy radicals are formed by the reaction of NMHCs with OH and subsequent reaction with O_2. The NO_2 produced in the following reaction with NO is photolysed by solar radiation. It is also formed through the reaction of HO_2 with NO. As a by-product, OH is produced, which can restart the cycle (OH-recycling). The photolysis product is NO, which is also reintegrated into the cycle. The oxygen radical reacts with O_2 to O_3.

Termination reactions of this cycle are the recombination of peroxy radicals and the reaction of OH and NO_2 to stable nitric acid.

For each NMHC oxidized by OH, two molecules of ozone (more for bigger larger hydrocarbon) are formed in the first step. The net reaction for the ozone production via hydrocarbon oxidation by OH is as follows:

$$R\text{-}CH_3 + 4\ O_2 + 2\ hv \rightarrow R\text{-}CHO + 2\ O_3 + H_2O \qquad [VI]$$

Figure 1-2 schematically summarizes the tropospheric formation of ozone.

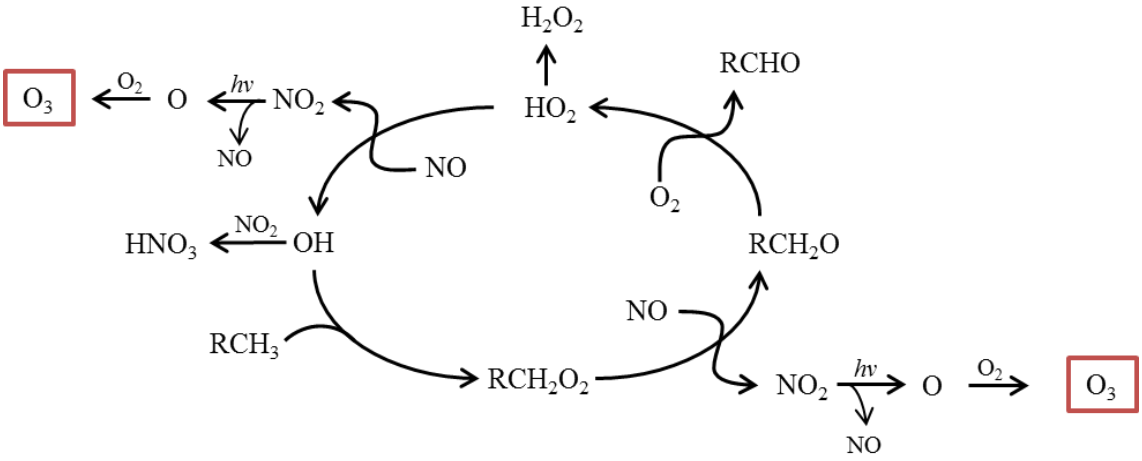

Figure 1-2: Schematic reaction cycle of ozone formation with OH-recycling and the termination reactions with HNO_3 and H_2O_2 as stable products

Alkenes are broken down by radical addition of the hydroxyl radical to the double bond. These radicals can then further react with oxygen to hydroxyalkyl peroxy radicals. The subsequent reaction with NO provides hydroxyalkoxy radicals. Another possible reaction pathway is the oxidation of alkenes with ozone. This reaction involves the 1,3-dipolar cycloaddition of O_3 and the decay of the unstable cyclic intermediate. This splits into a carbonyl compound and a Criegee intermediate, which is stabilized or further decomposed. (Becker and Berger, Organikum, 2009). This reaction also takes place with biogenically emitted terpenes.

The oxidation of aromatic compounds goes via H-abstraction at the side chain or OH addition to the ring and the associated subsequent reactions.

The oxidation degradation mechanisms described above, lead to products that have a lower vapor pressure compared to the initial compounds due to the introduction of polar groups. The solubility in water increases due to the increased polarity. Furthermore, some of the newly generated substances are able to oligomerise, which again considerably reduces the vapor pressure. This promotes the forming of secondary organic aero-

sols and finally removes NMHCs from the gas phase and expedites removal from the troposphere.

The reactions of NMHCs with oxidizing radicals (X= OH, Cl or NO_3) follow pseudo-first order kinetics described by equation [1].

$$[A]_t = [A]_0 e^{(-k[X]t)} \quad [1]$$

The lifetime τ of an atmospheric species is defined as the time for the organic compound to fall to $1/e$ of its initial value (Finlayson-Pitts and Pitts 1999) and is calculated as the reciprocal of the product of the reaction rate coefficient (k) and the concentration of the radical in molecules cm^{-3} (X). In presence of multiple radicals, the sum of the products from individual reactions is used (see equation [2]). Typical lifetimes of NMHCs at northern hemispheric mid latitudes, at an estimated average OH concentration of 10^6 molecules cm^{-3} (Spivakovsky et al. 2000) range from about 50 days for Ethane to about 3 days for the pentanes.

$$\tau = \frac{1}{\sum k[X]} \quad [2]$$

The fact that different NMHCs react differently fast with the respective radicals can be extremely useful for data interpretation and the assessment of radical abundance. On the one hand, conclusions can be drawn about the oxidative history of the air mass (Rudolph et al. 1997; Jobson et al. 1994). On the other hand, the changes in ratios can be used for source reconciliation (Kourtidis et al. 2002; Kouvarakis et al. 2002; Nelson and Quigley 1983; Stephens and Burleson 1967; Stephens and Burleson 1969; Mayrsohn and Crabtree 1976). Detailed descriptions are given in the chapter sections 1.2 and 1.3.

Table 1-1: reaction rate coefficients of NMHCs with OH, Cl, and NO_3 radicals ([a]Atkinson et al. 2006; [b]Anderson et al. 2007; [c]Anderson et al. 2004; [d]Atkinson 1991, [e]Herron & Huie 1974; [f]Treacy et al. 1992). The given reaction rate coefficients refer to IUPAC preferred values and can be looked up at http://iupac.pole-ether.fr/#

compound	reaction rate coefficient at 298 K in [cm³ molecules^{-1} s^{-1}]			
	k_{OH}	k_{Cl}	k_{NO3}	k_{O3}
Ethane [a]	2.40×10^{-13}	5.90×10^{-11}	1.00×10^{-17}	
Propane[a]	1.10×10^{-12}	1.40×10^{-10}	7.00×10^{-17}	
i-Butane[a, b]	2.10×10^{-12}	1.38×10^{-10}	1.10×10^{-16}	
n-Butane[a]	2.35×10^{-12}	2.05×10^{-10}	4.60×10^{-17}	
i-Pentane[a]	3.40×10^{-12}	2.62×10^{-10}	8.10×10^{-17}	
n-Pentane[c, b]	3.70×10^{-12}	1.93×10^{-10}	1.56×10^{-17}	
Benzene[a, d]	1.20×10^{-12}	1.50×10^{-11}	3.01×10^{-17}	
Toluene[a]	5.60×10^{-12}	5.65×10^{-11}	6.79×10^{-17}	
Ethene[a, e ,f]	7.90×10^{-12}	1.10×10^{-10}	2.10×10^{-16}	1.55×10^{-18}
Propene[a, e, f]	2.40×10^{-12}	2.54×10^{-10}	9.5×10^{-15}	1.05×10^{-17}

1.1.2 Organic Nitrogen Compounds

Reaction [Va] and [Vb] show two possible pathways of the reaction of alkyl peroxy radicals with NO. The branching ratio α describes the extent of nitrate formed in concurrence to the formation of alkoxy radicals [3] and depends on the reaction rate coefficients from reactions [Va] and [Vb]. The magnitude of α depends on temperature and pressure and increases with carbon number of the parent alkane. Additionally, secondary alkylperoxy radicals are favored and the ratio is smaller for primary and tertiary radicals (Atkinson et al. 1982; Atkinson et al. 1983; Atkinson 1997).

$$\alpha = \frac{k_{[Vb]}}{(k_{[Va]}+k_{[Vb]})} \qquad [3]$$

Table 1-2: Branching ratios of alkyl nitrate formation from alkylperoxy radicals (Lightfoot et al. 1992; Finlayson-Pitts and Pitts 1999)

R	α
Methane	
Methyl	≤ 0.0005
Ethane	
Ethyl	≤ 0.014
Propane	
1-Propyl (*n*-propyl)	0.02
2-Propyl (*i*-propyl)	0.05
n-Butane	
1-Butyl (*n*-butyl)	≤ 0.04
2-Butyl (*i*-butyl)	0.083
i-Butane	
2-Methyl-1-propyl	0.075
tert-Butyl	0.18

Atmospheric depletion of alkyl nitrates proceeds via OH reaction which is slower than the reaction of the mother alkanes. Reaction coefficients lie in the range from 0.23×10^{-13} cm³ molecules^{-1} s^{-1} to 2.9×10^{-13} cm³ molecules^{-1} s^{-1} for methyl, ethyl and *i*-propyl nitrate (Talukdar et al. 1997). Thus, the lifetimes of alkyl nitrates are longer with respect to OH chemistry.

An additional pathway of alkyl nitrate removal is photolysis via breaking the O-NO_2 bond, to generate NO_2. The lifetimes of alkyl nitrates with respect to photolysis are about a week or longer at the surface and decrease to several days with altitude where the influence of radiation is higher (Clemitshaw et al. 1997). Smaller alkyl nitrates are mostly removed by photolysis, and with increasing length of the alkyl chain, the reaction with OH becomes more important.

The lifetimes are long enough that alkyl nitrates can be transported long distances to remote regions. Therefore they serve as reservoir and intermediate transport mechanism for reactive nitrogen, promoting tropospheric ozone production in regions far away from the NO_x emission source (Elliot Atlas 1988). C_2-C_5 alkyl nitrates can account for

1-2% of the total reactive odd nitrogen species NO_y (Flocke, Volz-Thomas, and Kley 1991).

Further sources for methyl, ethyl and propyl nitrate can be direct oceanic emissions (Atlas et al. 1993; Chuck et al. 2002; Talbot et al. 2000; Blake et al. 1999).

Another organic nitrogen compound discussed in this work is acetonitrile. Its dominant source is emission during biomass burning processes and it is removed from the atmosphere by reaction with OH and ocean uptake (Hamm and Warneck 1990). Nevertheless, its lifetime is in the range of several months (Holzinger et al. 1999; Karl et al. 2008).

1.2 Oxidative history

Once emitted into the atmosphere or produced within it, VOCs are removed on characteristic time scales by physical or chemical processes. For NMHCs the dominant sink is oxidation by photochemically produced OH radicals. Based on kinetic considerations and different reaction rate coefficients NMHCs can be used as "photochemical clocks" to deduce the "age" of an air parcel because more reactive species are depleted faster than species with longer lifetimes. Consequently, their ratios change with travel time and oxidant impact. Under ideal conditions there is a linear relationship between the natural logarithms of different NMHC ratios. This has been extensively described by Jobson et al. 1994, Rudolph and Johnen 1990 and Parrish et al. 1992, 2007.

The reaction follows pseudo-first order kinetics and is described in equation [4]. The mixing ratio of a given NMHC $[A]_t$ at time t is a function of the initially released, source mixing ratio $[A]_0$, the reaction rate coefficient k, the travel time t of the air parcel and the temporal integral of the OH radicals concentration [X] between source and measurement location (Parrish et al. 1992).

$$[A]_t = [A]_0 e^{(-k[X]t)} \quad [4]$$

For the ratio of two chosen NMHC the relationship is given in equation [5]. One assumption which has to be made, is that during the travel time of an air parcel no mixing-in of other air parcels occurs or it is at least negligible.

$$\ln\frac{[A]_t}{[B]_t} = \ln\frac{[A]_0}{[B]_0} - (k_A - k_B)[OH]t \quad [5]$$

According to this assumption, [OH]t is equivalent for different hydrocarbon ratio pairs and another pair of NMHC can be added for comparison.

$$\ln\frac{[A]}{[B]} = \left\{\frac{k_A - k_B}{k_C - k_D}\right\}\ln\frac{[C]}{[D]} + \left\{\ln\frac{[A]_0}{[B]_0} - \frac{k_A - k_B}{k_C - k_D}\ln\frac{[C]_0}{[D]_0}\right\} \quad [6]$$

By simplifying the terms in braces a plot of $\ln\frac{[A]}{[B]}$ versus $\ln\frac{[C]}{[D]}$ shows the linear relationship described by equation [7]:

$$\ln\frac{[A]}{[B]} = b\ln\frac{[C]}{[D]} + a \qquad [7]$$

with the axis intercept a:

$$a = \ln\frac{[A]_0}{[B]_0} - b\ln\frac{[C]_0}{[D]_0} \qquad [8]$$

and the slope b:

$$b = \frac{k_A - k_B}{k_C - k_D} \qquad [9]$$

Typically, NMHC pairing with fairly equal rate coefficients with one oxidant and diverging rate coefficient with another radical of interest are chosen. An example is indicated by the "step" shown in Figure 1-3 which shows the NMHC reaction rate coefficients with Cl vs. OH.

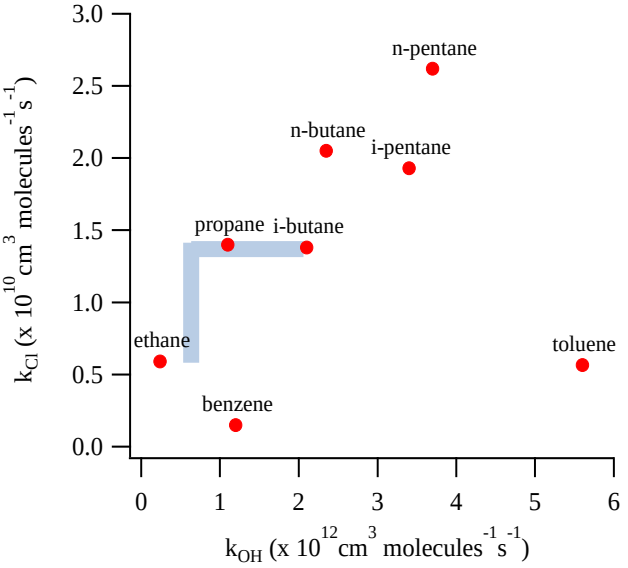

Figure 1-3: Graphical illustration of reaction rate coefficients of NMHCs with Cl and OH radicals

Based on the known reaction rate coefficients a theoretical slope can be calculated. This slope describes the course of the line where the data points should accumulate around if oxidation of the air mass was influenced exclusively by one radical species. The theoretical axis intercept a can be calculated from general average source concentrations.

Figure 1-4 shows the calculated results for the combination of ln (*i*-butane/ethane) vs. ln (*n*-butane/ethane). The initial mixing ratios were taken from a short measurement series in Mainz in May 2014. The rate coefficients are taken from Table 1-1. Although OH is the dominant radical for NMHC oxidation other radicals such as Cl or NO_3 can not be excluded a priori.

If oxidation was only based on the reaction with OH radicals, the data points show a linear behavior following a slope of 0.88. Solely Cl chemistry would show a slope of 0.54 and reaction only with NO_3 would result in a slope of 2.77. The advantage of this method is, that with experimentally derived slopes the ratio of two active radicals can be calculated with equation [9] (Arsene et al. 2007) by carefully choosing the NMHC pairs with respect to their reaction rate coefficients with each radical.

$$Cl/_{OH} = \frac{b\left(k_{D_{OH}} - k_{C_{OH}}\right) - k_{B_{OH}} + k_{A_{OH}}}{b\left(k_{C_{Cl}} - k_{D_{Cl}}\right) + k_{B_{Cl}} - k_{A_{Cl}}} \qquad [10]$$

The result is a sensitive method for analysis of the oxidative history of an air parcel. Less variable compounds are used as denominator (Parrish et al. 1992) to minimize the impact of dilution and mixing of different air masses.

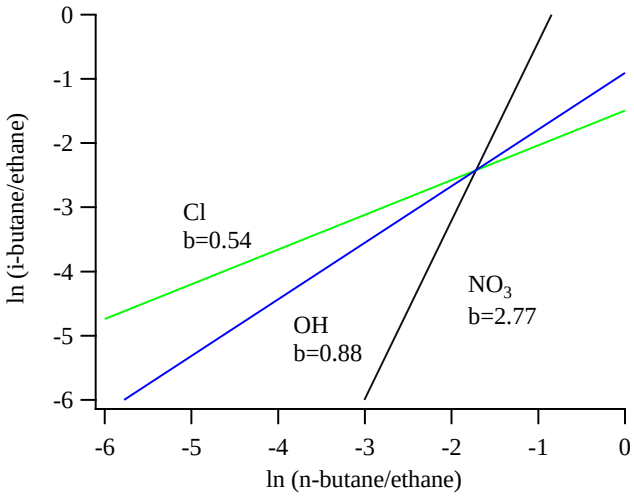

Figure 1-4: Theoretical slopes calculated on kinetics of OH, Cl and NO_3 with butanes and ethane

For the application of this method, several assumptions have to be made. Dilution by mixing with air masses with lower mixing ratios has to be negligibly low. If mixing is taken into account, the air masses have to have the same photochemical age. Further-

more the source signatures, meaning the initial ratios of NMHCs of mixing air masses have to be comparable.

1.3 The Junge relationship

Compounds which are emitted into the atmosphere have distinct lifetimes dependent on individual removal processes, see section 1.1.1. For example ethane, which is less reactive than other NMHCs, has a lifetime of approximately 45 days. It has a longer residence time in the atmosphere. With moving and mixing air masses ethane is globally distributed. Shorter lived compounds such as ethene ($\tau \approx 1$ day) will be depleted faster and they fate before they are equally distributed. This was described already in 1963 and was applied for NMHCs in 1974 by Junge. Atmospheric NMHC measurement data vary with time. Junge considered whether the observed variability in the measurement could be related to either the chemistry or transport and mixing of the particular species in the atmosphere. Generally he observed that longer lived species such as ethane varied much less than short lived species such as ethene. He therefore tried to relate the chemical lifetime of the compound to the variability in the measurement.

The standard deviation (σ) of a group of data points (X) can be used as a measure for the temporal variability. Junge used the relative standard deviation.

$$\sigma'(X') := \frac{\sigma(X')}{\overline{X}} \qquad [11]$$

In general and under steady state conditions, the lifetime τ of a compound can be described as the ratio of the total mass M_{TOT} of the compound and the global source strength Q_{TOT}.

$$\tau = \frac{M_{TOT}}{Q_{TOT}} \qquad [12]$$

M_{TOT} can be described as a product of the average of individual measured values and a constant C which comprises the molar masses of the compound and air and the total mass of air in the atmosphere.

$$M_{TOT} = C \cdot \overline{X} \qquad [13]$$

By inserting M_{TOT}, rearranging for $\overline{X}$ and putting it into the equation for relative standard deviation following expressions are received:

$$\overline{X} = \frac{Q_{TOT}}{C} \cdot \tau \qquad [14]$$

and [15]

$$\sigma'(X') = \sigma(X') \cdot \frac{C}{Q_{TOT}} \cdot \tau^{-1}$$

Making the assumption that organic compounds are solely depleted by photolysis and reaction with OH radicals the variability would only be influenced by the source strength, because the effect of depletion pathways is globally seen equally distributed. Therefore the ratio of standard deviation and source strength would be the same for every individual compound. Junge expressed it as follows:

$$\sigma'(X') = A \cdot \tau^{-1} \quad \text{or} \quad \sigma'(X') = A \cdot \tau^{-b} \qquad [16]$$

with [17]

$$\sigma'(X') = \sigma(X') \cdot \frac{C}{Q_{TOT}} \cdot \tau^{-1}$$

His model calculations showed an exponent $b = 1$ which he traced back to a non-equal distribution of sources and sinks. In the model of Gibbs and Slinn (1973) this was considered and they came to an exponent of $b = 0.5$.

Jaenicke (1982) and Slinn (1988) supposed that different air masses have traveled different transport distances between source and measurement location. That is the reason for Jobson et al. (1998) using the standard deviation of the natural logarithms of the mixing ratios as a better measure for variability. Without mixing the natural logarithm of the ratio of measured concentration X and concentration at emission X_0 is the negative ratio of travel time of the air mass and the lifetime of the compound.

$$\ln\frac{X}{X_0} = -\frac{t}{\tau} \qquad [18]$$

Because the variability is only caused by different transport times the equation above can be described as

$$\sigma(\ln\frac{X}{X_0}) = -\left(\frac{\partial}{\partial t}\ln\frac{X}{X_0}\right)\sigma(t) \qquad [19]$$

$\ln\frac{X}{X_0}$ can be replaced by $-\frac{t}{\tau}$. The variability is independent from the mixing ration at the source and can therefore be neglected.

$$\sigma(\ln X) = \frac{1}{\tau}\sigma(t) \qquad [20]$$

This corresponds to the relationship for the relative standard deviation being postulated by Junge.

$$\sigma(\ln X) = A \cdot \tau^{-b} \qquad [21]$$

With the experimental data Jobson shows a deviation from $b = 1$, as well.

The exponent b describes the relative locations of source and measurement point to one another. Typical values for measurement points in the vicinity of the source are $b \approx 0$, meaning there is no coherence between standard deviation of the natural logarithms of the measurement values and the lifetime. For remote or rural measurement sites b often is found to be around 0.5. For arctic measurements, where the only variability causing factors are the chemical processes, the exponent b approaches values of 1.

The interpretation of b is also the description of the relationship between sources and sinks. Is b approaching 0 then the air masses were strongly influenced by the source. If b is converging 1 sink processes are dominating the behavior of the measurement results.

The factor A can be an interpretation of the standard deviation of the transport times of individual air masses of which the sample consists of. Figure 1-5: Example diagrams for a remote and a strongly source-influenced measurement location from Jobson et al. 1998 shows experimental result for various NMHCs from Jobson from a remote station on the left. The fit through the data points is deviating from the "Junge relationship". On the right, a data set from York University Campus is shown. In this urban area where NMHC sources are close by there is no correlation between the variability and the lifetime of the measured compounds (Jobson et al. 1998). This means that the variability of the measurements is driven by the wind direction (and the measurements being exposed to the source), and not to chemical processes which would have generated a series of variabilities in the individual measurements that form an inverse relationship to lifetime.

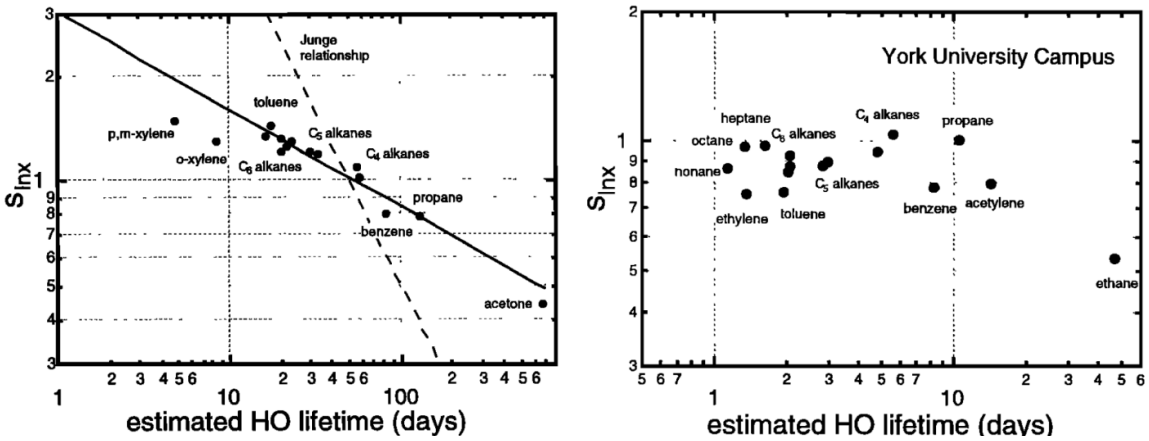

Figure 1-5: Example diagrams for a remote and a strongly source-influenced measurement location from Jobson et al. 1998

Another useful application of this analysis method is the estimation of a compounds lifetime based on its variability. Model calculations by Hamrud (1983) result in a uncertainty of a factor of ten if the variability is the only information available for a certain

compound. If there is further information on sources and sinks configurations, the overall uncertainty is significantly improved to a factor of two.

During LBA-CLAIRE in 1998 Williams et al. (2000) found acetonitrile deviating from the general trend of the other compounds. The variability was higher than it should be for a predicted lifetime of 3 years considering removal by OH radicals only. They came to the conclusion that additional sinks such as wet uptake and hydrolysis in acidic solution decreased the lifetime of acetonitrile to about three weeks.

A general approach of this method is data quality control. A deviating behavior from the predicted variability-lifetime-comparison can give hints on systematic errors. One example for GC measurements close to the detection limit is that background is continuously integrated with the peak. This would result in a lower variability for this special compound. It also can aid data interpretation with unidentified compounds (Williams et al. 2000).

By optimizing the fit quality the OH concentration or the radical composition in general may be estimated by using the lifetime variability relationship (Jobson et al. 1994; Ehhalt et al. 1998).

In this thesis the comparison of the standard deviation of the natural logarithm of individually measured NMHCs has been compared to their estimated lifetimes for the CYPHEX and the NOTOMO data sets.

1.4 Field campaigns

The species introduced in this chapter were measured during different field campaigns and the above discussed means of data analysis were applied.

In summer 2014 the CYPHEX campaign took place in the northwestern part of Cyprus. NMHCs were measured on-site and the analysis of organic nitrogen compounds from canister was conducted in the lab in Mainz after the campaign.

The use of the NCD-system and the good results during CYPHEX lead to the start of analysis of samples from the CARIBIC project from August 2014 to August 2015.

In summer 2015 the NOTOMO campaign was at the Kleiner Feldberg, Taunus, Germany and also involved measurements of NMHC and organic nitrogen compounds.

The plant rich environment and the knowledge that some plants are able to emit amines served as motivation for a small laboratory experiment.

The experimental details are explained in chapter 2 including the plant cuvette experiment and results of the campaigns are addressed in detail in chapters 3 - 5.

Chapter 2

Experimental

2 Experimental

The research presented in this thesis is based on two detection systems that measure NMHC and organic nitrogen species in the atmosphere. These systems have been deployed both in the field and have been used to analyze compressed air samples collected at surface sites, from chambers and at high altitude using custom made sampling devices mounted in a commercial aircraft. Details of the detectors and the sample collection devices are given in this chapter.

2.1 Measurement of Non-Methane Hydrocarbons

Non-methane hydrocarbons were measured using two coupled commercial gas chromatographs (GC) by AMA (GC 5000 VOC; GC 5000 BTX, AMA instruments, Ulm Germany). They were built especially for monitoring ozone precursors. GC 5000 VOC was used for the measurement of C_2-C_6 non-methane hydrocarbons and BTX for C_6-C_{12}. The common basis for both instruments was sampling on adsorbent filled enrichment cartridges, thermodesorption, chromatographic separation and detection of the eluting trace compounds by flame ionisation detectors (FID). The GCs were programmed to start in parallel with sample collection while separation and data acquisition of the last sample were still going on. Thus data points from both instruments represent the same timeframe at the best temporal resolution despite different chromatographic set ups. A hydrogen generator (HG 500, AMA instruments, Ulm Germany) and a zero-air generator (AirKat 6.1, INNOTEC, Pfinztal, Germany) were implemented into the rack to enable stand-alone combustion and carrier gas supply without using any additional high pressure gas cylinders. Ambient air was compressed up to 10 bar into a pressure reservoir. The air passed 3 purifying stages with a constant pressure of 5 bar to remove water, hydrocarbons and carbon dioxide (CO_2) (1. silicagel, 2. charcoal, 3. mixture of charcoal, molecular sieve and soda lime). Afterwards, remaining hydrocarbons and carbon monoxide (CO) were removed by oxidative catalysis over a Pd-catalyst at 430 °C and a final cartridge filled with molecular sieve. This zero air was also used with a dilution module by AMA for automatic calibration and dilution of standard gases by up to a factor of 2500. The dilution module housed a 2-100 ml/min mass flow controller (MFC) for calibration gas, a 100-5000 ml/min MFC for zero air and a solenoid valve to select between the calibration gas mixture and the sample inlet. During the CYPHEX field campaign (see chapter 3 for details) the system was calibrated against a commercial 30 component NMHC mixtures in nitrogen which was gravimetrically generated (National Physical Laboratory, Teddington, Middlesex, United Kingdom, 2010). Mixing ratios in the standard gas were around 4.00 ± 0.08 nmol/mol. Samples of a volume of 900 ml were taken with a flow of 45 ml/min representing an average NMHC compo-

sition for a sampling interval of 20 min. The sample volume could be adjusted by changing flow or time.

Table 2-1: Operational parameters for GC 5000 VOC and GC 5000 BTX

Step	Time [min]	Temperature [°C]
GC 5000 VOC		
Valve plate	-	40
Purging of sample line	2	-
Enrichment/sampling	20	15
Desorption	3	200
Focussing	-	30
Injection	3	270
GC 5000 BTX		
Valve plate	-	60
Purging of sample line	2	-
Enrichment/sampling	20	30
Injection	7	230

The crucial differences between the two systems were an additional focussing stage used in the VOC system, the capillary columns, and the temperature programs. Salient parameters of the system operation are summarized in Table 2-1. The enrichment stage of the BTX system was filled with Carbotrap, the VOC systems enrichment stage was additionally filled with Carbosieve (50:50). The VOC instrument houses an AMAsep WAX (30 m; 0.32 mm; 0.25 µm; polyethylene glycol) as a pre-column and an AMAsep ALUMINA (50 m; 0.32 mm; 8 µm, $Al_2O_3/NaSO_4$) as the main column. A ramped temperature program at constant carrier gas flow (40 ml/min) allows optimal separation. The initial temperature of 65 °C was held for 7 min, with a rate of 6 °C/min the oven was heated to 125 °C and held constant for 9 min. The final ramp to 200 °C was reached by heating with 20 °C/min. This temperature was held for 19 min. This sums up to an overall GC runtime off 48.75 min. An AMAsep1 (60 m; 0.32 mm; 1.5 µm, 100% poly methyl siloxane) was used for the BTX system. This was also operated with a temperature program at constant carrier gas flow of 37 ml/min. The inlet pressure of the carrier gas was 0.6 bar for the BTX system and 0.8 bar for the VOC system. The initial temperature of 50 °C was held for 15 min, followed by heating with a rate of 6 °C/min to 80 °C and 10 °C/min to 100 °C. This was kept for 7 min and an additional heating with 10 °C/min ended with holding 200 °C for 8 min. The total run time of the BTX

system was 47 min. All other parameters are summarized in Table 2-1. Since sampling started already during data acquisition the temporal resolution was to 60 min although overall runtime for the VOC instrument was around 74 min.

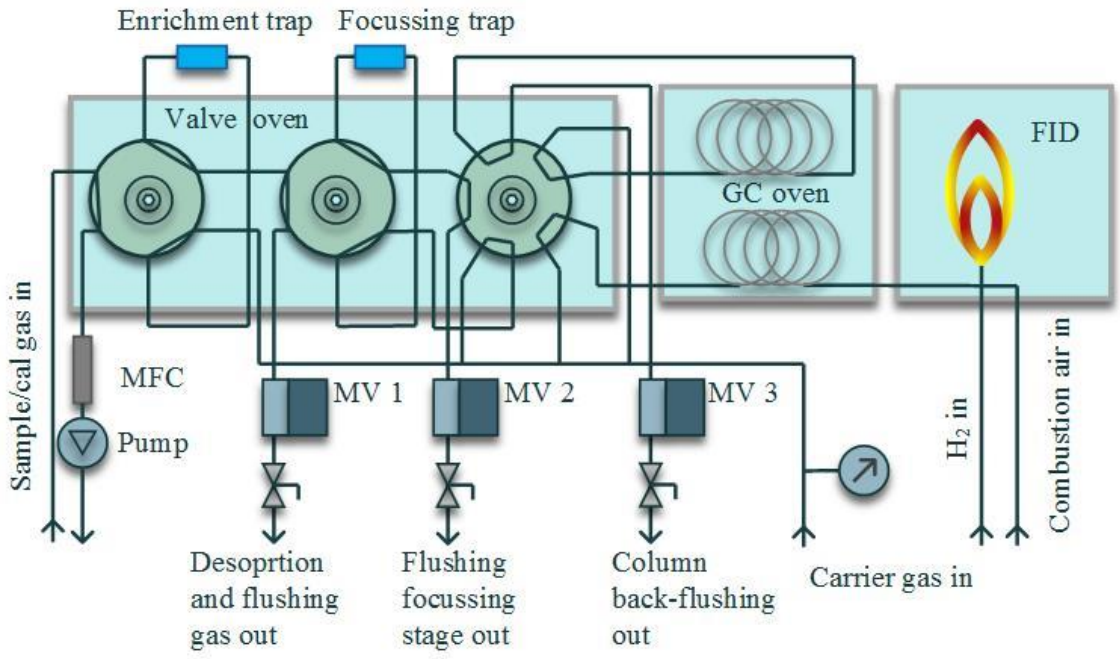

Figure 2-1: Schematic diagram of AMA GC 5000 VOC for measurement of C_2-C_6 NMHC

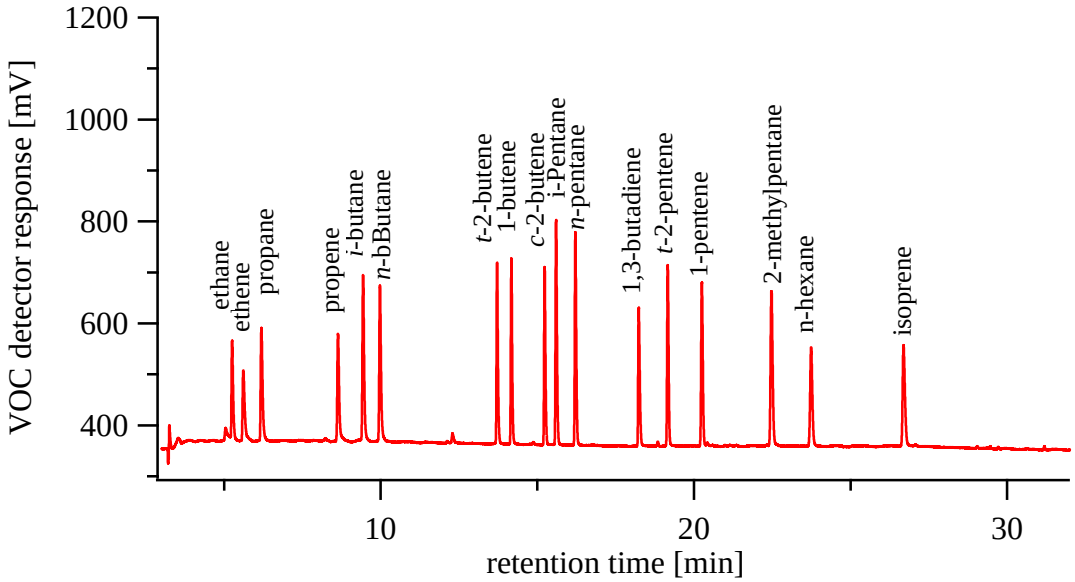

Figure 2-2: Chromatogramm of C_2-C_6 NMHC from 30 component calibration gas mixture

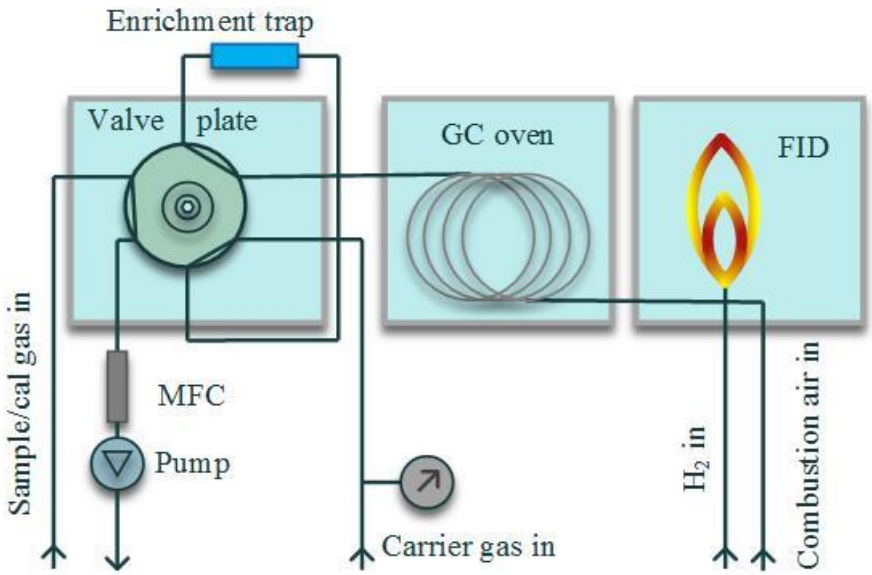

Figure 2-3: Schematic diagram of AMA GC 5000 BTX for measurement of C_6-C_{12} NMHC

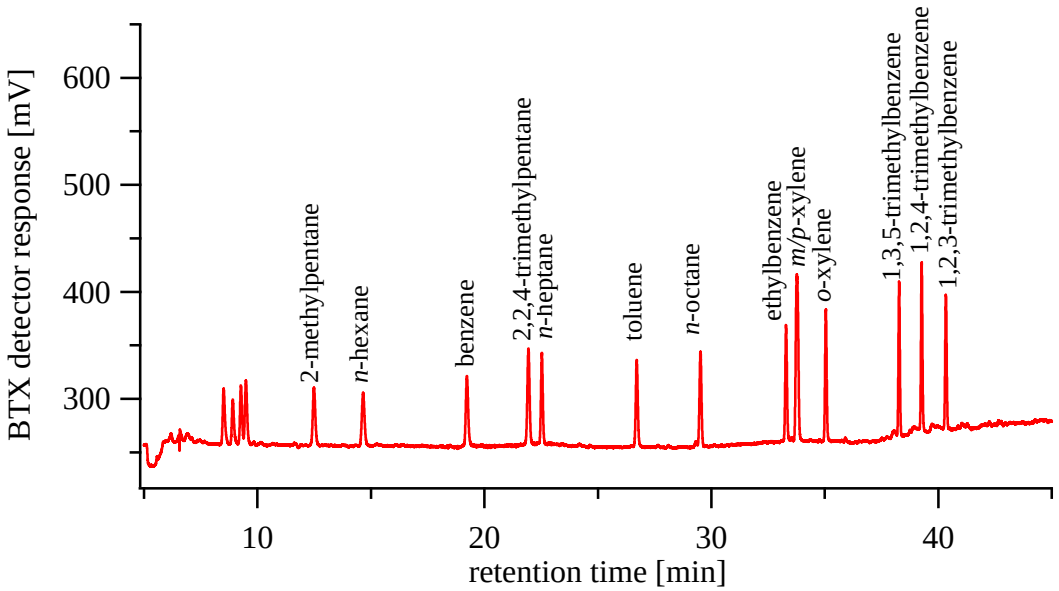

Figure 2-4: Chromatogramm of C_6-C_{12} NMHC from 30 component calibration gas mixture

Figure 2-2 and Figure 2-4 show chromatograms of the calibration gas. The limits of detection (LOD) were calculated by using three times the standards deviation of the blank signal over the retention time window of the associated compound. LODs typically ranged from 1-5 ppt. Exceptions with higher LOD were ethane (8 ppt),

ethane (16 ppt), propene (9 ppt), benzene (14 ppt) and toluene (48 ppt). For the more volatile compounds this was due to the lower response factors caused by the per carbon sensitivity of the FID (Figure 2-5). For the BTX compounds, which have much higher response factors, the higher LOD is caused by a background, possibly caused by traces of carbon containing compounds that were not removed by the zero air generator. Precisions were calculated for each species by using the standard deviation of 10 repetitions of the standard measurements and were 5% or less for all compounds considered in this work.

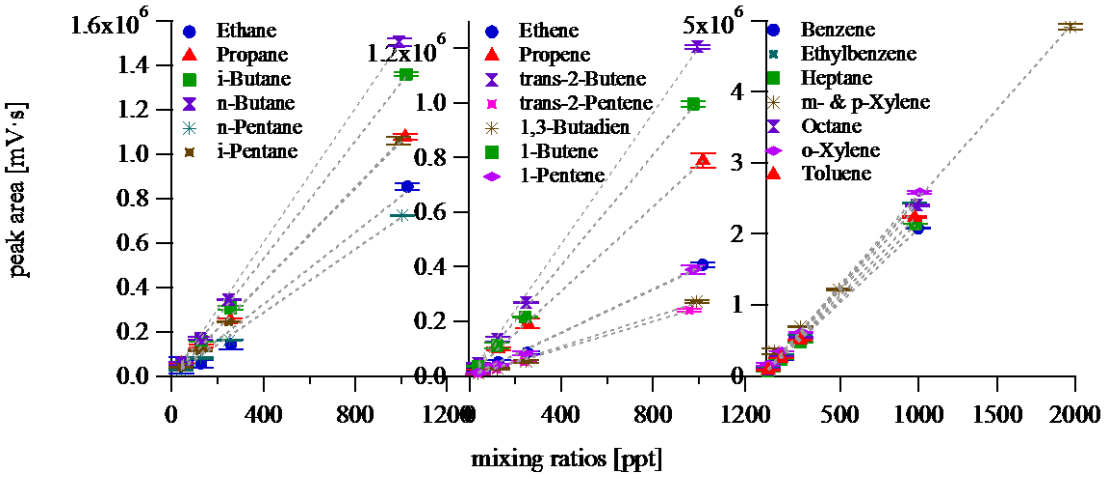

Figure 2-5: Calibration curves for NMHCs measured by GC-FID

In 2013 these instruments were evaluated along with the ACTRIS (Aerosols, Clouds, and Trace gases Research InfraStructure Network) comparative experiment (Hoerger et al. 2015). The results of the comparison between our NMHC analysis and the ACTRIS whole air standard are shown in Figure 2-6. The results are displayed as normalized fraction of the NMHC mixing ratios determined by GC-FID relative ACTRIS quoted

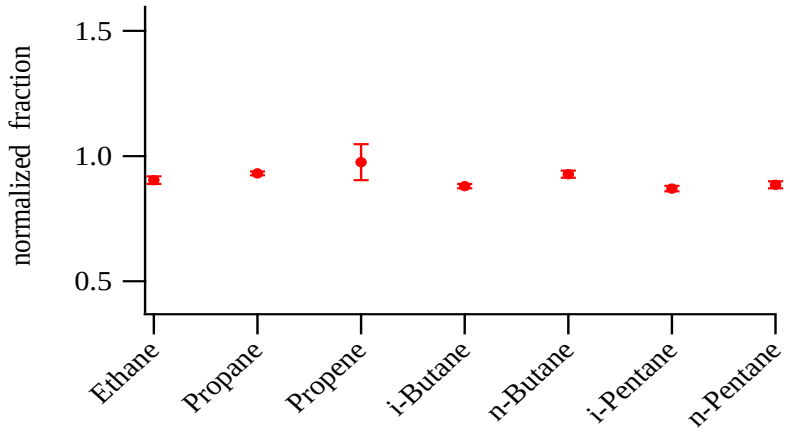

Figure 2-6: Comparison of NMHC analysis within the ACTRIS experiment

mixing ratios considered as 100%. The fractions were between 0.88 and 0.97.

2.2 Measurement of organic nitrogen species

Air samples were analyzed for organic nitrogen compounds using an Agilent 6850 gas chromatograph (Agilent Tech., Inc., Santa Clara, California, USA) equipped with an Agilent 255 nitrogen chemiluminescence detector (NCD). Prior to chromatographic separation the trace gases were enriched by cryofocussing using an ENtech 7200.

Figure 2-8 shows a schematic of the complete system. The ENtech 7200 is a commercial preconcentration system by ENtech Instruments, Inc., Agate Ct. Simi Valley, California, USA. All tubings and valves were passivated by Silonite® coating. For sample drying and enrichment, a reservoir of 1.4 l was evacuated to a pressure of 103 mbar (1.5 psi). Sample, internal standard and calibration standard were passively drawn through a dehydration module (empty 1/8" (3.17 mm) tubing) followed by an enrichment module (1/8" tubing filled with Tenax®). The sample volume was calculated by the pressure difference in the evacuated reservoir instead of using mass flow controllers, since the pressure can be determined more accurately than the flow. During sample preconcentration the dehydrating module (M1) was kept at a temperature of -10 °C and the enrichment module (M2) at -45 °C. Liquid nitrogen for cooling was provided at a pressure of 1.3 bar (20 psi). The gas flow through the modules was controlled by the pressure difference between the reservoir and the sample and the sequentially opening valves. To ensure an almost steady flow, the reservoir was re-evacuated at a pressure of 586 mbar (8.5 psi). To transfer retained analytes from M1 to M2 (see Figure 2-8), M1 was heated to 20 °C and flushed with 50 ml He (6.0) at a flow rate of 20 ml/min. Meanwhile the focusing module M3, a deactivated GC transfer line was cooled down to a temperature of -180 °C. During sample transfer M2 was heated to 210 °C and flushed with He for 2.5 min with a flow of 20 ml/min. From M3 the sample was injected over 1 min with carrier gas at 780 mbar (11.3 psi; 1.1 ml/min) into the GC. For the trace gas separation a combination of a HP-5 (30 m; 0.32 mm; 0.25 µm; 5% diphenyl; 95% dimethyl polysiloxane) and a Restek 1701-CB-0,5 (5 m; 0.25 mm; 0.5 µm; (14%-cyanopropyl-phenyl)-methylpolysiloxane), as post column for better separation of more polar components, was used. The oven was operated between 30 and 200 °C and also the carrier gas pressure was increased during the GC run to maintain carrier gas flow. Detailed information can be found in Table 2-2. The temporal resolution in continuous measurement mode, in which the preconcentration was also started during the last minutes of the GC run, was 29-32 min depending on sample pressure, because of the passive sampling procedure. The column was connected to a NCD. The first step of the detection process was the combustion of all eluting compounds at a temperature 800 °C

in a hydrogen/oxygen plasma over a platinum catalyst. The pressure in the plasma burner was at 150 mbar (114 Torr). During combustion all nitrogen containing compounds form nitrogen oxide (VII). Subsequently, the exhaust from the burner was lead to the reaction cell where it was reacted with ozone (O_3) in a chemiluminescent reaction at a pressure of 9 mbar (7 Torr). The relaxation of the resulting excited NO_2 produces light in the near infrared range which was detected by a photomultiplier. To reduce dark current the photomultiplier was cooled down by a Peltier element to -10 °C. Agilent Open Lab Chemstation (Rev.: C.01.05; Agilent Tech., Inc., Santa Clara, California, USA) was used for GC operation, data acquisition and data analysis.

$$R\text{-}N + O_2 \rightarrow CO_2 + H_2O + NO \qquad [VII]$$

$$NO + O_3 \rightarrow NO_2^* \rightarrow NO_2 + h\nu \text{ (NIR)} \qquad [VIII]$$

Table 2-2: Operational parameters for the GC-NCD

	Rate	Temperature	Hold Time	Run Time
	°C/min	°C	min	min
Initial		30	5	5
Ramp 1	15	50	3	9.3
Ramp 2	10	110	0	15.3
Ramp 3	20	200	0	19.8

Run Time	carrier gas pressure
min	mbar (psi)
0	780 (11.3)
8	924 (13.4)
9.5	1069 (15.5)
19	1310 (19.0)

For calibration and identification of acetonitrile and acrylonitrile a primary, gravimetrically prepared standard of 79 components by AiR Environmental, Inc. (Broomfield,

Colorado, USA, Ambient Air Quality Gas Standard) from 2011 was used. Mixing ratios of individual components in the standard ranged from 24 to 77 ppb with a quoted uncertainty of ±5%. The mixing ratio of acetonitrile was 47.7 ppb and 54.8 ppb for acrylonitrile. A second standard with a similar composition except for the addition of *i*-propyl nitrate, *i*- and *n*-butyl nitrate was available and used from June 2015 (Apel-Riemer Environmental, Inc., Boulder, Colorado, USA) Limits of detection at optimal instrument performance were between 1.5 and 3 ppt for those compounds.

Furthermore, a permeation source for peak identification and calibration was coupled to the system. Figure 2-7 shows a schematic diagram of the setup. The source consisted of a round-bottom centrifuge tube (56 mm; 145 mm) equipped with a glass impinger top (Neubert-Glas GbR, Geschwenda, Germany). The long tube reached down to the bottom of the centrifuge tube and was the inlet for synthetic air. The permeation source was constantly flushed with 300 ml/min of synthetic air. The short end of the impinger top was split by a Teflon Y-piece into one line to a rotameter, and one line to a sample inlet of the preconcentrator. The rotameter worked as a control of the total flow through the source and excess during sampling from the sample outlet. The centrifuge tube was housed in a heating aluminum block (152 mm; 90 mm; 100 mm) with a drilled hole with an inner diameter of 58 mm and a height of 90 mm with a round bottom optimally enclosing the glass. The temperature could be varied according to the volatility of the analyte. Pure compounds or solutions were filled in 2 ml GC auto sampler amber vials with open screw cap and virginal PTFE septum (Ø = 8 mm; 0.25 mm) for peak identification. The permeation source was used solely for peak identification, since no mass difference was observed to calculate the permeated amount of analyte. Measurements of samples with different humidity did not show an influence on retention times or peak shape.

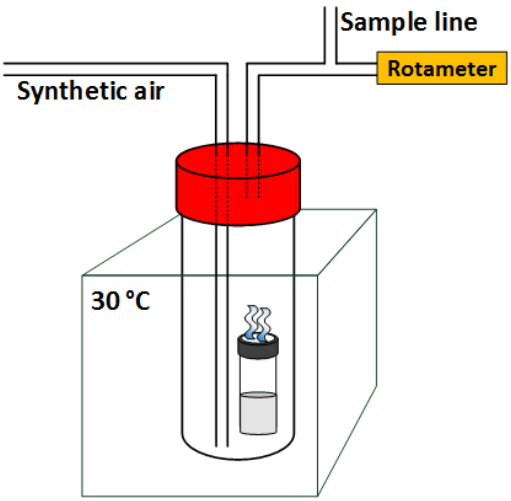

Figure 2-7: Schematic diagram of the permeation source

Different test runs were done to find the optimal conditions for analysis with the GC-NCD system. The NCD was tested with different plasma burner temperature ranging from 730 -900 °C in 20 degree increments. Hydrogen flow was tested with 4, 6 and 8 ml/min. The oxygen flow was also varied with 2 ml/min steps between 8-14 ml/min. In contrast to the results of Özel et al. 2011, we neither found significant improvement nor deterioration on system sensitivity. We adopted the conditions for dual plasma burner gas supply they found to be optimal.

However, the pressure within the reaction cell of the NCD was found to have a huge influence. The NCD was delivered with a Teflon membrane pump. This pump lost efficiency with run time. Therefore it was exchanged with a scroll pump (Agilent IDP-3) and the system was additionally equipped with a valve just before the pump to adjust the pressure. The optimal signal-to-noise ratio was found at a pressure of 7 torr (9.3 mbar) balancing quenching of the chemiluminescence reaction at higher pressures and short residence time of the reaction partners at lower pressures. Moreover, the traps of the preconcentration system were tested with different temperatures and also with glass beads as adsorbent material. The highest sensitivity could be achieved with the conditions described in Table 2-2. Furthermore the NCD was sensitive to the electromagnetic influence of the housing and was run with an open housing to ensure no fluctuation of the baseline.

Table 2-3: Nitrogen containing compounds for NCD measurement

Compound	Retention time [min]	CAS	Supplier	annotation
Hydrogen cyanide	2.20	74-90-8	Linde AG	4 ppm in N_2
Acetonitrile (Ethanenitrile)	2.38	75-05-8	Apel-Riemer	47.7 ppb in N_2
Acrylonitrile (2-Propenenitrile)	2.48	107-13-1	Apel-Riemer	54.8 ppb in N_2
Methyl nitrate	2.54	598-58-3	Envilytix GmbH	1000 µg/ml in 1-octanole
Propylnitrile (Propionitrile)	2.75	107-12-0	Sigma-Aldrich	99%
Ethyl nitrate	3.07	625-58-1	Envilytix GmbH	1000 µg/ml in 1-octanole
i-Propyl nitrate	3.70	1712-64-7	Sigma-Aldrich	99%

Compound	Retention time [min]	CAS	Supplier	annotation
n-Propyl nitrate	4.32	627-13-4	SelectLab Chemicals GmbH	99%
i-Butyl nitrate	5.90	543-29-3	SelectLab Chemicals GmbH	99%
n-Butyl nitrate	6.81	928-45-0	SelectLab Chemicals GmbH	99%

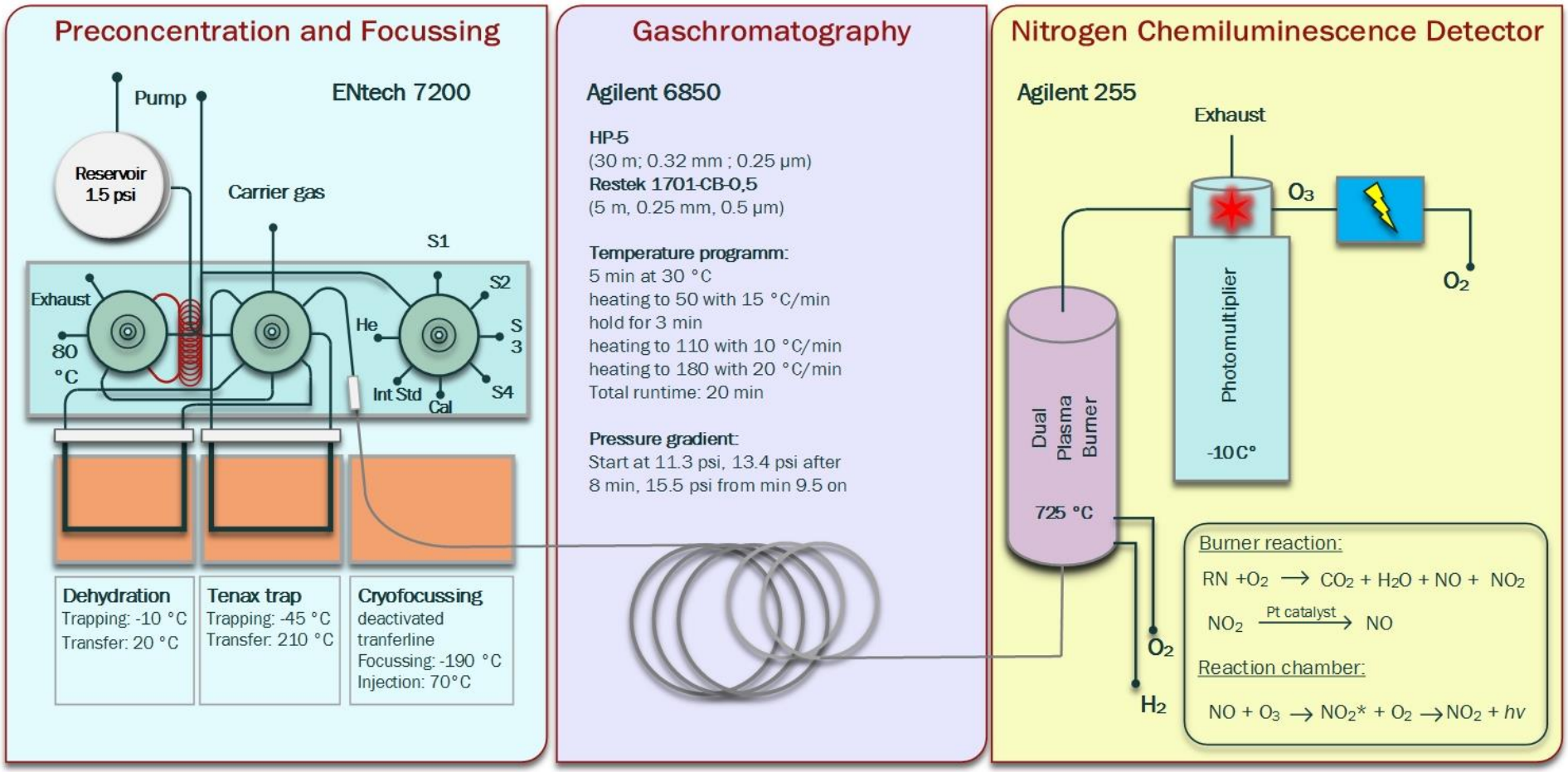

Figure 2-8: Schematic diagram of the GC-NCD system for measurement of organic, nitrogen containing compounds

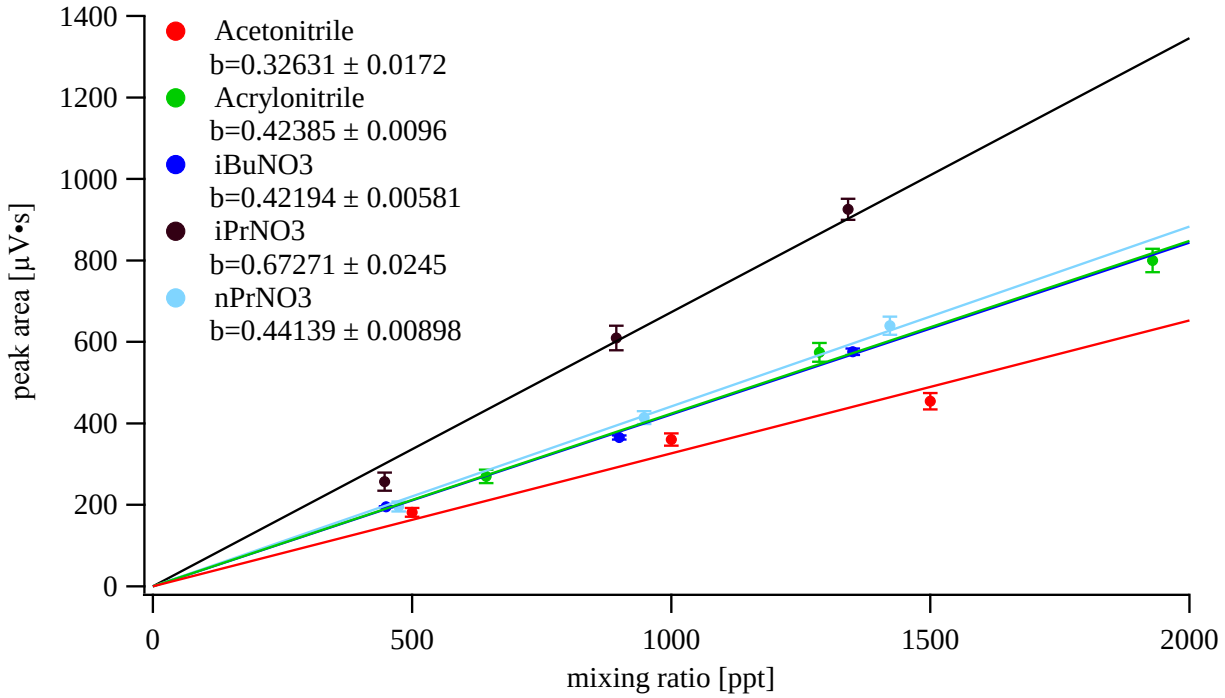

Figure 2-9: Calibration curves of organic nitrogen compounds from Apel-Riemer calibration gas mixture

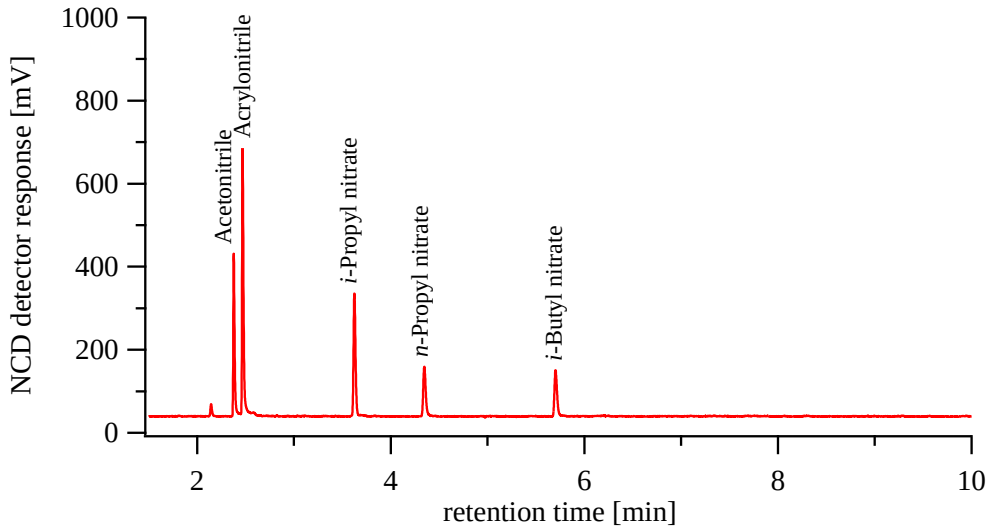

Figure 2-10: Chromatogram of organic nitrogen compounds from Apel-Riemer calibration gas mixture

2.3 Sample collection during measurement campaigns

During the CYPHEX measurement campaign (see chapter 3 for details) the GC-FIDs were installed in an air conditioned laboratory container, sampling air from a common inlet system for all other group containers. The containers were stacked in two by two with the common inlet of 8 m height and an inner diameter of 0.5 m sited in the middle. Air was drawn through this inlet at a high flow of 10 m^3/min. Individual instrument and container inlets were placed perpendicular to the main flow. The GC-FIDs were connected to the common inlet via a Teflon line (OD = 1.27 cm) in common with an OH reactivity system, a methane FID, a GC-MS and a PTR-ToF-MS. Sample flow in this line was 5 l/min. To prevent condensation in the line it was insulated and heated to 35 °C (Derstroff et al. 2016).

Whole air samples (WAS) were taken from a different inlet line (Teflon, OD = 0.625 cm, 10 m,) on the outer site of the container stacking. This was necessary to avoid inducing strong pressure fluctuations in the continuously measuring instruments. 2.4 l stainless steel canisters were filled with ambient air using a Teflon membrane pump to 3.5 bar and then the pressure was released to 0.2 bar. After four times of flushing the canisters were pressurized to 3.5–4 bar. The sample consisted of 1.8% from the first filling, 5.2% from the second, 19.5% from the third and 73.3% from the final filling. One filling took approximately 20 seconds. Thus the data points refer to that time frame of sampling. In total, 31 WAS were taken during the campaign and were analyzed within two months after the campaign for organic nitrogen species with the GC-NCD system in the lab in Mainz. The results of the CYPHEX campaign are shown and discussed in chapter 3.

During the NOTOMO field campaign (see chapter 5 for details) the FIDs were connected to a 3 m Teflon (OD = 0.625 cm) line with no additional constant sub flow to the same common high flow inlet as used during CYPHEX. To minimize the influence of residual air, the purging time of the sample line was set to 5 min (≈ 5 times flushing the inlet line volume). WAS were also taken from the common inlet tower next to the FID inlet line. Flushing and filling procedure was as described above. The canisters were analyzed within maximum four days after sampling with the GC-NCD system for organic nitrogen species. This campaign is addressed in chapter 5.

In addition to the ground based measurement campaigns, WAS from the CARIBIC project (Civil Aircraft for the Regular Investigation of the atmosphere Based on an Instrument Container) were analyzed with the GC-NCD system. Within this project a 1.5 t freight container equipped with laboratory instrumentation for online and offline analysis of the atmospheric composition was sent monthly on four consecutive long-distance flights with a Lufthansa Airlines Airbus A340-600 passenger aircraft

(Brenninkmeijer et al. 2007). A set of two TRACs (Triggered Retrospective Air Collector) with 14 glass sampling flasks (2.67 l; Louwe Hapert, the Netherlands) each and one HIRES (High REsolution Sampler) with 88 electropolished stainless steel flasks were deployed in the measurement container. Usually during each single flight either one TRAC or half of HIRES was filled. Sample collection automatically started when ambient pressure fell below 480 mbar to ensure no contamination by airport air. TRACs consisted of one VICI 16-port multiposition valve (VICI AG International, Schenkon, Switzerland), an inlet and an outlet. The flasks were flushed for 300 s before the outlet closes. The inlet closed at an absolute pressure of 4.5 bar. The filling procedures took 30 to 90 s which corresponded to a spatial resolution between 7 and 21 km at a flight speed of about 230 m/s (Schuck et al. 2009;. Baker et al. 2009). HIRES housed six 16-port dead-end VICI valves connected to 15 (13 for the last valve) sampling flasks and an inlet. Therefore the sampling process for HIRES was different to that of the TRACs. The canisters were filled to a pressure of 4 bar and released against cargo pressure (0.7-1 bar at flight altitude). This was repeated 8 times. The final filling was to 4.5 bar. CARIBIC samples were analyzed in Mainz for NMHC, greenhouse gases (SF_6, N_2O, CO_2 and CH_4), organic nitrogen and sulfur species. Having three sets of TRACs enabled an exchange among different laboratories between flights. Those samples were regularly analyzed for halocarbons at the University of East Anglia, Norwich, UK. Further information on the container set up and instruments can be found in Brenninkmeijer et al. 2007.

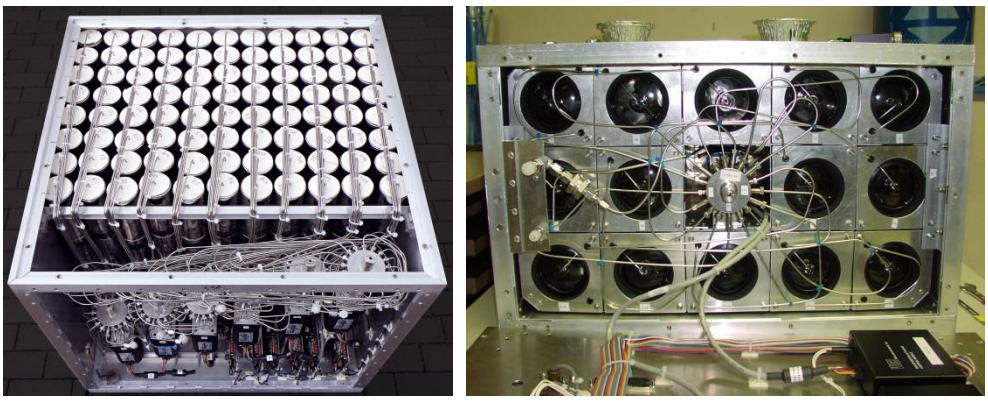

Figure 2-11: Left: open view of HIRES; right: open view of TRAC

Due to flight schedules and exchange between instruments and institutes it was not possible to test the influence of storage time on mixing ratios within the canisters intensively. From sample comparison between TRAC and HIRES we couldn't find any evidence for influences of canister material on the results. Repetitive measurements from stainless steel canisters used for CYPHEX and NOTOMO showed deviations within the un-

certainty of the instrument. However, no trend was identified whether the compounds were depleted or build up.

The result of this thesis from the CARIBIC project can be found in chapter 4.

To explore plant emissions and further applications of the GC-NCD system, a chamber experiment in collaboration with the department for biogeochemistry at the MPIC was carried out. In addition to offline analysis of flask measurements the system is also able to do quasi-online analysis. This capability was tested with a chamber experiment. The GC-NCD system was tested in quasi-online mode during a plant cuvette experiment.

2.4 Plant cuvette experiment

A small laboratory based campaign was conducted to explore the emission of nitrogen containing organic compounds from plants and also with the aim of testing the scope of the new system for measurement of organic nitrogen compounds.

Four different plants, stinking goosefoot (*chenopodium vulvaria*), pear (*pyrus*), hawthorn (*crataegus*) and mountain ash (*sorbus aucuparia*) were selected based on previous observations of trimethylamine (TMA) from those plants (Wicke 1862; Cromwell 1950). Chenopodia were cultivated in the MPIC greenhouse from seeds in a set of three each with three different fertilizer concentrations. The plants were labelled with "no" for no fertilizer, "w" for little and "v" for much fertilizer.

The plants were put into a flexible Teflon foil cuvette with their upper part enclosed around the stem above the soil to ensure that samples were influenced only by emissions from the leaves (see Figure 2-12). From pear, hawthorn and mountain ash a freshly cut branch with blossoms was put into the cuvette with the cut end outside being in nutrient solution.

The dynamic cuvette had a volume of 18 l. FEP foil (Saint Gobain Performance Plastics Corporation, USA) was used as mantle material to minimize trace gas interaction and wall losses. All tubings and tubing connections were of PFA-Teflon® (Swagelok, USA). A fan (APC Propellers, USA), which was coated with Teflon® was installed inside the cuvette to assure well-mixed conditions in order to reduce the aerodynamic resistance of the trace gas fluxes (Gut et al., 2002). By use of an additional perforated ring at the bottom of the cuvette the main air stream was divided into several small air streams to improve the distribution of the air addition inside the cuvette. Air samples were taken via the two sampling tubes entering the cuvettes from the top. The surplus of the air stream effused at the vent situated at the bottom of the cuvette (see Figure 2-12). To prevent ambient air from entering the cuvette, the flow rates were adjusted such that the cuvettes were slightly over-pressurized (Sun et al. 2016). The sampling line connecting the cu-

vette with the preconcentrator was a 3 m, ¼ “ (0.635 cm) Teflon® tubing. No heating of the lines was installed, so that the line was effectively at laboratory temperature (≈ 21 °C).

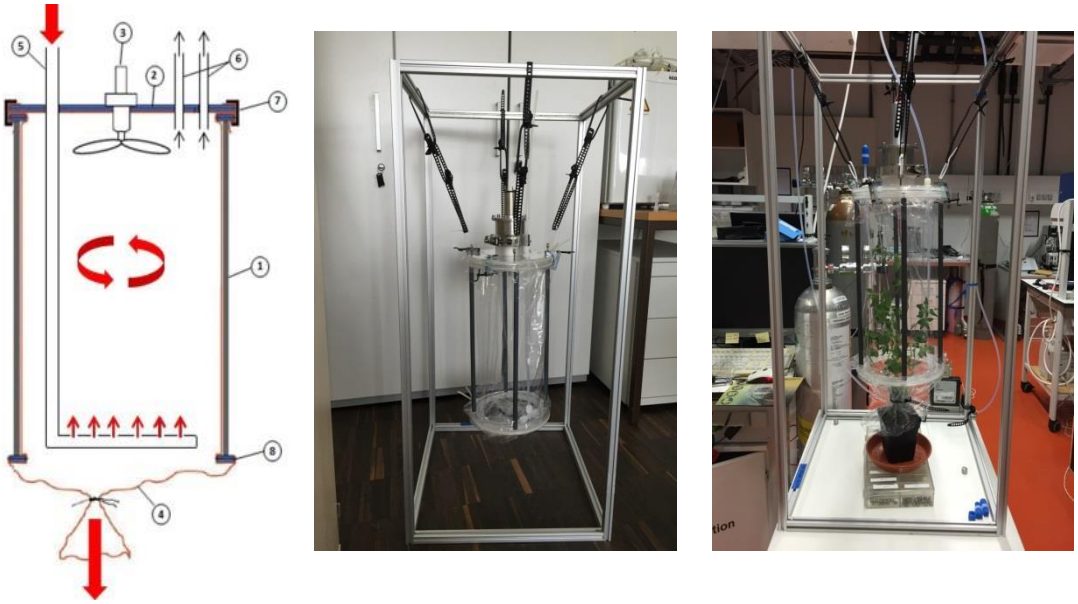

Figure 2-12: Sketch and photography of the plant cuvette

Before introduction of the plants, the air from the empty cuvette was measured until no peaks were observed, establishing the clean conditions. Prior to an experiment the cuvette usually was empty during nights and constantly flushed with zero air. Blank measurements showed that after an exchange of plants during the day a cleaning of the cuvette was complete after 3 hours of flushing (40 times turn over). The cuvette was generally flushed with synthetic air of 40 % relative humidity with a flow of 4 l/min. During measurements the flow was reduced to 2 l/min to keep the dilution of the emitted gases as low as possible still providing suitable conditions for the plant. Prior to the plant experiments an identification of TMA from the permeation source was completed. A comparison of a plant sample and a sample from the permeation source with TMA is shown in Figure 2-13. The results are briefly presented in chapter 5.3.

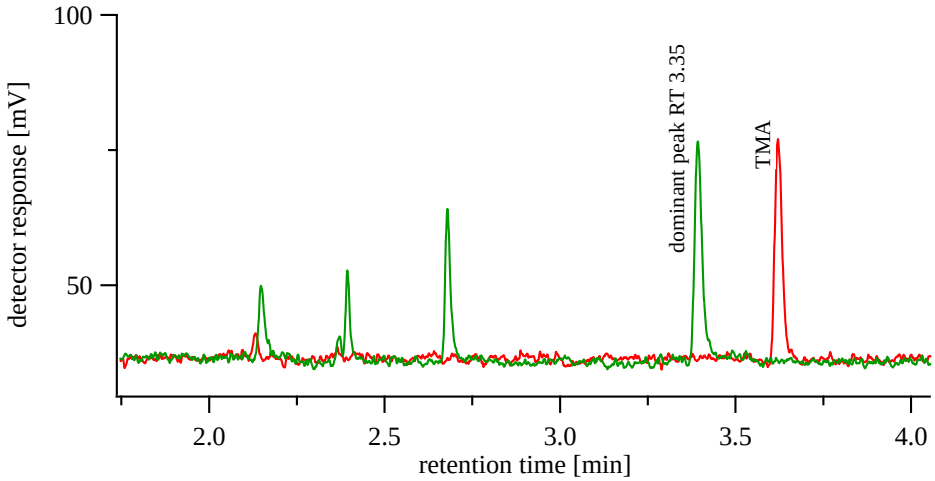

Figure 2-13: Comparative chromatograms for TMA from the permeation source (red) and measurement from *chenopodium* with different identified an unidentified peaks (green)

Chapter 3

CYPHEX 2014

CYprus PHotochemistry Experiment

Parts of the CYPHEX NMHC data set were published in:

Derstroff, B., Hüser, I., Bourtsoukidis, E., Crowley, J. N., Fischer, H., Gromov, S., Harder, H., Janssen, R. H. H., Kesselmeier, J., Lelieveld, J., Mallik, C., Martinez, M., Novelli, A., Parchatka, U., Phillips, G. J., Sander, R., Sauvage, C., Schuladen, J., Stönner, C., Tomsche, L., and Williams, J.: Volatile organic compounds (VOCs) in photochemically aged air from the eastern and western Mediterranean, Atmospheric Chemistry and Physics, 17, 9547-9566, https://doi.org/10.5194/acp-17-9547-2017, 2017.

Mallik, C., Tomsche, L., Bourtsoukidis, E., Crowley, J. N., Derstroff, B., Fischer, H., Hafermann, S., Hüser, I., Javed, U., Keßel, S., Lelieveld, J., Martinez, M., Meusel, H., Novelli, A., Phillips, G. J., Pozzer, A., Reiffs, A., Sander, R., Taraborrelli, D., Sauvage, C., Schuladen, J., Su, H., Williams, J., and Harder, H.: Oxidation processes in the eastern Mediterranean atmosphere: evidence from the modelling of HO_x measurements over Cyprus, Atmos. Chem. Phys., 18, 10825-10847, https://doi.org/10.5194/acp-18-10825-2018, 2018.

3 The CYPHEX field measurement campaign

Cyprus is an island in the eastern Mediterranean with a population of 1.12 million inhabitants. As it has little heavy industry, emission of anthropogenic NMHCs and organic nitrogen compounds should be modest. Nevertheless, diverse studies show that in the eastern Mediterranean and on Cyprus the ozone levels often exceed the European Union air quality standard of 60 ppb (8h average maximum value per day) defined by the World Health Organization (WHO) in 2001. Alternating high and low ozone periods were shown to be influenced by general European meteorological conditions rather than abundance of local precursors such as NO_x and VOCs. Hence, ozone is not necessarily produced locally under high NO_x and VOC conditions, it is rather transported to the eastern Mediterranean by long-range transport and photochemical processing along during air mass movement (Kourtidis et al. 2002; Kouvarakis 2002; Kalabokas et al. 2007; Kleanthous et al. 2014; Kalabokas et al. 2008; Kalabokas et al. 2013; Doche et al. 2014). The photochemical processes leading to the production of ozone are described in chapter 1 of this thesis.

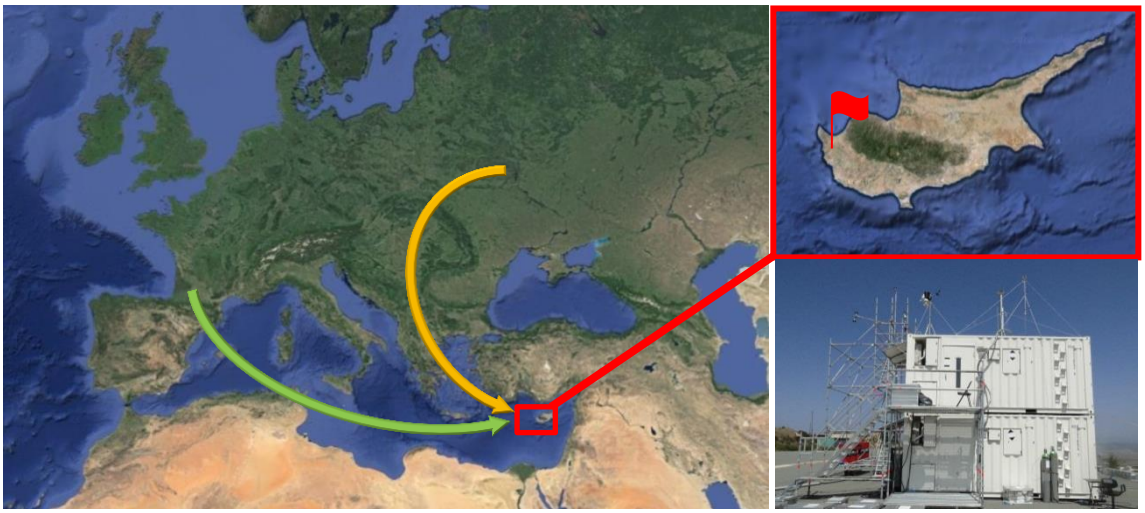

Figure 3-1: Main pathways of transport; site location; measurement containers

In summer 2014 the CYprus PHotochemistry EXperiment (CYPHEX) field campaign took place in the north western part of Cyprus in order to investigate the photochemistry and air mass transport of the eastern Mediterranean. NMHCs, as primary anthropogenic emissions and ozone precursors are an important component of this experiment as they can be used to investigate chemical processing using the methods described in chapter 1. While NMHCs react away during transport across the Mediterranean, several organic nitrogen species can be formed when NO_x is present in the air mass.

3.1 Site description and data overview

The four laboratory containers were placed at an elevated (600 m) measurement site close (5 km to the west and 10 km to the north) to the coast (35,96N, 32,4E). The next villages are Dhroushia and Inia, each with just a few hundred inhabitants at a distance of 2 km east-south-east of the site. A few other villages of this size are in this corridor. The next town in the north is Polis with ca. 3500 inhabitants. The next biggest city with 33000 inhabitants is Paphos with its airport and habour 20 km south of the site. The location was surrounded by sparse vegetation, mostly maquis or garigue. Maquis describes a mixture of not fully regenerated forest vegetation of evergreen shrubs and/or small trees of 3-5 m height. Garigue vegetation consists of low-growing shrubs (ca. 50 cm). Also agricultural fields are spread over the area around the measurement site. Orchards of Citrus species, *Ceratonia* (carob) or *Olea* (olive) and vineyards can be found (Fall 2012). In the northern part of the Akamas peninsula a pine and juniper forest lies between the measurement site and the coast.

3.1.1 Meteorology and air mass origin

The local meteorology was characterized by temperatures ranging from 18-29 °C and 23.4 °C on average. The relative humidity was varying from minimum 11% to 97% (70% on average) without any rain events during the campaign. The local wind was mainly coming from SW with an average wind speed of 3.3 ms^{-1} (Figure 3-2), though overall the transport pattern of air arriving at the site was dominated by northerly and westerly flows (Figure 3-1).

During the campaign the measurement site was influenced by two main transport patterns. A high pressure region over northern Greece, Macedonia and Bulgaria opposed to a low pressure area over Turkey caused Etesian winds coming from Eastern Europe and reaching Cyprus from the northern coast. Air masses originating from there typically showed higher mixing ratios in trace compounds which indicate that they were recently influenced by continental emissions. In contrast there were periods where the main transport to the measurement site was influenced by the Mistral. This wind pattern is caused by high pressure regions over the Atlantic and low pressure regions over the Baltic Sea and northern Italy. During these times the air masses were characterized by generally lower mixing ratios and more aged and photochemically processed trace gas compositions due to the longer transport ways over the Mediterranean Sea.

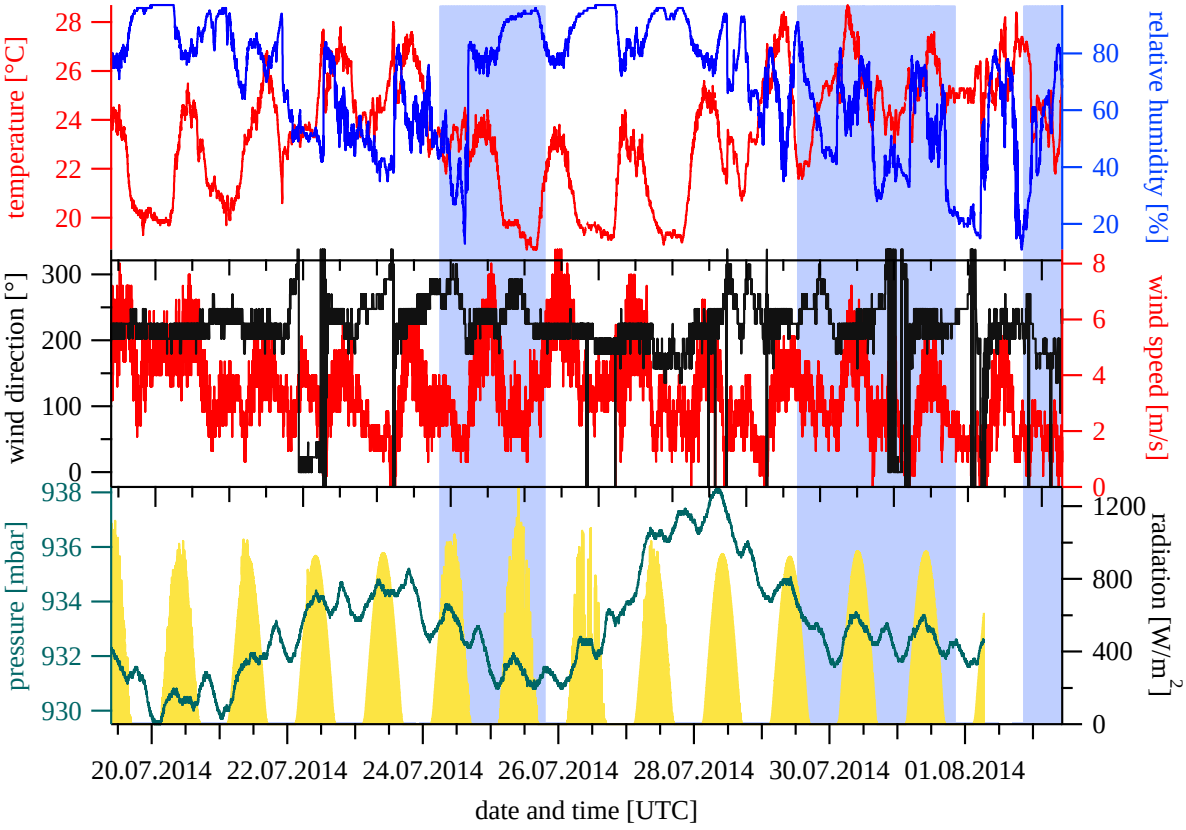

Figure 3-2: Meteorological conditions during CYPHEX

Trajectory analysis and studies on effective source region footprints were done with Flexpart (FLEXible PARTicle dispersion model). Based on this analysis (Figure 3-3) and comparison with VOC data the time series was divided into 6 individual time frames with respect to source regions from Europe and Northern Africa. Continental and oceanic parts were segmented into distinct source regions. The lower map shows the exact distribution.

The upper part of the plot shows the percentage of modelled particles coming from the individual grid cell. This data includes the results to a height of 1.5 km. In the lower panel the PTR-ToF-MS data for methanol can be seen. The red vertical lines indicate the air mass origin changing between Western and Eastern Europe. The measurement of NMHC started on the 19.07.2014. So the sectors were labelled from sector 1 to sector 6 as indicated in Figure 3-3. Additionally the Flexpart calculations were separated in air mass origin from free troposphere and planetary boundary layer (PBL). Detailed explanation can be found in Derstroff et al. 2016.

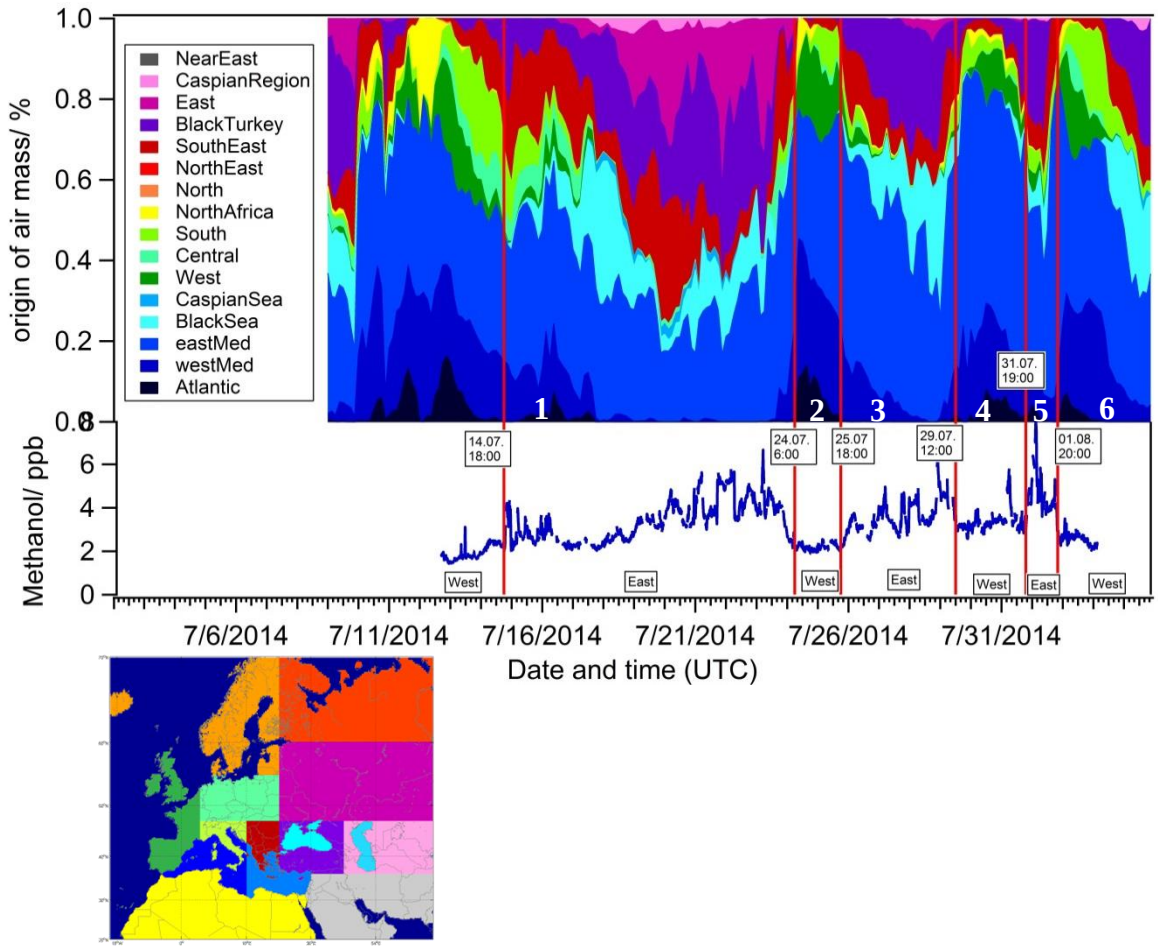

Figure 3-3: Upper panel: Results from Flexpart modelling. The campaign was split into six sectors of influence from Eastern and Western Europe based on comparison of Flexpart results with measurement of VOC (methanol from PTR-ToF-MS measurements).
Lower panel: gridding of Europe and Northern Africa

3.2 Results and Discussion

Non-methane hydrocarbons were measured with the GC-FID (AMA instruments GmbH, Ulm, Germany) described in chapter 2. The final dataset consisted of two weeks of continuous, hourly measurements of 10 different NMHCs. A methane FID, a PTR-ToF-MS for VOC, in particular OVOCs (oxygenated VOC), a GC-MS for halogenated compounds and terpenes and a CRM-OH-reactivity (comparative reactivity method) instrument were running in parallel inside the same container. Along with these, other measurements for CO, NO, NO_2, O_3, formaldehyde, hydrogen peroxide and various other atmospheric tracers were carried out.

Some VOC species were measured by more than one instrument. A comparison of GC-FID and PTR-ToF-MS results for the measurement of benzene and toluene gave R^2=0.88 and 0.76, respectively, and showed generally good agreement between the two different measurement techniques within uncertainty limits. However, the slopes of 0.89 for benzene and 0.78 for toluene show that the GC-FID measurements give slightly lower values than PTR-ToF-MS measurements (see Figure 3-4). This suggests that the less molecularly specific PTR-ToF-MS may be measuring a small fraction of break-down fragments of higher molecular weight species at these masses.

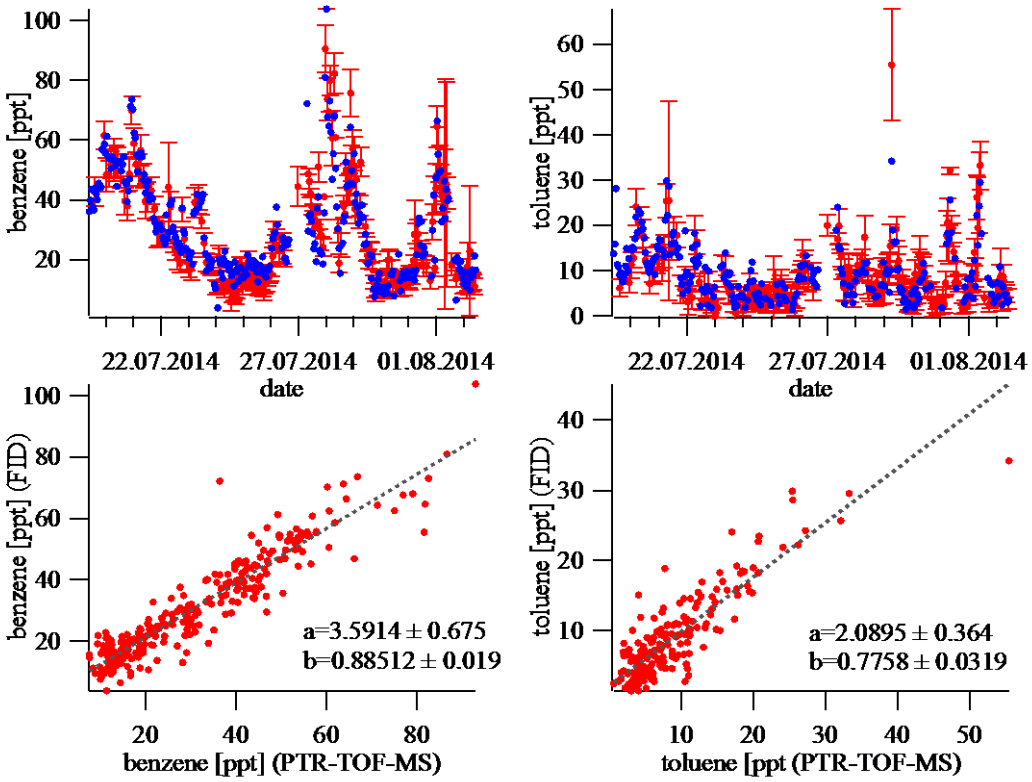

Figure 3-4: Comparison of GC-FID and PTR-ToF-MS measurements of benzene and toluene

Figure 3-5 shows the timeline of ethane, propane, *i*-/*n*-butane, *i*-/*n*-pentane, benzene, toluene, ethene and propene. In the white shaded areas the main air mass origin was from Eastern Europe. The easterly sectors in which the air masses were more recently influenced by anthropogenic emissions were characterized by generally higher NMHC mixing rations and higher variability. The westerly sectors, which are highlighted in blue, showed lower mixing ratios and a chemical composition being more influenced by photochemical processing. Ethene and propene as alkenes showed a slightly different behavior compared to the alkanes and aromatics. They were not as variable and also the contrast between easterly and westerly air masses was not as pronounced as for the other NMHCs. Table 3-1 shows the NMHCs in comparison with other measurement campaigns in the Eastern Mediterranean, Greece mainland and from Crete. Also a seasonal comparison is given with higher mixing ratios in wintertime when on one hand anthropogenic emissions are enhanced by combustion for heating and on the other hand depletion is less because OH chemistry is suppressed by lower insolation during wintertime. The mixing ratios measured during CYPHEX were about 50% or less compared to the other summertime measurement campaigns (Table 3-1).

In addition to on-site measurements stainless steel canisters were filled as described in chapter 2.3. In total, 31 samples were collected from 17.07.2014 until 25.07.2014. They were analyzed for organic nitrogen compounds and HCN with a GC-NCD system in the laboratory in Mainz within 2 months after the campaign.

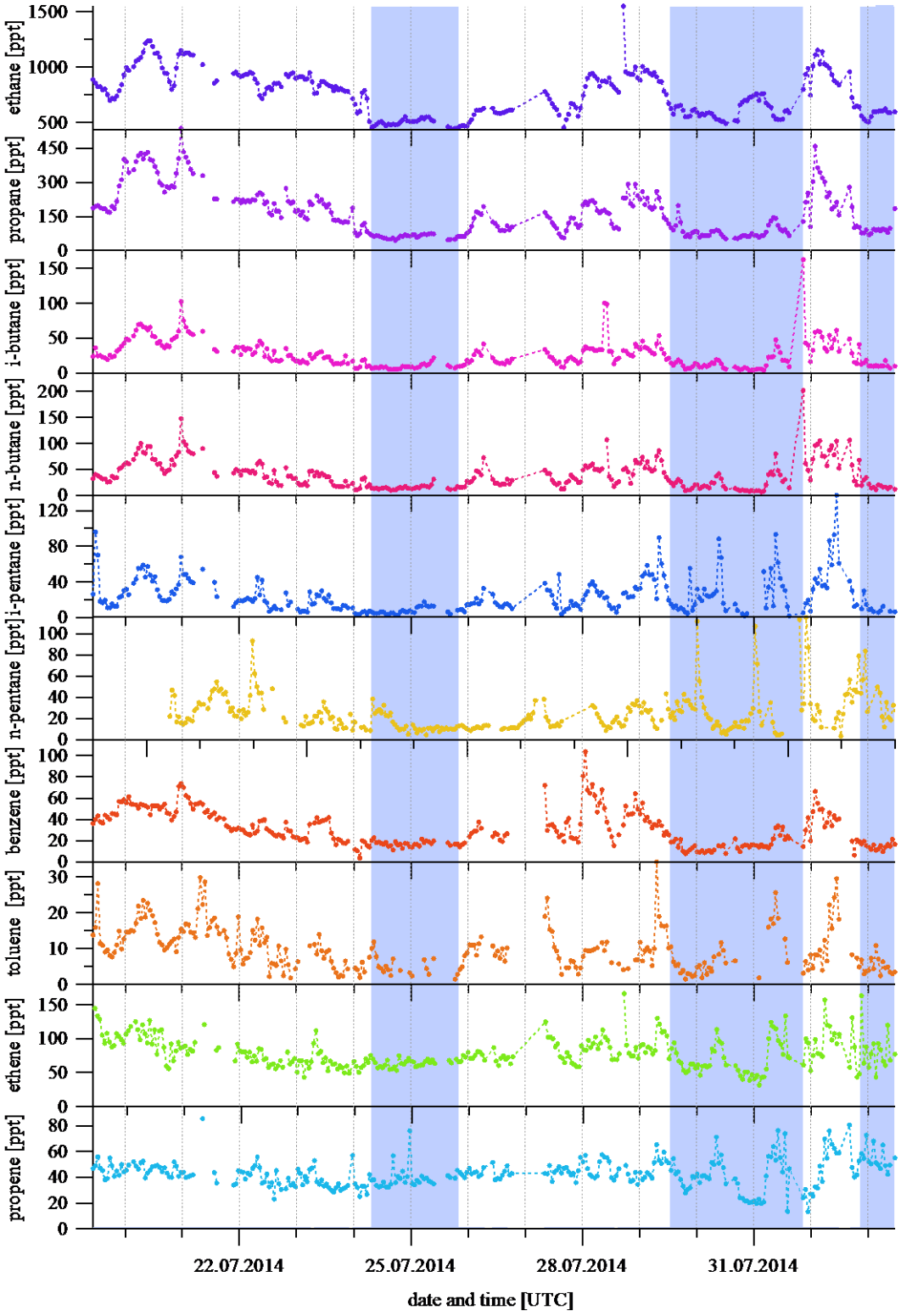

Figure 3-5: Timelines of NMHCs from GC-FID measurements

Table 3-1: NMHCs during CYPHEX and comparison with other measurement campaigns (winter and summer) in the Mediterranean

Season (year) location area	Summer (2014) Inia, Cyprus marine	Summer (2004–2006) Finokalia, Greece marine	Summer (2001) Finokalia, Greece marine	Summer Thessaloniki Greece (290–680 m height)	Summer (1996) Messorougion Greece (mountain)	Winter (2004–2006) Finokalia Greece (marine)	Fall (2004–2006) Finokalia Greece (marine)	Fall (1996) Messorougion Greece (mountain)
Ref.	this work	(Liakakou et al. 2009)	(Gros et al. 2003)	(Moschonas, et. al 2001)	(Moschonas and Glavas 2000)	(Liakakou et al. 2009)	(Liakakou et al. 2009)	(Moschonas and Glavas 2000)
Compound								
Ethane	753 ± 201	1353 ± 598				2432 ± 936	1952 ± 836	
Propane	164 ± 100	418 ± 322	235 ± 121	360–580	640 ± 330	757 ± 306	471 ± 264	950 ± 420
i-Butane	26 ± 19	451 ±115	72 ± 178		40 ± 20	544 ± 192	174 ± 89	70 ± 30
n-Butane	38 ± 27	258 ± 96	86 ± 93	80–1310	110 ± 70	561 ± 326	235 ± 117	320 ± 180
i-Pentane	24 ± 20	121 ± 71	97 ± 278	10–850	90 ± 80	221 ± 173	227 ± 96	110 ± 60
n-Pentane	25 ± 19	140 ± 68	36 ± 64	90–540	40 ± 30	210 ± 98	196 ± 76	70 ± 50
Benzene	31 ± 17	118 ± 41	101 ± 56	210–610	80 ± 60	269 ± 58	231 ± 102	170 ± 100
Toluene	10 ± 6	141 ± 95		180–1270	160 ± 130	174 ± 285	174 ± 188	130 ± 70
Ethene	79 ± 23						75 ± 27	
Propene	43 ± 11						235 ± 68	60 ± 40

Figure 3-6 displays the timelines of the regularly observed nitrogen compounds HCN, acetonitrile, methyl-, ethyl, *i*-/*n*-propyl- and *i*-/*n*-butyl nitrates. The campaign averages, standard deviations, maximum and minimum values are listed in Table 3-2. The average mixing ratio of acetonitrile of 162 ppt was in agreement with measurements during MINOS at Finokalia in August 2001 (154 ppt). The PTR-ToF-MS measurements during CYPHEX are also displayed in Figure 3-6. On average NCD values were higher than PTR-ToF-MS values by a factor of 1.3 ± 0.5. One reason for this deviation and also the relatively high standard deviation amongst individual WAS could be caused by the fact that PTR-ToF-MS measurements are averaged over 10 min. The WAS represents a time frame of only a few seconds of sampling (see chapter 2.3). The PTR-ToF-MS measurements with a higher temporal resolution of 1 min also showed higher variability and spiking of acetonitrile.

Table 3-2 Results from WAS analysis for organic nitrogen compounds by GC-NCD measurements

Compound	average ± SDEV	min.	max.
HCN	1698 ± 415	315	2798
Acetonitrile	162 ± 70	90	397
Methyl nitrate	24 ± 15	8	74
Ethyl nitrate	69 ± 87	14	448
i-Propyl nitrate	40 ± 54	6	293
n-Propyl nitrate	61 ± 83	9	446
i-Butyl nitrate	59 ± 61	11	215
n-Butyl nitrate	63 ± 53	25	191

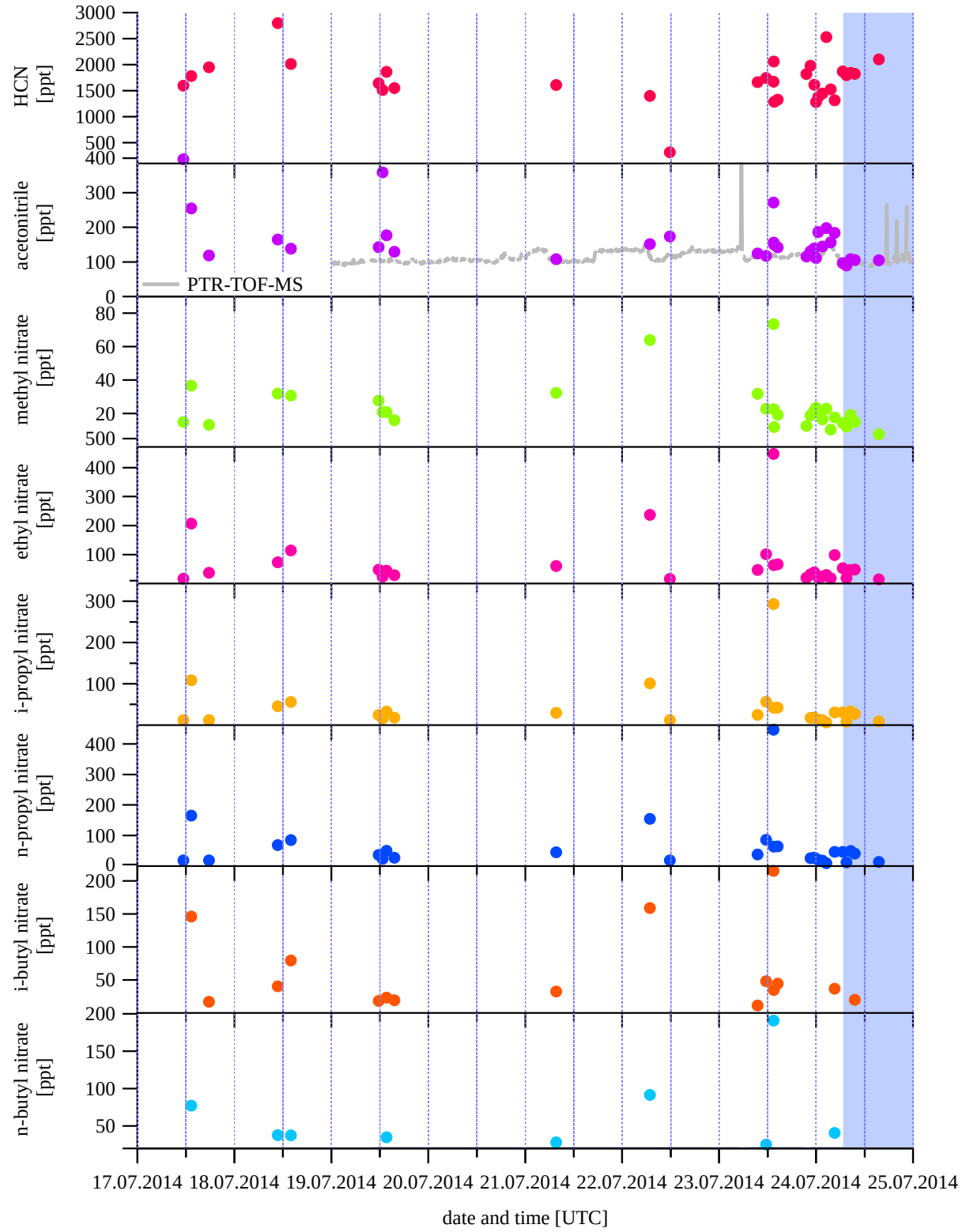

Figure 3-6: Timelines of nitrogen compounds from GC-NCD measurements. Grey lines show acetonitrile data from PTR-ToF-MS

Ethyl nitrate was the alkyl nitrate with the highest observed mixing ratio, methyl nitrate showed the lowest. For the *i*-/*n*-propyl and butyl nitrates a strong correlation with ethyl nitrate of $R^2 \approx 0.97$ was observed. The ratios determined by slope were 1.6 for *i*-propyl nitrate, 1.0 for *n*-propyl nitrate, 1.7 for *i*-butyl nitrate and 2.4 for *n*-butyl nitrate. The correlation of methyl nitrate with ethyl nitrate was with R^2=0.64 weaker and showed a ratio of 4.5. Except for methyl nitrate, the mixing ratios during CHYPHEX were higher than the ones reported by Flocke et al. (1991) for methyl, ethyl, *i*-/*n*-propyl and butyl nitrates of 109.0, 47.7, 27.4, 8.4, and 27.3 ppt at Jülich in Germany which was categorized as a polluted area and 10.0, 9.5, 19.9, 3.2, 13.3 respectively at *Schauinsland*, a rural location. Simpson et al. (2003) observed alkyl nitrates at different altitudes in Asian outflow during the aircraft measurement campaign TRACE-P at mean mixing ratios of 1.7-4.2 ppt (*i*-butyl > *n*-butyl > ethyl > *i*-propyl). These were about an order of magnitude lower than the results presented in this doctoral thesis. During PEM-West A (September-October 1996) and B (March-April 1999) Blake et al. (2003) found alkyl nitrates from 0.18-4.82 ppt at altitudes from 0-2 km. The comparison of the mixing ratios showed a different order between the two seasons (PEM-West A: methyl > ethyl > *i* propyl > *i* butyl > *n* propyl; PEM-West B: *i* butyl > *i* propyl > methyl > ethyl > *n* propyl). In spring time the alkyl nitrates which are formed from mother alkanes at higher branching ratios are dominating over the ones at the lower branching ratios but higher mixing ratios of mother alkanes.

To our knowledge this thesis is the first time measurements of individual short chained alkyl nitrates from the Mediterranean are presented. The only measurement of pentyl nitrates were performed by Glavas and Moschonas (2001) in Athens with a GC-ECD system in July 2000. They were found to between 20 and 90 ppt. During CYPHEX pentyl nitrates were not measured because they were not identified at the GC system. Nevertheless, additional unidentified peaks showed up in the chromatograms at retention times higher than butyl nitrates. Looking at the relation of the measured nitrate homologues, mixing ratios of pentyl nitrates consistent with the values previously reported by Glavas could be expected. Furthermore this study confirms the high mixing ratios found during CYPHEX in comparison with the mentioned studies in other regions.

During CYPHEX ethyl, *n*-butyl, *n*-propyl and *i*-butyl nitrates were found at quite equal mixing ratios, the average *i*-propyl nitrate was slightly lower and methyl nitrate the lowest.

Production rates of for alkyl nitrates $P(AN_i)$ were calculated using equation [21] with the branching ratios $\alpha_{i(OH)}$ from

Table 1-2, the reaction rate coefficients k_{OH+RH_i} from Table 1-1, the campaign average mixing ratios of the mother alkanes [RH_i] and an average OH concentration of 2.47×10^6 molecules cm^{-3}(Spivakovsky et al. 2000). The production rates decreased continuously from *i*-propyl nitrate to ethyl nitrate as illustrated in Table 3-3.

$$P(AN_i) = \alpha_{i(OH)} k_{OH+RH_i}[OH][RH_i] \qquad [22]$$

Table 3-3: Calculated production rates of alkyl nitrates

	i-Propyl	i-Butyl	Methyl	n-Propyl	n-Butyl	Ethyl
$P(AN_i)$ in [ppt h^{-1}]	0.080	0.066	0.055	0.032	0.032	0.022

Though photochemistry is the source of alkyl nitrates, it is also the most important sink. The photochemically initiated reaction with OH , as well as the direct photolysis of alkyl nitrates, lead to their removal from the atmosphere. The lifetimes of alkyl nitrates decrease with carbon number from about 8.5 days for methyl nitrate to 2 days for *n*-butyl nitrate with increasing chain length, whereas the *n*-isomers are removed faster than the *i*-isomers.

The measured alkyl nitrate mixing ratios deviated from expectations based on calculated production rates and atmospheric lifetimes.

Methyl nitrate has the longest lifetime and a moderate production rate (in comparison to the other measured alkyl nitrates). Therefore the mixing ratios were expected to be closer to the other alkyl nitrates. But it was the nitrate species with the lowest observed mixing ratio. Also the mixing ratios of *i*-propyl and *i*-butyl nitrate are lower than the mixing ratios of their isomers though they are the favored reaction products and were observed to be the dominating isomers in other studies. Though the production rate of ethyl nitrate was the lowest, it was the most abundant alkyl nitrate. Sinks apart from the reaction with OH and photolysis are excluded. A possible explanation of these results is an additional source for the ethyl, *n*-butyl and *n*-propyl nitrate next to photochemical production. Alkyl nitrates also were found to be photochemically produced in surface seawater and emitted from the Pacific Ocean (Chuck et al. 2002; Blake et al. 2003; Neu et al. 2008). The Mediterranean Sea as a conceivable source of alkyl nitrates could have influence on the alkyl nitrate ratios observed during CYPHEX which were contradictory to expectations based on photochemical production and depletion.

Table 3-4: OH reaction rate coefficients (Talukdar et al. 1997) and Photodissociation rate coefficients for alkyl nitrates (Warneck and Williams 2012[a)]; Clemitshaw et al. 1997[b)])

	Methyl	Ethyl	*i*-Propyl	*n*-Propyl	*i*-Butyl	*n*-Butyl
OH reaction rate coefficients [cm^3 $molecules^{-1}$ s^{-1}]	2.3×10^{-14}	1.8×10^{-13}	2.9×10^{-13}	5.8×10^{-13}	8.6×10^{-13}	1.6×10^{-12}
Photodissociation rate coefficients [s^{-1}] [a)]	1.3×10^{-6}	1.8×10^{-6}	3.4×10^{-6}	-	-	-
[b)]	-	1.415×10^{-6}	2.21×10^{-6}	1.56×10^{-6}	1.63×10^{-6}	1.82×10^{-6}

[a)] Calculated with overhead sun with a surface albedo of 0.03, from the summary of Jacobson (2005).

[b)] Calculated for summertime and surface at 40°N.

3.2.1 Diel cycles

The diel cycles of the NMHCs are shown in Figure 3-8 as box and whisker plots. The boxes represent 50% of the data points. 25 % of the data points lie below the lower border of the box and 75% below the upper end. The whiskers indicate the limit of 10% and 90% of the data. In these plots all data is summarized with no regard to air mass origin. For the longer lived compounds ethane, propane and benzene which have an atmospheric lifetime between 4 and 20 days no clear diel cycle could be observed. The lifetimes refer to average concentration of 2.47×10^6 OH molecules cm^{-3} (Spivakovsky et al. 2000), and were calculated as shown in chapter 1. Also the variability throughout the day is equally distributed. The more reactive compounds, which have lifetimes of less than three days (butanes, pentanes toluene, and alkenes), showed a slight diel cycle becoming more pronounced with decreasing lifetimes and showing a maximum between 07:00 and 08:00 UTC which corresponded to 10:00 and 11:00 local time. This maximum was also characterized by a higher variability. In the afternoon the average concentration of the shorter lived compounds reached their minimum, likely caused by higher OH radical concentrations and therefore enhanced depletion of NMHCs as well as enhanced turbulent mixing with the less polluted free troposphere. Due to lower reaction rate coefficients the longer lived NMHCs did not show this minimum. Either the longer lived species are not removed as fast in the boundary layer, or the older air in the free troposphere contains proportionally more of the longer lived species. Either way this temporal trend is related to the lifetime of the species. This behavior was in agreement with other studies in the Eastern Mediterranean where the diel cycles were domi-

nated by OH chemistry (Liakakou et al. 2009; Arsene et al. 2007). Those measurements were done at *Finokalia* station, on Crete, at a hill top 150 m above sea level.

The morning maximum in the shorter lived NMHC data which was observed during CYPHEX was not observed in the previous Finokalia studies. The increase in mixing ratios in the late morning resulted from boundary layer dynamics particular to the ele-

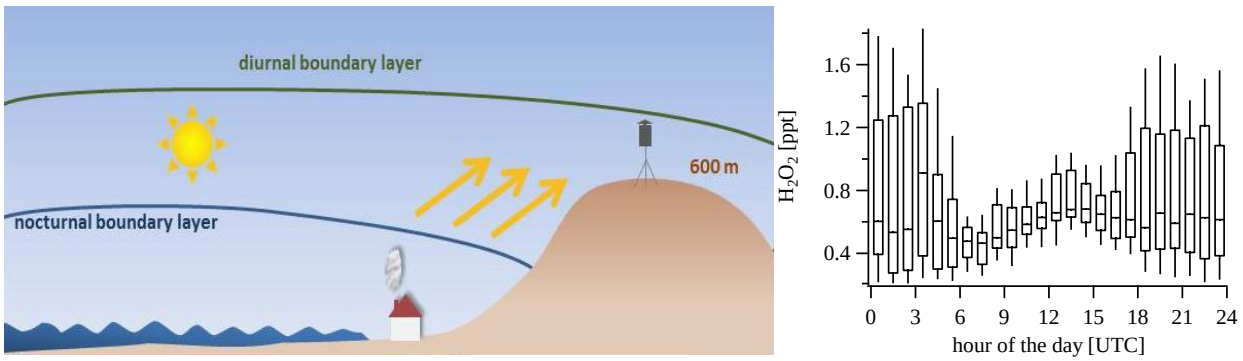

Figure 3-7: Left: Sketch of boundary layer evolution after sunrise. Right: Diel cycle of H_2O_2

vated measurement site which was at 600 m height above sea level. As illustrated in Figure 3-7 the stable nocturnal boundary layer was low and the measurement site was within the free troposphere. Through heating after sunrise the boundary layer expanded via turbulent mixing and reached the measurement site bringing air masses more recently influenced by fresh emissions either anthropogenic or biogenic to the site. When the measurement site was within the convective internal boundary layer the diel cycles are dominated by OH chemistry. This interpretation is supported by the diel cycle of hydrogen peroxide, a molecule that is highly sensitive to surface contact. This showed a decrease parallel to hydrocarbon increase. Also this period was usually accompanied with a slight change in wind direction between day and night. Since the diel cycles were weak compared to other species, such as biogenic VOC (Derstroff et al. 2016), the focus of NMHC analysis will be on the different transport patterns and the comparison of westerly and easterly flow regimes.

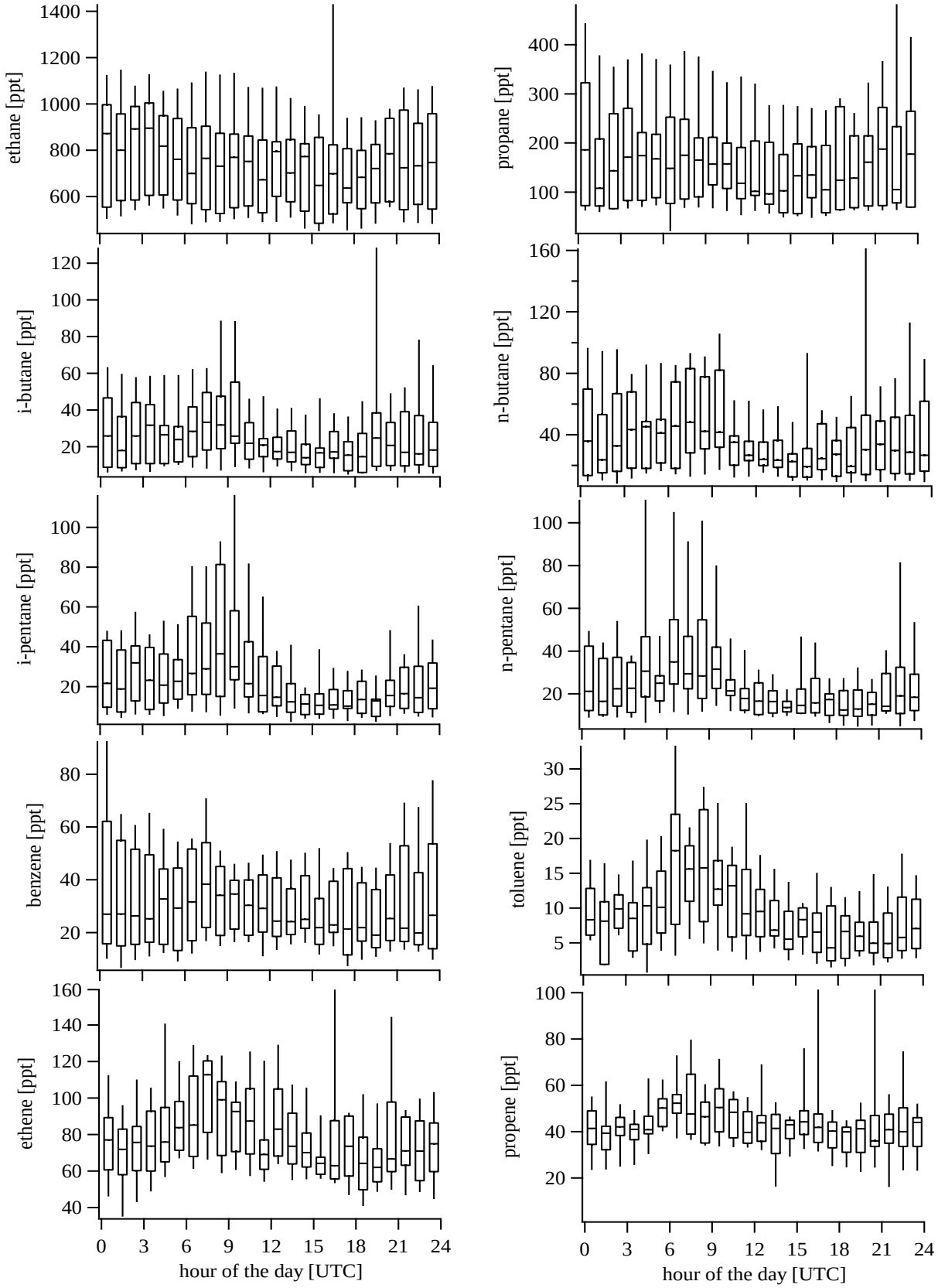

Figure 3-8: Diel cycles of NMHCs (UTC = local time -3 h)

3.2.2 Air mass origin and compositional characteristics

As mentioned previously, the site was influenced alternately by air masses coming from Eastern Europe and Western Europe. In Figure 3-9 the different regimes and sectors are shown as box and whiskers plots. Generally the air masses coming from Eastern Europe showed higher average mixing ratios (higher median values are represented as vertical lines within the boxes) in NMHCs and more variability (longer boxes and whiskers) during the measurement period. This higher variability was caused by stronger and more recent influence of Eastern European sources. The average mixing ratios of the westerly air masses were ~50% or less of the average mixing ratios coming from Eastern Europe. This difference became larger with increasing lifetime of the NMHCs. The unsaturated compounds ethene and especially propene did not show this intensive contrast between east and west. Several reasons can be conceived for this behavior of alkenes deviating from saturated alkanes and aromatics. Hence ethene and propene will be discussed individually.

The depletion of NMHCs by oxidants such as OH radicals has a strong influence on the absolute concentrations as described above and illustrated in Figure 3-9. In addition, the rates of reaction of the NMHCs with OH are markedly different. The atmospheric lifetimes of propane at Cyprus' latitude in presence of 2.47×10^{6} OH molecules cm^{-3} (Spivakovsky et al. 2000) is about 4 days. Under the same conditions CO has a lifetime of 20 days ($k_{OH}=1.54\times10^{-13}$ cm^3 $molecules^{-1}$ s^{-1}) (Atkinson et al. 1976). In the following paragraph we will focus on hydrocarbon ratios with carbon monoxide. This is a good method to have a more detailed look at air mass age as well as origin and sources of trace gases in the atmosphere.

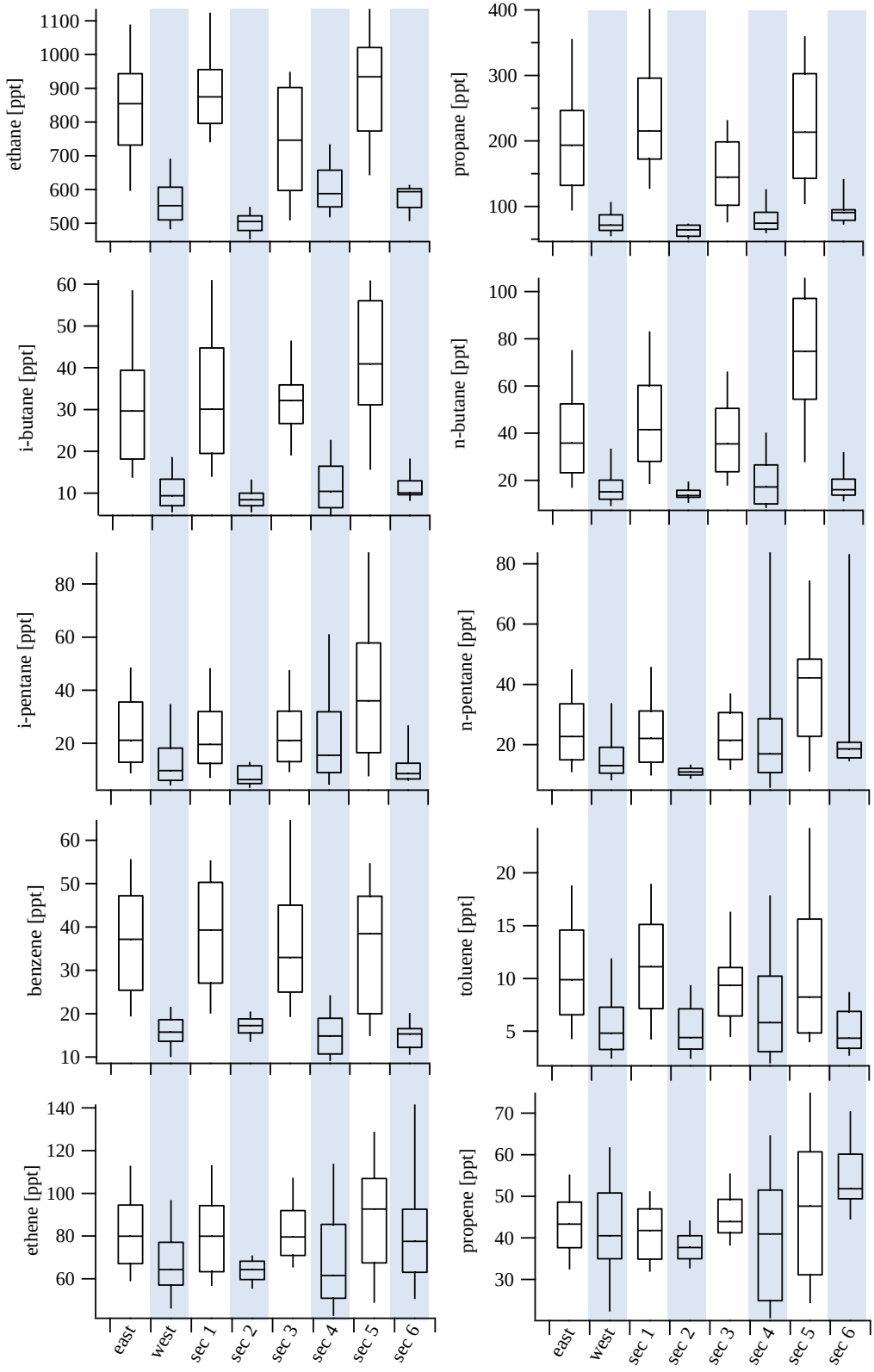

Figure 3-9: Box and whisker plots of individual NMHCs divided into east, west and the single sectors. Vertical lines within the boxes represent mean values, 25% of the data lies above the lower limit of the box, 75% below the upper limit, whiskers represent 10% and 90% of the data points

Hydrocarbon ratios

Focusing on ratios of hydrocarbons the effect of individually decreasing mixing ratios with more dilution is reduced to some extent. This is because mixing is expected to act equally on all compounds and therefore have less influence on the ratio than the absolute concentrations (Baker et al. 2011).

The ratios used here were deduced by geometric means rather than from linear regression of data from scatter plots of NMHCs vs. carbon monoxide, which have common sources dominated by anthropogenic influence (Parrish et al. 2009; von Schneidemesser et al. 2010). This method was chosen because the correlation of these plots was rather poor (R^2=0.30-0.55). It was best for benzene due to common combustion sources for both compounds. Also the correlation of ethane with CO was better than for the other hydrocarbons. The poor correlations can be explained by the high differences in lifetimes of CO and the hydrocarbons, combined with the effective photochemical aging during transport. The units of the ratios are given in ppt/ppb. The hydrocarbon ratio comparison between Eastern and Western Europe is listed in Table 3-5. Furthermore the table contains ratios from urban sites in London, Paris and Berlin and from the remote site Hohenpeissenberg (von Schneidemesser, Monks, and Plass-Duelmer 2010; Borbon et al. 2013; Bonn et al. 2016).

In the following discussion hydrocarbon ratios (emission ratios) at time t = 0, meaning at the source without chemical processing will be called HR_0. In contrast, the measured or calculated ratios at time t will be labelled HR_t. All ratios were calculated using the longer lived CO as denominator and with shorter lived species as numerator. There are three factors which have an influence on HR_t. The first factor to be discussed is the photochemical age and oxidative processing time since emission. As mentioned above, HR_t will then be smaller for air masses with higher photochemical age because the more reactive species will be depleted faster than CO.

Throughout all hydrocarbon/CO combinations HR_t from Eastern Europe were higher than those from Western Europe. This is consistent with HYSPLIT and Flexpart calculations which showed travel times of 12-48 hours for air masses coming from Eastern Europe and up to 120 hours for westerly air masses. These differences were more or less pronounced for different NMHC/CO pairings. One reason is the different rate of reactions with OH. For shorter lived species such as the butanes the differences in HR_t were more obvious, because longer transport times lead to higher extents of depletion. In contrast the difference for the longer lived ethane was not that strong. Despite their short lifetimes the pentanes showed comparable HR_t between the easterly and westerly source regions. A possible reason could be that by using the geometric means to determine HR_t the impact of local source influenced spikes in the pentane data is higher

(Figure 3-5). Another exception was benzene. Although this compound is one of the longer lived ones, the difference between East and West was more pronounced.

This leads to the second factor influencing HR_t. NMHCs are emitted to the atmosphere by different, mainly anthropogenic, processes. Examples are various types of combustion such as biomass or fossil fuel burning (Andreae and Merlet 2001; Akagi et al. 2011). Also evaporative processes from gas leakage or gas stations and the use of LPG (liquefied petroleum gases) are sources for NMHCs (Blake and Rowland 1995). In areas with higher population and various industry sectors a differentiation of those diverse source type dependent emission ratios is difficult because of the mixing of air masses. One approach to obtain HR_0 is to use literature data from ground based measurements directly from the source regions. This is a useful tool when the area of source region is limited and quite homogeneous in land use and the transport pathways are quite short and direct. In Table 3-5 the ratios of NMHCs to CO from a kerbside in London from 1998-2008, from a site in Paris, known for well mixed urban air, in summer 2009 and from a site in Berlin considered as urban background from the BAERLIN2014 campaign are listed. Additional values from the remote site Hohenpeissenberg are also displayed. Ratios from London, Paris and Berlin can be considered as HR_0 without any influence of chemical processing and mixing with background air. To allow a comparison with HR_0 from these sites with HR_t measured on Cyprus an age correction to adjust for oxidation during transport time has to be applied.

Scheeren et al. (2003), de Gouw et al. (2001) and Baker et al. (2011) showed that with estimated travel times such an age correction can be made based on the following equation. HR_t being the ratio of two species $\frac{A_t}{B_t}$, k_A and k_B as their reaction rate coefficients for the reaction with OH radicals, $\{[OH]\}$ as average concentration during the travel time Δt between the source and the measurement site (2.47×10^6 molecules cm^{-3}). By applying this equation HR_0 can be estimated and compared to different source types and areas of origin. Δt can be estimated by backwards trajectory analysis.

$$HR_t = HR_0 e^{-(k_B - k_A)\{[OH]\}\Delta t} \quad [23]$$

$$\frac{A_t}{B_t} = \frac{A_0}{B_0} e^{-(k_B - k_A)\{[OH]\}\Delta t} \quad [24]$$

HYSPLIT calculation showed that the average transport times for air masses coming from Eastern Europe were around 24 hours; westerly air masses needed around 48-120 hours to reach the measurement site. Transport times refer only to the time the air parcels spent over the Mediterranean Sea implying that no fresh anthropogenic emissions were introduced. In Table 3-5 the HR_t are corrected for these time intervals.

Table 3-5: Hydrocarbon ratios during CYPHEX with and without age correction in comparison to urban and rural values from Europe. Ratios are given in ppt/ppb

Season (year) location area	Summer (2014) Inia, Cyprus marine					Hohenpeissenberg remote	London urban	Paris urban	Berlin urban background
Ref.	this work					(von Schneidemesser, Monks, and Plass-Duelmer 2010)		(Borbon et al. 2013)	(Bonn et al. 2016)
HR (X/CO)	Eastern EU	Age corr. (24 h)	Western EU	Age corr. (48 h)	Age corr. (120 h)				
Ethane	7.59	7.59	6.07	6.06	6.06	1.30	7.1	23.4	8.39
Propane	1.85	2.22	0.83	1.20	2.08	0.44	2.7	9.02	4.01
i-Butane	0.29	0.43	0.12	0.27	0.87	0.1	1.2	10.1	2.51
n-Butane	0.42	0.66	0.20	0.49	1.90	0.16	2.0	4.53	8.10
i-Pentane	0.24	0.47	0.17	0.65	4.95	0.12	1.6	10.8	2.31
n-Pentane	0.24	0.50	0.22	0.96	8.82	0.071	0.52	3.08	1.20
Benzene	1.25	1.53	0.20	0.30	0.56	0.092	0.32	1.07	11.3
Toluene	0.10	0.31	0.07	0.69	21.31	0.088	1.0	12.3	2.02

In case of the CYPHEX campaign a comparison with HR_0 from different European cities is quite difficult and can only be done on a qualitative and approximate basis because the source regions of the air masses reaching the measurement site were spread over several countries and were diverse in distinct sources.

The age corrected ethane/CO ratio was in the range, though slightly lower than the HR_0 from London and Berlin. Paris HR_0 was about three times higher. Also this particular ratio is quite independent from transport time and photochemical processing because ethane and CO have almost the same lifetimes. This means that ethane emissions relative to CO from Western Europe were lower than from Eastern Europe. This was the same for propane. The age corrected ratios showed comparable but slightly higher values for Eastern Europe after one day transport time in comparison to Western Europe after 5 days. HR_0 from London was slightly higher, but Berlin and Paris were higher by factors of 2-5. The age corrected HR for the butanes from Eastern Europe laid between the 2 and 5 days corrected values for Western Europe. Keeping up with 5 days of transport from there means that the HR_0 from Western Europe had to be higher due to enhanced emission of butanes. For the pentanes the corrected HR differed a lot. This can again be explained by the short duration concentration spikes towards the end of the campaign having a big impact on the geometric mean. The corrected values showed a much higher ratio from Eastern Europe even higher than HR_0 from London and Paris, but lower than Berlin. The westerly air masses are comparable with HR_0 from London. The corrected HR from Eastern Europe for toluene is lower than the HR_0 from the urban areas. The 5 days corrected HR for Western Europe with a value about 21 was much higher than all other ratios. This shows that the age correction has to be used with caution. Toluene is one of the compounds with the shortest lifetime and therefore the results are quite sensitive to kinetic calculations like age correction.

The ratios from Cyprus can also be compared to emission inventory model results. The disadvantage of this approach is that usually such models do not distinguish between individual hydrocarbons and consolidate them as non-methane volatile organic compounds (NMVOC) and they are also found to underestimate the emissions (Karl et al. 2008; Lei et al. 2007; Warneke et al. 2007).

In Figure 3-10 the results from the MACCity emission inventory for the month July 2014 are shown for Europe (Granier et al. 2011; Lamarque et al. 2010; van der Werf et al. 2006). In the upper part the Figures a-c show the total anthropogenic emissions of CO, ethane and propane including the emission sectors transportation, energy, solvents waste, industry, residential, ships, agriculture and agricultural waste. The unit is $kg/m^2/s$ and the scale is logarithmic. It must not be mistaken with mixing ratios in ppt. Nevertheless, it can be seen that the emission of CO from Western Europe, in particular

France and Germany was higher than for Eastern Europe. For ethane and especially propane it's the opposite. The emissions of those NMHCs were higher in Eastern Europe. Ethane is elevated in Serbia and Poland. Propane emissions were also stronger in this region compared to Western Europe.

In the lower part of this figure the HR_0 values were calculated by normalizing the emissions to the molecular weight. This is only a rough point of reference. The color code has a cut off at HR=25 which was considered as a high but still realistic HR_0. Values above 25 are represented in a redish brown. The cut off has been applied because calculated HR from model results went up to 2.6×10^7 for ethane and 5.0×10^7 for propane. And even with a color coding even on a logarithmic scale a distinction of HR_0 from the different regions would not be possible. Western Europe showed extraordinarily low HR_0 in the range of 0-3 for both hydrocarbon/CO combinations. Ethane/CO is again elevated in Serbia. Propane/CO is increased over the Balkans and Turkey. One possible reason for this could be that Turkey, Poland and Italy are among the world's leading countries in LPG use (DVFG e.V.; Annual Report 2014). Consequently higher HR for propane and *n*-butane could be expected for the times when the easterly flows were dominant. This was not observed during CYPHEX. Quite the contrary, the data showed enhanced *n*-butane/CO ratio from Western Europe.

We do not consider the values displayed in Figure 3-10 d and Figure 3-10 e as realistic; especially the very low HR_0 for Western Europe which lie even lower than the results from the remote station Hohenpeissenberg. Also HR_0 for propane were higher than ethane. This contradicts general understanding of the meaning of HR.

Nonetheless, the trend for higher HR_0 from Eastern Europe for both components was in agreement with our findings during CYPHEX. It is to be expected that enhanced emissions in ethane and propane go along with enhanced emissions of other hydrocarbons. This was found for benzene. Its HR_0 from East is by a factor of 3 higher than HR_0 from West. The other hydrocarbons do not show this behavior. But due to their short lifetime they are much more sensitive to age correction. Small amounts of fresh pollutant injection would have an impact on the age corrected HR_0 and give higher values.

The comparison between the two different areas of origin showed that the air masses coming from Western Europe were generally characterized by lower mixing ratios and lower HR_t indicating a higher influence of photochemical processing during transport times which were overall longer than for air masses approaching the measurement site from source areas in Eastern Europe. Air masses from there were enriched in hydrocarbon and showed higher HR_t. A quantitative discussion is very difficult because hydrocarbon ratios are dependent on 3 factors all having influence. The first is the chemical processing during transport. Chemical processing is dependent on oxidant availability

and processing time. In theory, ratios can be corrected for this transport time but this is prone to errors because transport times, oxidant type and concentration can only be estimated. Also shorter lived NMHCs are more sensitive to kinetic calculation and small variations would lead to very different results. Age correction provides calculated HR_0, which leads to the second factor having influence on quantitative discussions. Those HR_0 are different for various sources such as biomass/fossil fuel burning or use of LPG and hard to compare quantitatively to source regions which are very diverse in land use and population as it is for areas spanning several countries like in this study. Overall, neglecting the discussed exceptions pentanes and toluene, the age corrected HRs for Eastern as well as for Western Europe were lower than the urban HR_0. The third factor which influences hydrocarbon/CO ratios is mixing and dilution of air masses. The HR_0 were measured directly within the cities where fossil fuel use and anthropogenic emissions in general are higher compared to rural areas. On one hand the source regions upwind of Cyprus vary in the source composition. Mixing with air masses from less populated areas where anthropogenic emissions are less would show other HRs. Another point is mixing with background air which cannot be neglected. Flexpart calculations showed that the proportion of air from the free troposphere measured on Cyprus can be up to 90%. Background air is highly photochemically aged air. After a few days of processing without any introduction of fresh pollutants, most of the NMHCs, except ethane, would be depleted to background mixing ratios. Mixing of boundary layer air masses with background air would therefore result in lower HRs than expected without mixing. This was also observed in the CYPHEX data set. In order to explore this further, a theoretical “time in the marine boundary layer” has been calculated using the FLEXPART results and a comparison of NMHC data and model results were made according to their photochemical depletion during transport time.

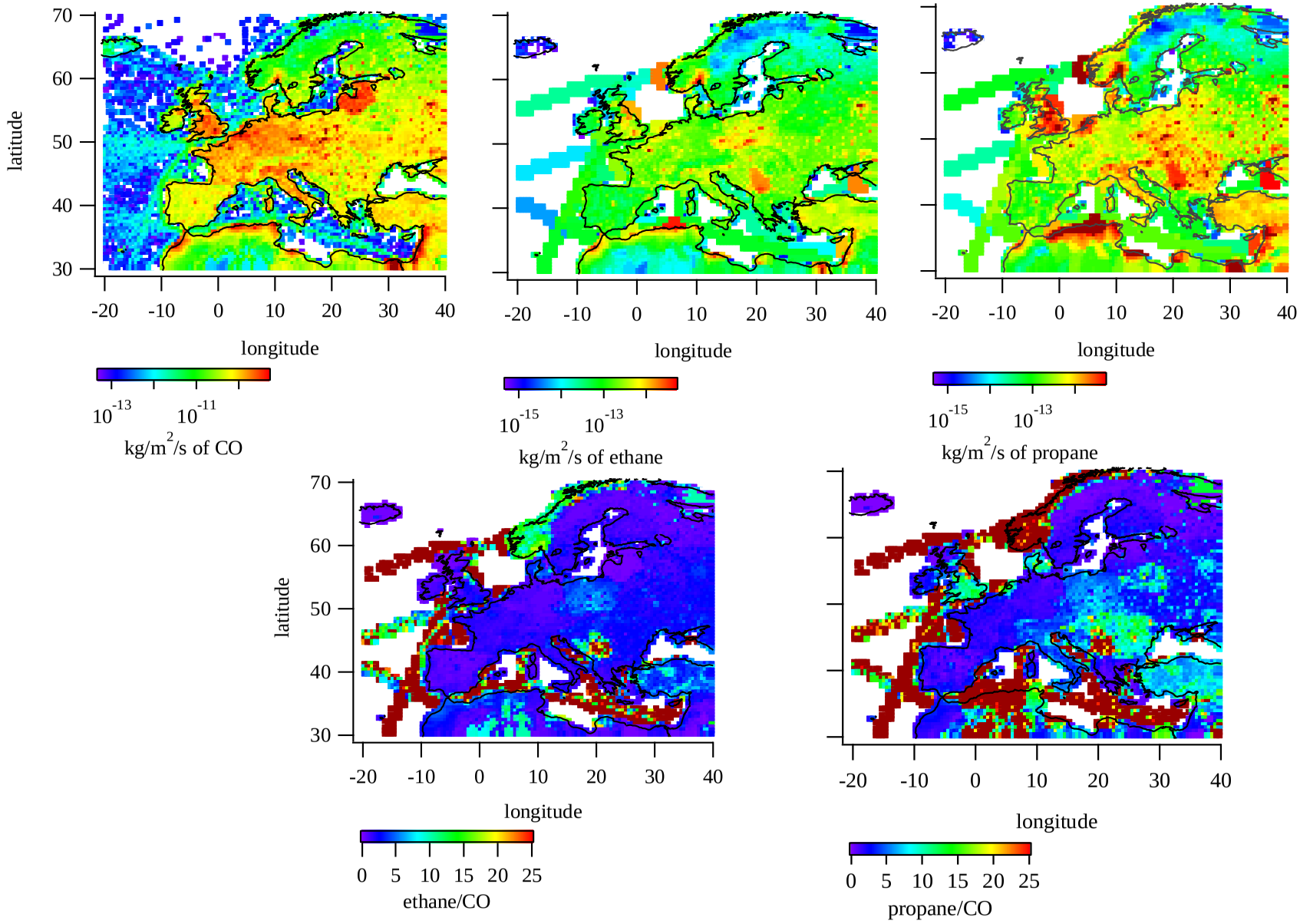

Figure 3-10: Emission of CO, ethane and propane and hydrocarbon ratios from MACCity emission inventory for the July 2014

NMHC depletion rates

The reaction with ozone is one characteristic which differs for alkene from the other NMHCs. From the FLEXPART data set a theoretical "time in the marine boundary layer (MBL)" was calculated. Depletion rates were determined for the individual NMHCs from the linear regressions from the scatterplots of species vs. time in the MBL. They are listed in Table 3-6. The depletion of NMHC via OH radical oxidation is a pseudo-first order reaction. Therefore the decrease over time follows an exponential function with a higher loss rate in the beginning becoming less with the passing of time.

All NMHCs show a higher depletion rate in air masses from Eastern Europe due presence of precursors and oxidants. In comparison the westerly air masses show progressed photochemical aging and the depletion rates are accordingly lower.

Table 3-6: Depletion rates of NMHCs in dependence of transport time over sea

Compound	Depletion rate [ppt/h]	
	east	west
Ethane	20.5 ± 2.9	5.8 ± 1.5
Propane	7.2 ± 1.9	0.8 ± 0.6
i-Butane	1.05 ± 0.4	0.07 ± 0.1
n-Butane	1.4 ± 0.5	0.18 ± 0.23
i-Pentane	0.64 ± 0.4	1.1 ± 0.4
n-Pentane	0.64 ± 0.4	0.35 ± 0.3
Benzene	0.85 ± 0.4	0.12 ± 0.1
Toluene	0.18 ± 0.1	0.16 ± 0.1
Ethene	0.09 ± 0.5	0.02 ± 0.5
Propene	0.08 ± 0.2	0.06 ± 0.3

3.2.3 NMHC and ozone interactions

NMHCs, in the presence of NO_x (NO + NO_2), are precursors for tropospheric ozone production (chapter 1.1.1). As mentioned, the Cyprus ozone levels often exceed the European Union air quality standard of 60 ppb. In Figure 3-11 the ozone mixing ratios are plotted versus the ratio of propane/ethane (Parrish et al. 2004; Thorenz et al. 2017). This ratio is a proxy for air mass age. With progressing air mass aging this ratio decreases. It can be seen from this diagram that the mixing ratios of ozone decreased with age. This means that at the measurement site, independent from source region, the chemical regime was ozone depleting.

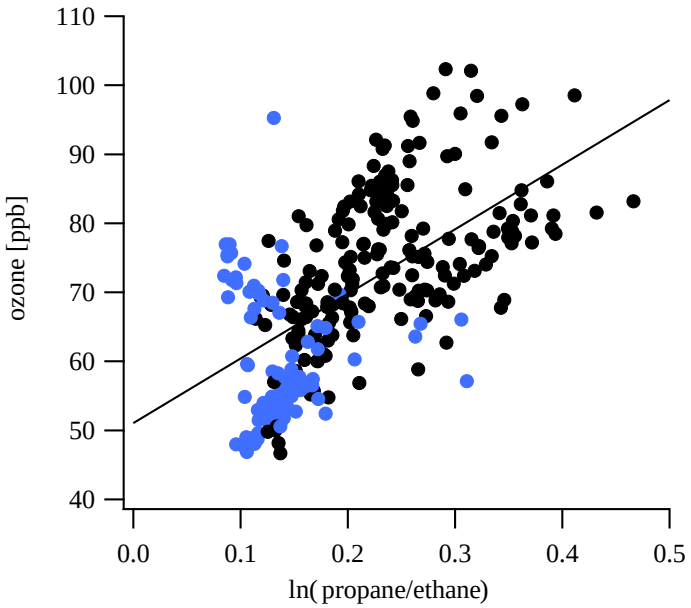

Figure 3-11: Ozone vs. ln (propane/ethane). a=51 b =93; R^2=0.35

This implies that during the CYPHEX campaign the elevated ozone levels were induced by transport from the European continent rather than local sources. Air masses reaching the site were of advanced photochemical age and conclusively with the lack of additional key precursors such as NO_x leading to no additional ozone production.

As mentioned previously, the alkenes ethene and propene showed different characteristics to the other NMHCs. Their timelines were not as variable throughout the campaign (Figure 3-5). This can also be observed in the box and whisker plots from Figure 3-9 which shows the comparison between easterly and westerly air masses on a statistical basis. In contrast to the saturated or aromatic NMHCs which clearly showed decreased mixing ratios from Western Europe and a lower variability indicated by shorter boxes and whiskers, the unsaturated alkenes did not show this explicit contrast in mean mixing

ratios between East and West and also the variability amongst the six different sectors was comparable. The relative standard deviations of the average mixing ratios of 0.2-0.3 for the short lived species ethene and propene were comparable with ethane which has a lifetime more than 30 times longer. The other shorter lived compounds showed much higher relative standard deviations for easterly and westerly sectors (> 0.4). As mentioned in the introduction the spatial and temporal variability of a species is dependent on its atmospheric lifetime and the distribution of sources and sinks and their vicinity to the measurement point. For ethene and propene the characteristics, which are responsible for their behavior, deviate from the other NMHCs.

In contrast to saturated species, unsaturated compounds with a double bond can undergo ozonolysis reactions. This means that while alkenes are depleted via OH oxidation they build up ozone. If they are depleted by ozonolysis they fate while ozone also reacts away. This has as consequence that for alkenes there is a competition between ozone production and ozone depletion (Atkinson and Carter 1984).

In Figure 3-12 the correlation plots of *i*-/*n*-pentane, ethene and propene vs. ozone are displayed. The pentanes were chosen as compounds for comparison, because they are, as ethene and propene, among the shorter lived species which have been measured. The pentanes were positively correlated with ozone with slopes between 0.17 and 0.56.

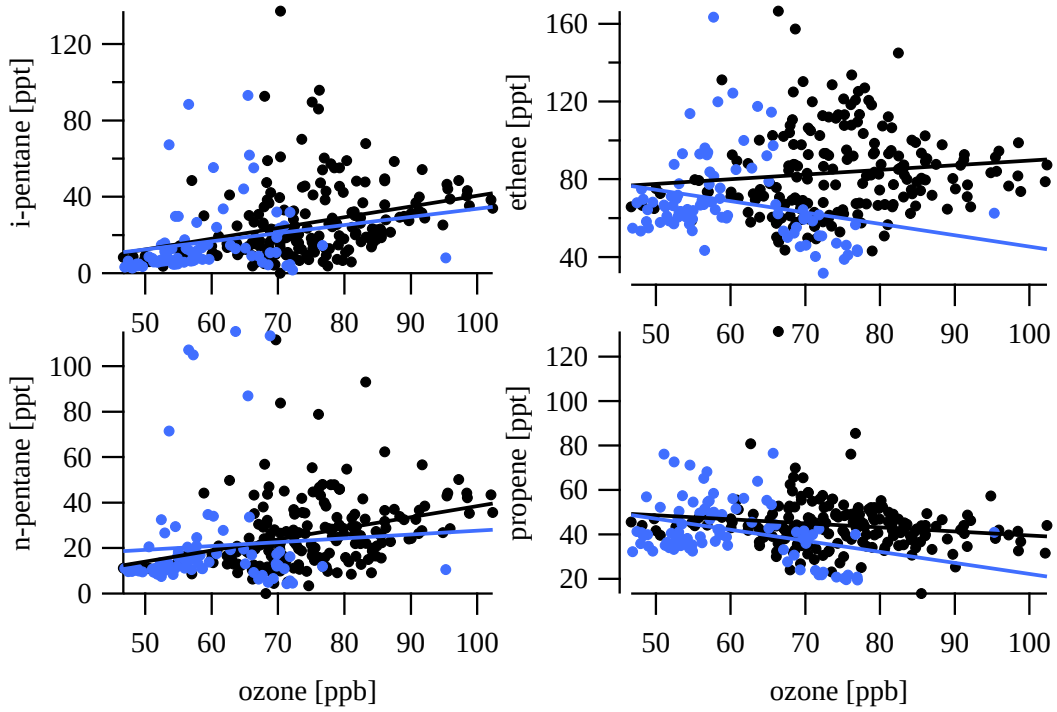

Figure 3-12: Pentanes, ethene, propene vs. ozone

Table 3-7: Fitting parameters of correlation plots of shorter lived NMHCs with ozone

	east		west	
NMHC/ozone	b	R^2	b	R^2
i-Pentane	0.56	0.001	0.43	0.04
n-Pentane	0.49	0.11	0.17	0.003
Ethene	0.24	0.014	-0.59	0.064
Propene	0.18	0.029	-0.50	0.13

It is a sign for generally more polluted air masses in which higher concentration of NMHCs go hand in hand with elevated ozone levels. Other than the positive correlation of the saturated pentanes, ethene and propene showed a different behavior. While ethene from Eastern Europe still showed a positive correlation with ozone, although reduced in comparison to the pentanes, ethene from Western Europe and propene from both source regions were negatively correlated with ozone showing that they were depleted by ozonolysis rather than ozone is formed by their oxidation with OH and NO_x.

3.2.4 Logarithmic ratios

Figure 3-13 shows ln (*i*-butane/ethane) vs. ln (*n*-butane/ethane) for the individual easterly and westerly sectors. Also the calculated slopes for single radical chemistry are displayed in each plot. Table 3-8 summarizes the experimental slopes b and the axis intercepts a calculated with linear least square fit. Also correlation coefficient R^2 and the number of data points are given in this table. The theoretical courses of the lines are based on simple model calculations using average mixing ratios of NMHCs from a one week measurement campaign at MPIC in Mainz, Germany, from 7.4. to 11.4.2014. The institute is close to a main traffic road and mixing ratios are considered to represent typical values for northern hemispheric urban environment. The average values were 2400 ppt for ethane, 425 ppt for n-butane and 210 ppt for *i*-butane.

OH reaction based calculations give a slope of 0.88 and an axis intercept of -0.91 (blue line); for Cl b is 0.57 and a is -1.5 (green line) and for NO_3 b was calculated with 2.77 and a with 2.3 (black line) (see Figure 3-14). The red lines are the linear regression fit lines from the measured data during CYPHEX.

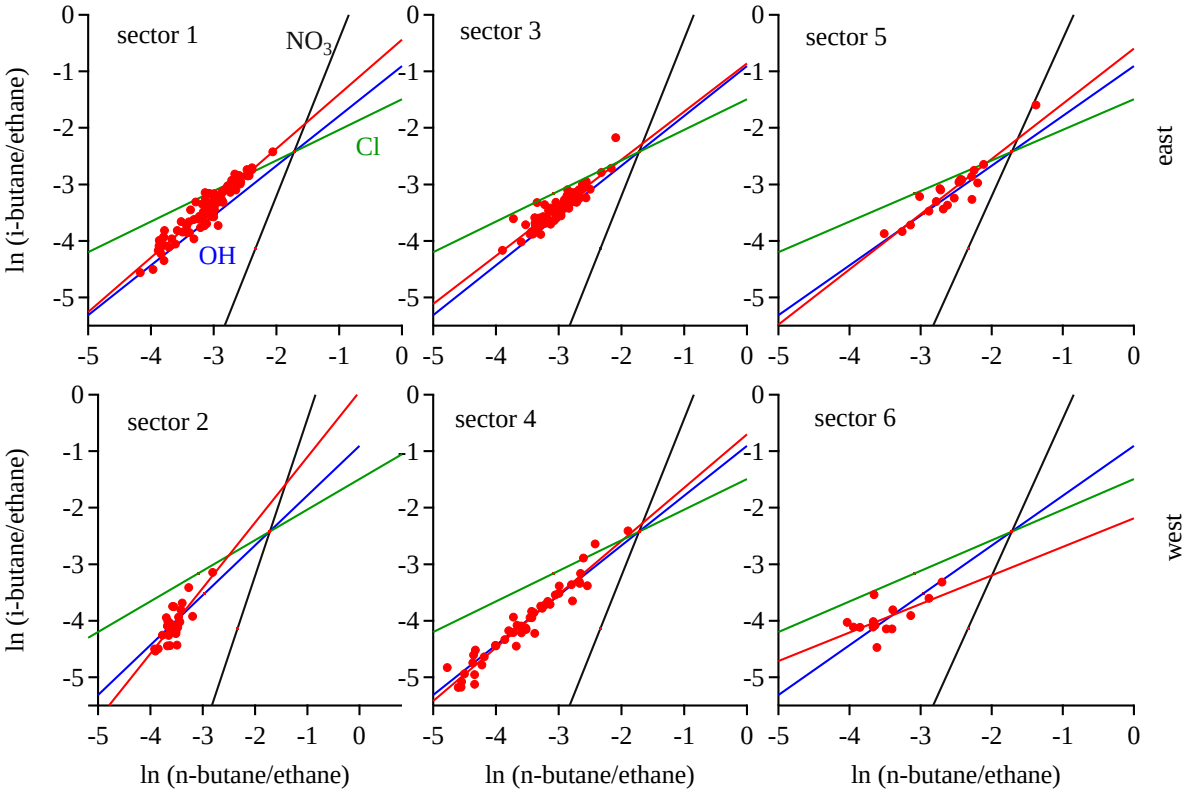

Figure 3-13: Plots of natural logarithms of the ratios of *i*-butane to ethane against *n*-butane/ethane

Table 3-8: Parameters from linear regression of logarithmic ratio plots

Sector	b	a	n	R^2
		East		
Sector 1	0.96 ± 0.031	-0.44 ± 0.10	100	0.91
Sector 3	0.85 ± 0.05	-0.86 ± 0.14	71	0.82
Sector 5	0.98 ± 0.09	-0.60 ± 0.25	21	0.85
		West		
Sector 2	1.16 ± 0.17	0.06 ± 0.59	31	0.63
Sector 4	0.94 ± 0.04	-0.70 ± 0.13	47	0.94
Sector 6	0.50 ± 0.17	-2.19 ± 0.61	14	0.41

Sectors 1, 2, 4 and 5 show a deviation from the OH reaction line towards the NO_3 reaction line. Also the axis intercept tends towards more positive values for these time frames. The data for sector 3 describes the OH line both with b and with a very well. The most obvious deviation of the data from the calculated courses occurred in sector 6. The slope as well as the axis intercept was below the line for chlorine chemistry. This section is the shortest time frame during the measurement campaign represented only by 14 data points. Also the correlation coefficient R^2 was only 0.41. Nevertheless, this strong deviation from the other sectors can be explained by influence of Cl radicals. Since the experimentally derived slope was below the theoretical one, no quantitative conclusion on Cl radical concentration can be drawn from this plot. This sector was also the one with the highest influence of marine planetary boundary layer. The potential influence of chlorine chemistry can also be backed up by lifetime-variability-analysis and will be discussed in section 3.2.5. Possible sources for chlorine radicals can be the photolysis of HCl or NO_2Cl.

Also sector 2 showed a higher deviation in combination with a lower correlation factor.

NO_3 is only measurable during night time because it is depleted by photolysis after sunrise to mainly NO_2 [IXa] and to a lesser extent to NO [IXb] (Vrekoussis et al. 2004).

$$NO_3 + hv \rightarrow NO_2 + O(^3P) \qquad [IXa]$$

$$NO_3 + hv \rightarrow NO + O_2 \qquad [IXb]$$

OH radicals are produced photochemically during the day. A direct comparison between daytime and nighttime, neglecting the sectors, showed that during the night when NO_3 is active the slope is steep with 1.02. But also during daytime when no NO_3 is present and oxidation is dominated by OH the slope with 0.97 was still higher than the calculated slope. But as shown in equation [1] ($\tau = \frac{1}{\sum k[X]}$) the radical concentration [X] is the temporal and spatial average during transport from the source to the measurement location. So with longer transport times differences in nocturnal and diel radical compositions are balanced.

Simple calculations based on this equation were done with the NMHC mixing ratios from the measurement campaign in Mainz as $[RH]_0$ and variable radical composition. During the CYPHEX campaign there were two nights of NO_3 measurement with an average of 7.6×10^7 molecules cm^{-3} and a maximum of 3.9×10^8 molecules cm^{-3}. During the MINOS campaign in summer 2001 at Finokalia station on Crete NO_3 concentrations of 1.1×10^8 molecules cm^{-3} on average with maximum values of 9×10^8 molecules cm^{-3} were observed (Vrekoussis et al. 2004). The MINOS results were used for the calculations in combination with an average OH concentration of 2.47×10^6 molecules cm^{-3} (Spivakovsky et al. 2000). Even with those values which were higher than those ob-

served during CYPHEX, the slopes will not exceed 0.89. The average NO_3 concentrations had to be between 4.87×10^9 molecules cm^{-3} and 2.49×10^{10} molecules cm^{-3} to reach the slopes observed in sector 1, 2, 4 and 5. For Western Europe high average NO_3 concentrations of 4.35×10^{10} molecules cm^{-3} were found also by using the indirect approach of logarithmic NMHC ratios (Penkett et al. 2007).

For sector 3 we obtained a slope of 0.85. This can be explained by the influence of Cl radicals. Already a concentration of 1.5×10^3 molecules cm^{-3} would result in this lower slope, still with NO_3 concentrations at MINOS average conditions.

Mixing with extensively oxidized air from the free troposphere has influence and cannot be excluded from discussion since Flexpart calculations showed that the majority of the air masses measured comprised of air from the free troposphere. If aging was advanced, then only the longer lived compounds would have influence on the slope of the plot of logarithmic ratios. As consequence the slope would follow a 1:1 line. No clear trend could be observed dependent on fraction of air from the free troposphere and the experimentally derived slopes. For example comparison of sectors 2 and 6 show that they have comparable content of free tropospheric air but show the highest and lowest slopes from ln (*i*-butane/ethane) vs. ln (*n*-butane/ethane) plots.

3.2.5 Lifetime-variability relationship

A detailed introduction into the relationship between atmospheric lifetime of an individual compound and its temporal variability at a certain measurement point was given in chapter 1.3. The variability described by the standard deviation of the logarithm of the measured mixing ratio of the hydrocarbon X is linked to the calculated lifetime via equation [21] from chapter 1.3 ($\sigma(\ln X) = A \cdot \tau^{-b}$). The lifetime τ was calculated by assuming a temporal and spatial average radical composition which was driving oxidation during transport from the hydrocarbon source to the measurement point. A and b describe independent variables. The exponent b describes the relative locations of source and measurement point to one another. Typical values for measurement points in the close vicinity to the source are $b \approx 0$, meaning there is no coherence between standard deviation of the natural logarithms of the measurement values and the lifetime. For remote or rural measurement sites b often is found to be around 0.5. For arctic measurements, where the only variability causing factors are the chemical processes, the exponent b approaches values of 1.

The interpretation of b is also the description of the relationship between sources and sinks. Is b approaching 0 then the air masses were strongly influenced by the source. If b is converging 1, sink processes are dominating the behavior of the measurement results.

The factor A can be interpreted as the standard deviation of the transport times of individual air masses. If the data contains some fresh and some old pollution, then A will be high. If the age spectrum of the air masses is more comparable then A will be lower.

In Figure 3-14 the lifetime-variability plots are shown for different sectors. An OH concentration of 2.47×10^6 molecules cm^{-3} was used to calculate τ. The black plot on the

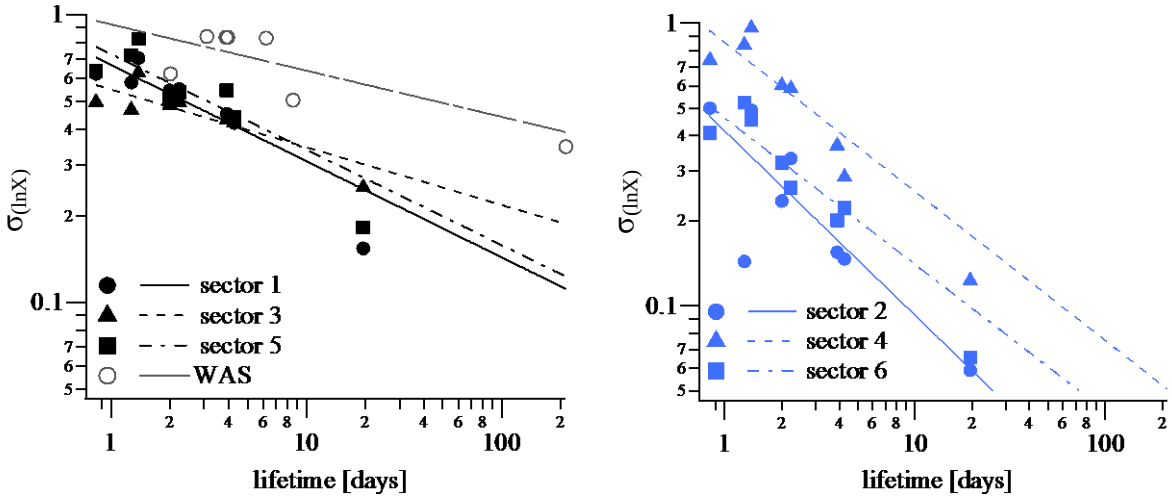

Figure 3-14: Lifetime-variability plots for easterly (black) and westerly (blue) sectors. lifetimes were calculated using an OH concentration of 2.47×10^6 molecules cm^{-3}. The results for WAS are illustrated as open circles but were not included in the analysis

left side shows the sectors 1, 3, and 5 coming from Eastern Europe while the blue plot on the right side shows the westerly sector 2, 4 and 6. The fit through the data points was made by using equation [21]. As measure of the quality of the fit the χ^2 value was used. The χ^2 indicates the discrepancy between the function and the data and evaluates the correlation of the least squares fit; lower values of χ^2 mean a better fit to the data (Williams et al. 2000). For the first scenario, where only OH as an oxidizing reagent is considered, the values for b lay between 0.20 and 0.33. This is an intermediate value between b exponents around 0 which were found for measurement points where sources were dominating the variability of the hydrocarbon mixing ratios such as the Harvard Forest site or the York University campus (Jobson et al. 1998; Jobson et al. 1999) and b exponents around 0.5 observed in rural and remote regions as for example during PEM-West B and at Amsterdam Island in the Indian Ocean (Jobson et al. 1999; Williams et al. 2001).

The b values obtained during CYPHEX were in good agreement with those found at Finokalia during MINOS in 2001 (b=0.23). Also during MINOS the main source of air masses was from Eastern Europe (Salisbury et al. 2003). As Crete, Cyprus showed val-

ues for b representing a site with intermediate conditions between source dominated and remote sites, where chemistry is the driving factor for variability. In contrast, for the westerly flow regimes, where transport times were longer, the values for b show that Cyprus not only represents intermediate conditions but also can show characteristics of remote sites. The values for b were between 0.52 and 0.62.

Varying the OH concentration for calculation of τ from 0.5×10^6 molecules cm^{-3} to 5×10^6 molecules cm^{-3} did not show any improvement on χ^2 or even lead to higher values. This shows that the OH chemistry during transport time was well represented.

An improvement of χ^2 was found for sectors 4 and 6 by addition of 1×10^4 molecules cm^{-3} and 5×10^4 molecules cm^{-3} of Cl radicals to calculate τ. Those sectors were the two, where the influence of marine planetary boundary layer with about 30% on average was the highest during CYPHEX. This finding showed evidence for chlorine chemistry observed during the last day of this campaign.

Table 3-9: Fitting parameter for lifetime-variability-plots

sector	A	b	χ^2
1	0.66	0.33	0.031
3	0.55	0.20	0.025
5	0.73	0.33	0.068
WAS	0.92	0.16	0.10
2	0.42	0.65	0.079
4	0.85 (0.79)[a]	0.53 (0.64)[a]	0.122 (0.101)[a]
6	0.46 (0.28)[b]	0.52 (0.89)[b]	0.030 (0.017)[b]

[OH]=2.47×10^6 molecules cm^{-3}

[a]: add. [Cl] 1×10^4 molecules cm^{-3}

[b]: add. [Cl] 5×10^4 molecules cm^{-3}

The exponents b for the different sectors showed that during CYPHEX Cyprus was influenced by air masses of different source/sink distributions and proximities between emission areas and measurement point.

The results for the WAS are also displayed in the diagram for the easterly sectors. However, they were not included in the analysis and the fitting was done separately. A large part of the WAS were taken before the start of NHMC measurements. Furthermore, the time periods of the samples differ. As mentioned earlier, also the variability was quite

high due to the very short sampling time (chapter 3.2). In comparison to NMHCs the results for acetonitrile and the alkyl nitrates showed higher variability in comparison to their calculated lifetimes (photolysis of alkyl nitrates was included). The 10 min averaged acetonitrile data from PTR-ToF-MS fits perfectly well with the fitting line for sector 1. This shows that measurement results and analysis are highly sensitive to sampling methods and durations. Nevertheless, the lifetime-variability results for the individual components measured from WAS showed good consistency ($\chi^2 = 0.10$).

Further reasons for the deviation from the NMHC data, especially for alkyl nitrates, can be the additional removal by photolysis. Although, this was included in the calculation of the lifetime, it could only be calculated approximately because of the estimated photolysis parameters. And as mentioned before (see chapter 3.2), an additional marine source cannot be excluded. Sources close to the measurement site would also increase the variability.

Figure 3-15 shows the factor A vs. the percentage of air from the planetary boundary layer calculated from Flexpart modelling. A refers to the results from plots shown in Figure 3-14.

With Flexpart results a portion of the air masses in contact the planetary boundary layer was calculated and compared to the results from lifetime-variability analysis.

As Figure 3-15 shows, A was linearly correlated with the PBL portion described by the equation $A = 1.27 - 0.028 \times \mathrm{PBL}\ [\%]$ from a linear regression.

During MINOS an A factor of 0.85 was found for the complete campaign which is also in the range of our measurements. As mentioned in chapter 1.3 A can be an interpretation of the range of the different transport times or air mass ages of individual air parcels of which the sample consists of and is mixed from. These low numbers show a narrow distribution of mixing by air masses of different photochemical ages and are below A factors found by Jobson (1998) at different locations at low altitudes within the PBL. During airborne measurement campaigns Williams et al. (2000) found values of A ranging from 2.9 to 4.23 at higher altitudes. At the surface the air masses are well mixed due to turbulence. Nevertheless, the proximity to sources suggests that the range of individual air masses ages is quite small. At high altitudes, the air is composed of a multitude of air masses, all of which originate from different regions and therefore have very varying transport times and age sepctra. During CYPHEX the direct and also apparently linear influence of the source proximity by means of PBL portion on A was shown.

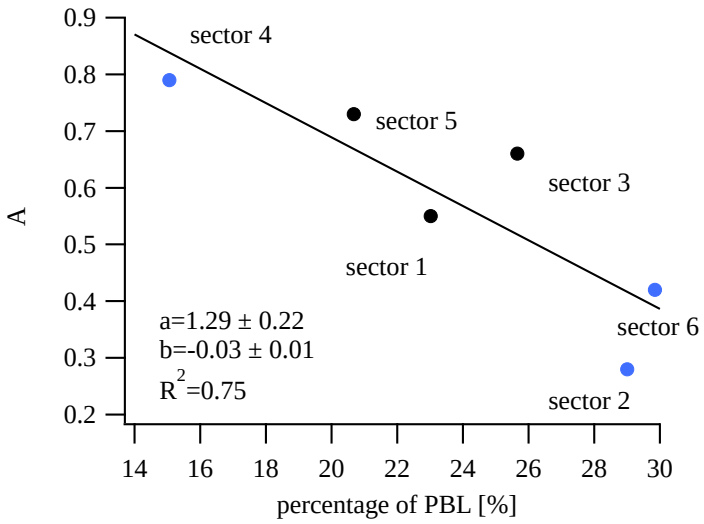

Figure 3-15: The A factor showed a linear correlation with the average fraction of air coming from the planetary boundary layer

3.3 Summary

In summer 2014 an extensive field campaign was performed in the north-western part of Cyprus by MPIC in collaboration with the Cyprus institute. During this campaign the photochemistry and air mass transport of the eastern Mediterranean was investigated. NHMC measurements showed that the site was influenced by two main flow regimes originating in Eastern and Western Europe. Easterly air masses were characterized by recent anthropogenic influence expressed by generally higher mixing ratios and higher emission ratios relative to CO.

The transport time of air masses from Eastern Europe was around 24 h. Westerly air masses needed transport times from 48 to 120 h. The longer transport times were mirrored by trace gas composition typical for more aged air masses with lower concentration of NMHCs and lower emission ratios.

The predominant oxidizing radical was found to be OH based on the relationship of ratios of hydrocarbons. Evidence for the influence of NO_3 and Cl was found in the data set by applying the means of logarithmic ratio comparison and lifetime-variability-analysis.

It was observed that air masses coming from Eastern Europe as well as from westerly sector showed ozone depleting regimes, confirming that local ozone levels are determined by transport and not local production.

To our knowledge CYPHEX was the first campaign in the Mediterranean where measurement of lower alkyl nitrates have been performed. The mixing ratios of those compounds reached maximum values of about 400 ppt.

With the analysis of the WAS taken during CYPHEX, the newly built GC-NCD system was successfully applied for the first time. The measurement of air samples of low pollution gave the confidence to use the system also for the CARIBIC project. Samples are collected in the UT/LS where generally lower mixing ratios of organic tracers are expected.

Chapter 4

Airborne Measurements

(CARIBIC 2014-2015)

The close collaboration among people, working with CARIBIC whole air samples, lead to following publications:

Umezawa, T., Baker, A. K., Oram, D., Sauvage, C., O'Sullivan, D., Rauthe-Schöch,A., Montzka, S. A., Zahn, A., Brenninkmeijer, C. A. M.: Methyl chloride in the upper troposphere observed by the CARIBIC passenger aircraft observatory: Large-scale distributions and Asian summer monsoon outflow, Journal of Geophysical Research: Atmospheres, 119, 5542-5558, doi:10.1002/ 2013JD021396, 2014.

Baker, A. K., Sauvage, C., Thorenz, U. R., van Velthoven, P., Oram, D. E., Zahn, A., Brenninkmeijer, C. A. M., Williams, J.: Evidence for strong widespread chlorine radical chemistry associated with pollution outflow from continental Asia; Nature, Scientific Reports 6, 36821, doi:, 2016.

Thorenz, U. R., Baker, A. K., Leedham Elvidge, E. C., Sauvage, C., Riede, H., van Velthoven, P. F. J., Hermann, M., Weigelt, A., Oram, D. E., Brenninkmeijer, C. A. M., Zahn, A., Williams, J.: Investigating African Trace Gas Sources , Vertical Transport , and Oxidation Using IAGOS-CARIBIC Measurements between Germany and South Africa between 2009 and 2011, Atmospheric Environment, 158. Elsevier Ltd: 11–26, doi:10.1016/j.atmosenv.2017.03.021, 2017.

4 Airborne measurements (CARIBIC)

Since 1997 the CARBIC project (Civil Aircraft for the Regular Investigation of the atmosphere Based on an instrumented Container) is a platform for regular observation of trace constituents of the free, upper troposphere and lower stratosphere (UT/LS).

A common airfreight container is equipped with instruments for online measurement of trace gases and aerosol particles. Sampling devices for whole air samples and particle collection are installed within the container for offline analysis after the flights. During CARIBIC phase #1, from 1997 to 2002, the air freight container was operated on a monthly basis onboard a Boeing 767-300 RT of LTU International Airways. Since 2004 until present, phase #2 is running using a more advanced container with larger capacity and additional equipment in combination with an improved inlet system (Figure 4-2 c) and d)). The inlet system is permanently installed in the belly of an Airbus A340- 600 of the Lufthansa German Airlines (Star Alliance). Once a month, the container is installed at the back of the cargo hold for four consecutive intercontinental, long-distance flights. The destinations are different airports in North and South America, southern Africa and Asia.

Between 2005 and 2016 CARBIC #2 completed 412 flights in 107 flight sequences and flew in total 3196463 km for 3635 hours departing from Frankfurt, Germany, (since August 2014 from Munich, Germany) to 26 destinations (see Figure 4-1).

In Figure 4-2 a picture of the Airbus A340-600 is shown. The inlet is mounted at its belly (see Figure 4-2 b)). It comprises different probes for aerosols, trace gases, gaseous and total water. Furthermore, it houses a video camera and three telescopes for differential optical absorption spectrometers (DOAS). The probes of the inlet system are connected to the instruments inside the freight container. This is equipped with instruments for in-situ measurement of O_3 (UV absorption and DOAS), CO (UV fluorescence), CO_2 (NDIR), H_2O (gaseous: laser photoacoustic, dew point; total: laser photoacoustic), NO (chemiluminescence), NO_y (chemiluminescence with gold converter), O_2 (electrochemical cells), Hg (enrichment and atomic fluorescence), aerosol number concentration (CPCs > 4nm; > 12 nm; > 18 nm), aerosol size distribution (OPC, 150-5000 nm), black carbon particles (SP2) and OVOCs (PTR-MS). Aerosol samples are collected for further analysis on elemental composition and particle morphology.

This work mainly focuses on measurement of whole air samples from TRAC and HIRES collectors (see chapter 2.3). Those canisters are analyzed for greenhouse gases, NMHCs, nitrogen and sulfur containing compounds. Glass samplers are also sent for further analysis of halocarbons. More detailed information on the project, container

equipment and the scientific consortium can be found in Brenninkmeijer et al. 2007 and references herein and on www.carbic-atmospheric.com.

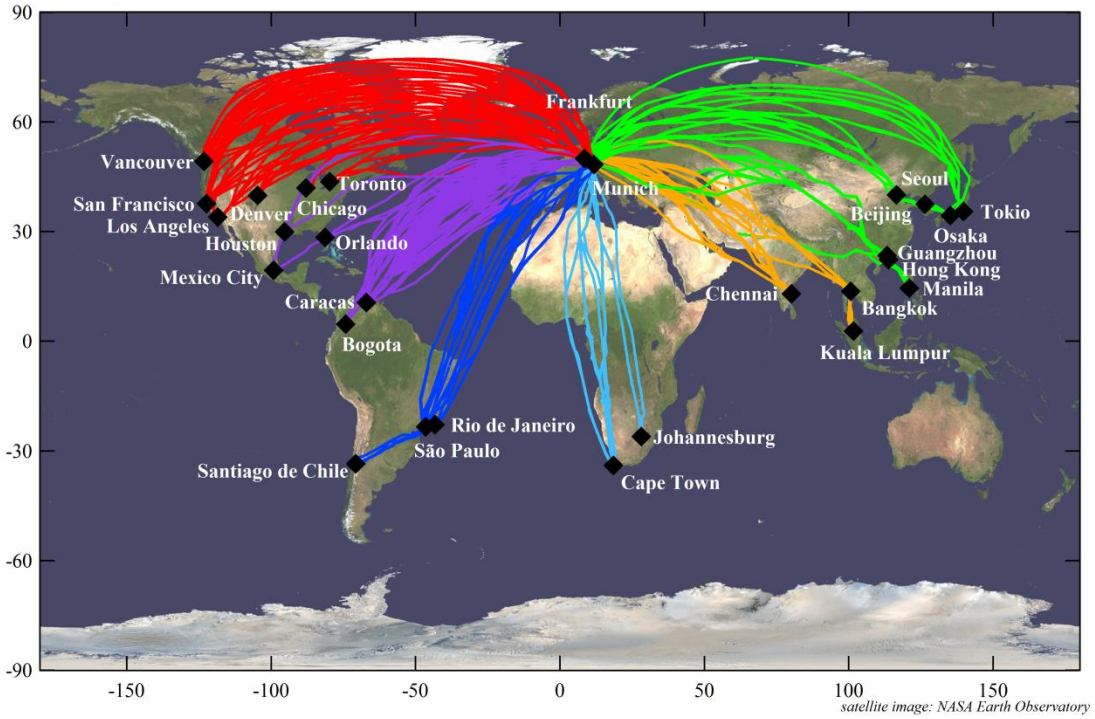

Figure 4-1: Flight routes of CARBIC from 2005 until 2016

Figure 4-2: a) Airbus A340-600 with inlet system b) inlet system c) instrument container (front) d) instrument container (rear)

4.1 Data overview

From August 2014 until August 2015 48 single long range flights were conducted within 12 different monthly flight sequences. From these flights the TRAC samplers and a selection of HIRES samples were analyzed resulting in 22 individual flights. The measurement of organic nitrogen species was done with the GC-NCD system and the analytical procedure was made as described in chapter 2.2. CARIBIC NMHC measurements which are mentioned were done with a GC-FID which was described in detail by Baker et al. (2009). 8-days-backwards trajectory analysis for each WAS along the flight track was based on ECMWF re-analyzed data (van Velthoven 2016).

The destinations during that year of monthly measurements were San Francisco (USA), São Paulo (Brazil), Tokyo (Japan), Beijing (China), Cape Town (South Africa), Mexico City (Mexico), Los Angeles (USA) and Hong Kong (China). Table 4-1 shows a summary of the single flights from which WAS samples were analyzed with the GC-NCD system.

The flight altitude of 10-12 km is around the UT/LS region and the tropopause where stratosphere-troposphere exchange (STE) takes place. Because physical and therefore also chemical processes differ for troposphere and stratosphere, it is necessary to assign the samples to one of these atmospheric layers. Different criteria can be used to define and locate the tropopause, which delineates the troposphere from the stratosphere. Ozone above a certain threshold (chemical tropopause) and the potential vorticity (PV) (dynamical tropopause) can be used to distinguish samples from the troposphere from samples with stratospheric influence (Gettelman et al. 2011). As shown by Assonov et al. (2013) N_2O can also be used as a tracer for the tropopause region. To strictly mark any sample which might have interference from stratospheric air three criteria were used. A possible stratospheric influence was assigned if PV was lower than 1.5, O_3 above 130 ppb and, N_2O being 1.3 ppb lower than the long term trend observed at the Mauna Loa Observatory (MLO), Hawaii, USA (http://www.esrl.noaa.gov/gmd/obop/mlo/). Samples were tagged with possible stratospheric influence if only one criterion was fulfilled. In Figure 4-3 the flight routes and sampling locations are mapped. The blue markers show samples being influenced by the stratosphere and the red ones show tropospheric samples. From 331 WAS in total 142 (43%) were ascribed as tropospheric samples and 189 (57%) as possibly influenced by stratospheric air masses. From these, 111 samples fulfilled at least one criterion, 28 fulfilled two and 50 samples fulfilled all three criteria. The vertical expansion of the troposphere and subsequently the altitudes of the tropopause and UT/LS regions show a latitudinal and an ancillary seasonal dependency. The tropopause is higher at the equator decreasing in altitude polewards. During wintertime (anticyclical for northern and

southern hemisphere) the troposphere is also shallower. This is also observable in Figure 4-3. The flights going to Southern Africa and America crossing the equator were intermitting mostly in the troposphere. Flights in the northern hemisphere to Northern America and Asia were intermittently crossing the tropopause and show tropospheric as well as stratospherically influenced air masses. According to the various destinations and also seasonal variation of destination within this year of measurement the flights will be discussed on a regional basis.

Table 4-1: Individual flights analyzed with the GC-NCD system

Flight number	month	Departure	destination
473	August 2014	San Francisco	Munich
475	August 2014	São Paulo	Munich
477	September 2014	San Francisco	Munich
479	September 2014	São Paulo	Munich
481	October 2014	Tokyo	Munich
483	October 2014	Beijing	Munich
484	November 2014	Munich	San Francisco
485	November 2014	San Francisco	Munich
490	January 2015	San Francisco	Munich
492	January 2015	São Paulo	Munich
495	February 2015	Munich	Cape Town
502	April 2015	Tokyo	Munich
504	April 2015	Mexico City	Munich
506	May 2015	São Paulo	Munich
508	May 2015	Los Angeles	Munich
510	June 2015	San Francisco	Munich
512	June 2015	Hong Kong	Munich
514	July 2015	São Paulo	Munich
515	July 2015	Munich	Los Angeles
516	July 2015	Los Angeles	Munich
518	August 2015	São Paulo	Munich
520	August 2015	Los Angeles	Munich

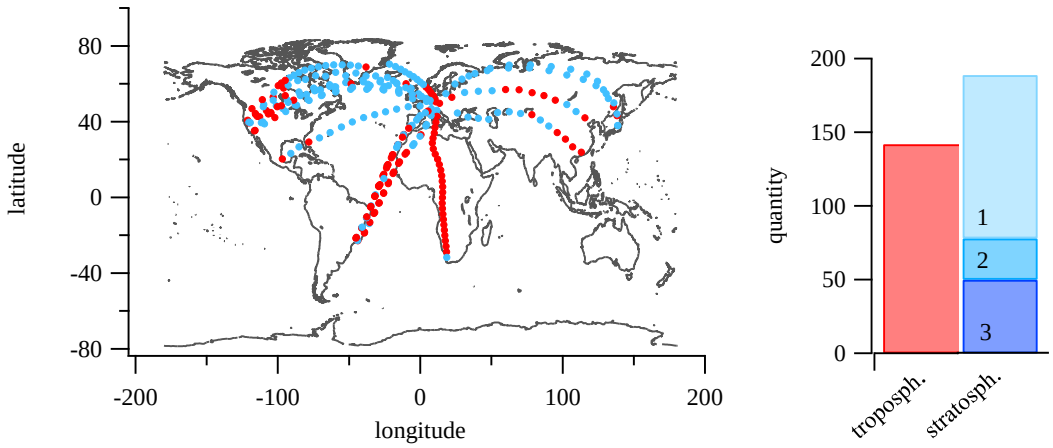

Figure 4-3: Left: flight routes between August 2014 and 2015 are represented by sampling location. Red markers indicate tropospheric air masses, blue markers possible stratospheric influence. Right: Bar chart of quantitative tropospheric and stratospheric sample distribution. Numbers 1-3 indicate the matched tropopause criteria

4.2 Flights to California

Flights between Los Angeles and San Francisco in California and Munich (Figure 4-4) were performed 10 times between August 2014 and August 2015 with intervals providing an annual/seasonal comparison. Most of the samples showed influence by the stratosphere. Over the main continent of Northern America and Europe a few tropospheric samples were collected (34 out of 141).

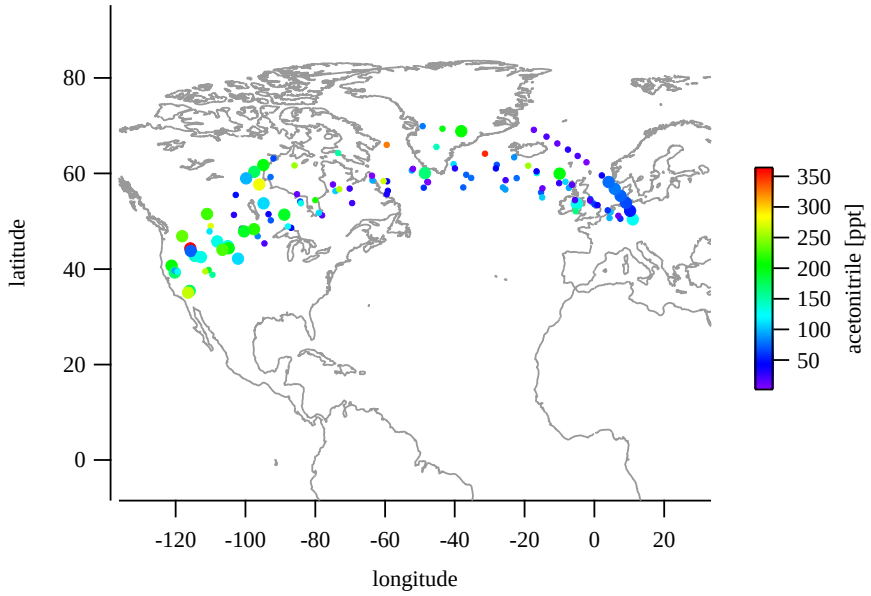

Figure 4-4: Flights to California, USA from August 2014 to August 2015. The color coding refers to mixing ratios of acetonitrile. Bigger markers represent tropospheric samples, smaller markers stratospheric samples

During these flights acetonitrile was regularly observed above the detection limit of 1.5 ppt. The average concentration of stratospheric samples was 91 ± 83 ppt and for tropospheric samples an average concentration of 178 ± 104 ppt was found. In Figure 4-5 the acetonitrile measurements during the flight is shown representing the seasonal cycle as box and whisker plots. Vertical lines within the boxes represent mean values, 25% of the data lies above the lower limit of the box, 75% below the upper limit, whiskers represent 10% and 90% of the data points. The plot only represents stratospherically influenced samples because the available amount of data was higher leading to a better representativeness. Nevertheless, tropospheric data shows the same seasonal trend.

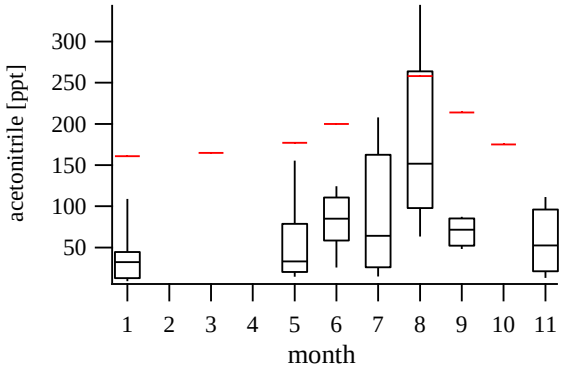

Figure 4-5: Seasonal cycle of acetonitrile (stratospheric samples) from flights between Munich, Germany and San Francisco or Los Angeles, USA displayed as box and whisker plot. Red lines indicate monthly mean measured by PTR-MS

It can be seen that the maximum average acetonitrile mixing ratio was observed in the summer months peaking in August. Although the variability indicated by longer boxes and whisker was higher in these times the minimum summer values were still higher or at least in the range of the wintertime mean concentrations. Acetonitrile is known to be a marker for biomass burning (Lobert et al. 1990; Holzinger et al. 1999; Karl et al. 2008) and boreal forest fires are known sources for acetonitrile in the troposphere and stratosphere (I. J. Simpson et al. 2011; Livesey et al. 2004). In northern hemispheric summertime, meaning from June to August, the biomass burning is enhanced leading to higher acetonitrile concentrations. In Figure 4-5 the monthly means of acetonitrile measured with the on-board PTR-MS was added as red lines. The absolute values were up to 300% higher than the data from WAS with GC-NCD but the seasonal cycle showed also a maximum during the summer. PTR-MS data comprises tropospheric and stratospheric samples. This has an overestimating influence on the average offset between those two instruments when from WAS only the stratospheric samples are considered as comparison, because of the tropospheric/stratospheric trend of acetonitrile. During TRACE-P Singh et al. (2003) found average mixing ratios of acetonitrile of 149 ± 56 ppt over the Pacific at altitudes of 0.1 to 12 km over a region that extended from 10 to 45 °N latitude and 100 °E to 120 °W longitude. The measurements were made from February to April 2001. PTR-MS measurements agree well with these results while GC-NCD measurements are lower.

The comparison of acetonitrile data from glass canisters (TRAC) in comparison to electropolished canisters (HIRES) didn't show a discrepancy. If wall losses were responsi-

ble for the discrepancy between PTR-MS measurements and GC-NCD measurements, than they are comparable for the two different materials or occurred already during the sampling process and lines prior to the collectors. The comparison between acetonitrile from PTR-ToF and canisters during the CYPHEX campaign showed reduced acetonitrile from PTR-ToF contrasting the results from the instrument comparison for CARIBIC. GC-NCD measurements from WAS also showed average HCN mixing ratios of 260 ppt which is in good agreement with results from the TRACE-B campaign (243 ppt). Methyl nitrate was found in 22 WAS on the way between California and Germany at average mixing ratios of 7 ± 3 ppt mainly in tropospheric but also in a few stratospherically influenced samples. Blake et al. (1999) found methyl nitrate not higher than 3 ppt at comparable latitude over the Pacific with a decreasing trend in mixing ratios with increasing altitude.

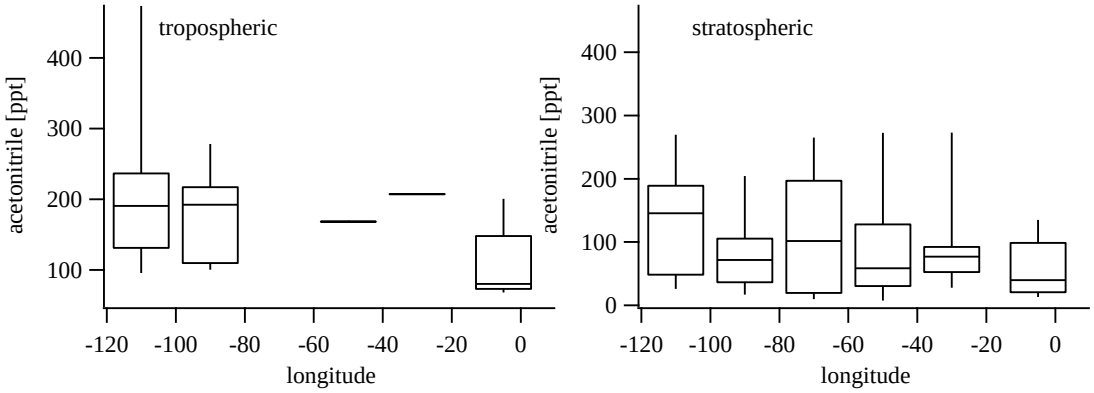

Figure 4-6: Longitudinal trend of acetonitrile on the flights between California and Munich for tropospheric and stratospheric samples

The longitudinal trend along the flight paths was also investigated for acetonitrile by sorting the data in 20° bins. Acetonitrile was found to be quite equally distributed over the longitude band between -120° and +10° for stratospheric samples as well as for tropospheric ones, although acetonitrile data is slightly elevated from -120 to -100° over the US and lower over central Europe Trajectories for those samples showed influence of continental emissions. Despite that, the variability is lowest over Europe although data density, especially for stratospheric samples is much higher. The corresponding plots are shown in Figure 4-6.

4.3 Flights to East Asia

Within the year of CARBIC WAS analysis with the GC-NCD systems four individual flights to East Asia were analyzed. In October 2014 two consecutive flights flew from Tokyo and Beijing, another one from Tokyo was conducted in April 2015 and one from Hong Kong in June 2015. The routes to Asia can be divided into three different regions over Europe and Western Asia, Central Asia and South East Asia. The origins of air masses which were encountered during the flights were Northern America, the Atlantic and Europe/Mediterranean for sampling regions over Europe. Over Central Asia the common sources are Europe, Central Asia, the Arabian Peninsula and the Indian subcontinent. South East Asia was dominated by more recent emission from Eastern China and the Indochinese peninsula, were tropospheric samples being lifted up from regions with pressures above 650 hPa are typical (Baker et al. 2011; Baker et al. 2012; Baker et al. 2014).

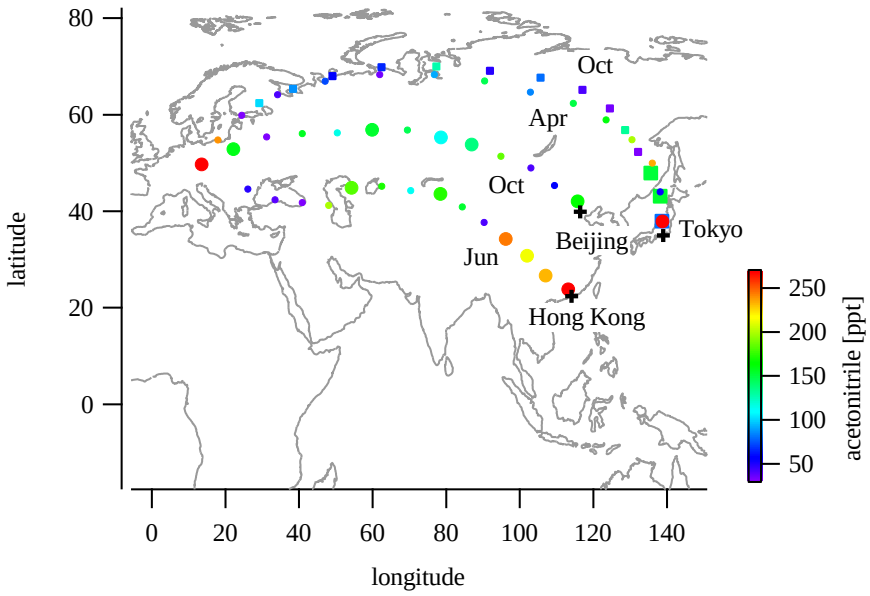

Figure 4-7: Flights between Munich and Asian destinations. The color coding refers to acetonitrile mixing ratios, bigger markers show tropospheric and smaller markers show stratospheric samples. The markers for the flight to Tokyo in October were chosen as squares for a better differentiation

The portion of tropospheric samples got higher with routes being more in the south and in the summer when the tropopause region is found at higher altitudes. Among 55 samples in total, 16 were tagged as tropospheric and 39 samples as stratospheric. Acetonitrile was the only organic nitrogen compound which was regularly observed. Figure 4-7 shows the four individual flights to Asia. Tropospheric samples are represented as big-

ger markers; smaller markers show stratospherically influenced samples. The color coding refers to mixing ratios of acetonitrile.

In October 2014 the flights analyzed with the GC-NCD system took place between Munich and Tokyo and Beijing. The average mixing ratios of acetonitrile were 85 ± 40 ppt for the route between Tokyo and Munich when almost exclusively stratospherically influenced air masses were sampled. On the more southern route to Beijing the portion of tropospheric samples is higher and also the stratospherical samples show higher levels of acetonitrile and on average 125 ± 53 ppt were observed on this route.

8 days-backwards trajectories showed that on the route to Tokyo the air masses encountered originated mostly from latitudes north of 50° N and at pressures below 250 hPa which corresponds to altitudes roughly between 10 and 15 km. On the route to Beijing the trajectory analysis showed sources further south and coming from lower altitudes with pressures > 500 hPa (0-5 km). The main regions which influenced those samples were North America, the Gulf of Mexico and the western Atlantic. The higher mixing ratios of acetonitrile on this route can be explained by more recent and fresh emissions while on the route to Tokyo air masses were sampled which spent more time in the UT/LS and were more photochemically processed.

The April flight between Tokyo and Munich showed acetonitrile mixing ratios of 75 ± 31 ppt on average for the complete flight. This is ca. 10 ppt lower compared to the flight in October. In contrast to the flight in April in October, the samples taken after departure, were tropospheric and therefore showed higher mixing ratios in acetonitrile. If only stratospheric samples were taken into account the average mixing ratios for those two flights to Tokyo with 73 ± 33 ppt in October and 71 ± 27 ppt in April are in good agreement.

On the route between Hong Kong and Munich, high mixing ratios of acetonitrile were observed in the first four samples taken after departure (216-268 ppt). The shorter lived non-methane hydrocarbons *i*-/*n*-butane and *i*-/*n*-pentane showed comparable trends during the flight (Figure 4-8). The global atmospheric lifetime of acetonitrile is about 1.4 years ($k_{OH}=2.2\times10^{-14}$ cm³ molecules^{-1} s^{-1} (DeMore et al. 1997); [OH]= 9.7×10^{5} OH molecules cm^{-3}(Prinn et al. 1995)). So it is expected that acetonitrile is more equally distributed when the air masses which were sampled were of a certain photochemical age. Therefore rather sources and recent pollution influenced the comparable trends in those organic compounds. The trend for ethane and propane was not as distinct as for the other hydrocarbons. Backwards trajectories showed that air masses during this flight were coming from India and were uplifted in an anticyclone possibly showing the influ-

ence of the Indian summer monsoon. The Indian monsoon is known to be a system for the fast uplift and transport of polluted air masses from East Asia where the air pollution is increasing over the last decades (Kurokawa et al. 2013; Ohara et al. 2007; Zhang et al. 2009). Air masses within the monsoon are characterized by high mixing ratios of anthropogenic pollutants. Furthermore the oxidation capacity within the monsoon is enhanced by efficient recycling of the OH radical. Due to high lightning activity NO_x is produced within the anticyclonic cell and reforms OH ($NO + HO_2 \rightarrow NO_2 + OH$) (Lelieveld et al. 2018).

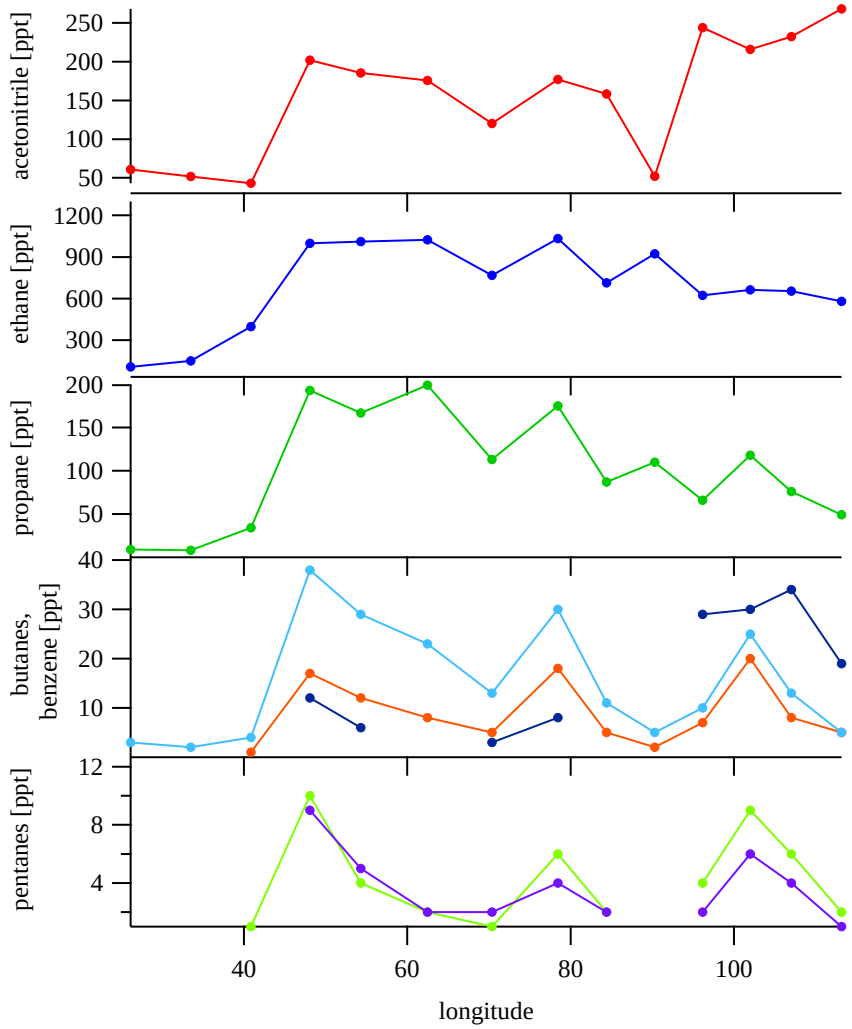

Figure 4-8: Longitudinal profile of acetonitrile and NMHC during the flight from Tokyo to Munich in April 2015.

On CARIBIC flights between May 2005 and March 2008 Baker et al. (2014) found mixing ratios of acetonitrile from ranging from 93 ± 27 to 141 ± 36 on average increas-

ing on the way from Europe towards South East Asia with maximum values observed in springtime. This is in contrast to the above discussed flights to California across the Atlantic when maximum values were reached in summertime.

Additionally to high acetonitrile mixing ratios directly after departure over Tokyo in April and over Hong Kong in June, methyl nitrate was found in those samples (Tokyo: 3 ppt; Hong Kong: 18 ppt)

4.4 Flight to Africa

In February 2015 a flight from Munich to Cape Town, South Africa was conducted. Along the flight track 28 WAS were collected. All of them could be assigned to the troposphere by using the three different criteria mentioned above. Figure 4-9 shows the sampling location over a map of Africa. In the left panel the markers are color coded with acetonitrile mixing ratios. The color coding in the right panel refers to mixing ratios of methyl nitrate which was also found in all samples. Furthermore, the background is shaded in black and white representing the outgoing longwave radiation (OLR) in Wm^{-2} observed by satellites.

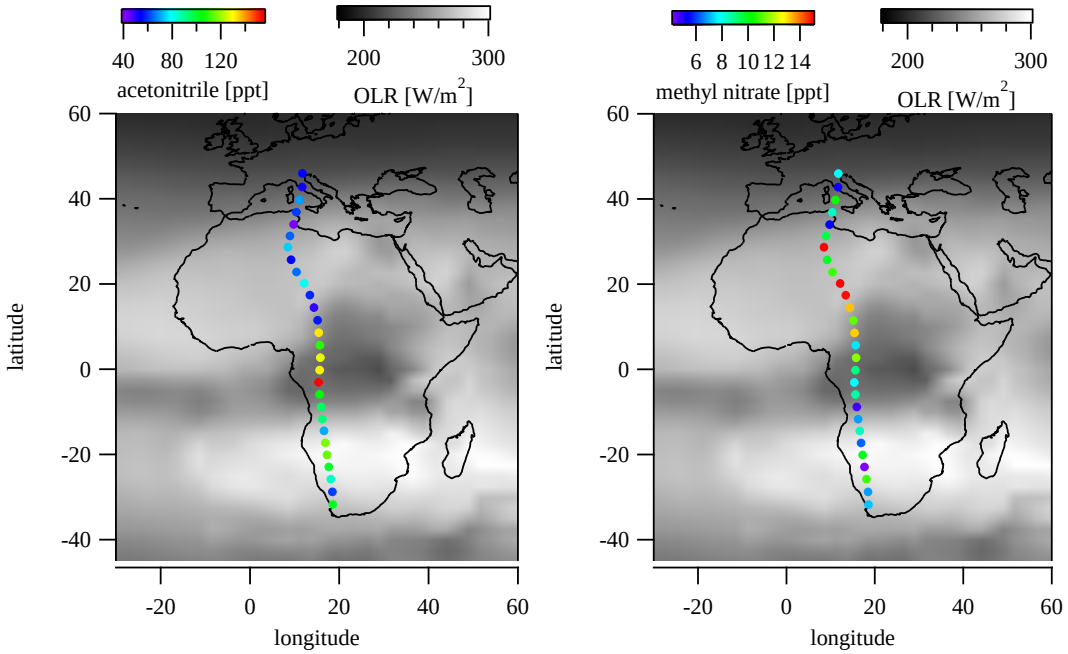

Figure 4-9: Latitudinal trends of acetonitrile and methyl nitrate on the flight from Munich to Cape Town in February 2015

The OLR is an index for tropical deep convection and therefore also for the intertropical convergence zone (ITCZ) (Waliser et al. 1993). For these plots the uninterpolated OLR data provided by the NOAA/OAR/ESRL PSD, Boulder, Colorado, USA (http://www.esrl.noaa.gov/psd/ downloaded at 26.11.2016) was used. Data is provided

in 2.5° latitude × 2.5° longitude global grid (144×73) as daily mean. The shading shows the average of the date of flight and the prior four days. As can be seen in Figure 4-9 in February the ITCZ was between 0 and -10° southwards of the equator. Also areas of high convective activity were observed over central Africa northwards the equator. During the flight the plane passed this region. Higher mixing ratios and relative compositions of atmospheric trace gases typical for fresh and less aged air masses are characteristic for this region of fast vertical transport (Thorenz et al. 2017). Mixing ratios of the biomass burning tracer acetonitrile showed a maximum across the ITCZ (up to 153 ppt). The seasonal cycle of acetonitrile discussed in chapter 4.2 shows a wintertime minimum for the northern hemisphere. This is also visible on the flight to Cape Town were acetonitrile mixing ratios north of the convective areas were found to be low (40-85 ppt). Separate from maximum acetonitrile mixing ratios crossing the ITCZ, higher mixing ratios were observed in the samples south of the ITCZ (60-115 ppt). This can be explained by a mirrored seasonal cycle of acetonitrile for the southern hemisphere.

The right panel in Figure 4-9 shows the markers color coded with the mixing ratio of methyl nitrate. Methyl nitrate was found in each sample and ranged from 6 - 19.5 ppt with an average of 12 ± 4 ppt. In contrast to acetonitrile, the predominant source for methyl nitrate is secondary photochemical production. On the flight to Cape Town the maximum mixing ratios were found over the northern part of Africa between 5 ° and 30 °N and not in the region of high convective activity as found for acetonitrile. Nevertheless around the ITCZ the mixing ratios were around the average of the whole flight. The backwards trajectory analysis showed that air masses sampled in the beginning of the flight originated around the Gulf of Mexico. The source of highest mixing ratios in methyl nitrate was located above the Pacific. The Pacific was previously identified as source of alkyl nitrates (Chuck, Turner, and Liss 2002; N. J. Blake, Blake, and Swanson 2003; Neu et al. 2008). The acetonitrile/methyl nitrate ratios were on average 10 ± 5 ppt/ppt and were found to be highest over the ITCZ region origination from the African continental boundary layer along with the acetonitrile maximum. This ratio was chosen arbitrarily to have a comparison amongst the components measured from the same samples with the same measurement technique. Despite that acetonitrile and methyl nitrate did not correlate (R^2=0.007).

The result from the flight between Munich and Cape Town showed the formation and advection of acetonitrile in the ITCZ and the secondary production of methyl nitrate by photochemical oxidation from NMHC and that it is not primarily emitted by biomass burning. Also backwards trajectory analysis identified the equatorial Pacific region as source of methyl nitrate.

4.5 Flights to South America

The six individual flights between Munich and São Paulo were conducted in August and September 2014 and January, May, July, and August 2015. During these flights acetonitrile was observed and later within the year of measurement due to sensitivity improvement of the NCD instrument also methyl nitrate (see chapter 2.2). Because of the latitudinal range and the vertical extension towards the equator the tropospheric samples were found to be 67 and the ones with stratospheric influence 17 (see Figure 4-3). The annual cycle of acetonitrile observed among the flights to California with maximum during summer and minimum during winter and spring was also represented in the flights to South America. For methyl nitrate higher mixing ratios were also observed during summertime when photochemical processing is more pronounced than in wintertime. Average mixing ratios and standard deviations, distinguished between stratospheric and tropospheric samples, are listed in Table 4-2. Apart from the seasonal cycle, as seen also in the flights to California, the tropospheric samples showed generally higher mixing ratios in acetonitrile, as well in methyl nitrate, than in stratospherically influenced samples. This was in agreement with the decreasing trend with increasing altitude observed by Singh (2003) and Blake (1999).

Table 4-2: Average acetonitrile and methyl nitrates mixing ratios (with standard deviation) in tropospheric and stratospherically influenced samples. Where no standard deviation is given, only one data point exists

Month	acetonitrile [ppt]		methyl nitrate [ppt]	
	tropospheric	stratospheric	tropospheric	stratospheric
January	112 ± 17	53 ± 20	7 ± 2	4 ± 2
May	104 ± 9	18 ± 2	11 ± 4	
July	245 ± 63	201 ± 64	15 ± 9	
August	198 ± 60	89 ± 63	16 ± 7	7
September	229 ± 78	58		

Figure 4-10 shows the individual flights between Munich and São Paulo and the OLR in shades of black and white. The darker the shaded background is, the more convective activity is observed in the individual region. In the summer months the ITCZ showed a sharp band slightly south of the equator. In January the ITCZ is not as clearly illustrated and showed a fluctuation south towards the Atlantic.

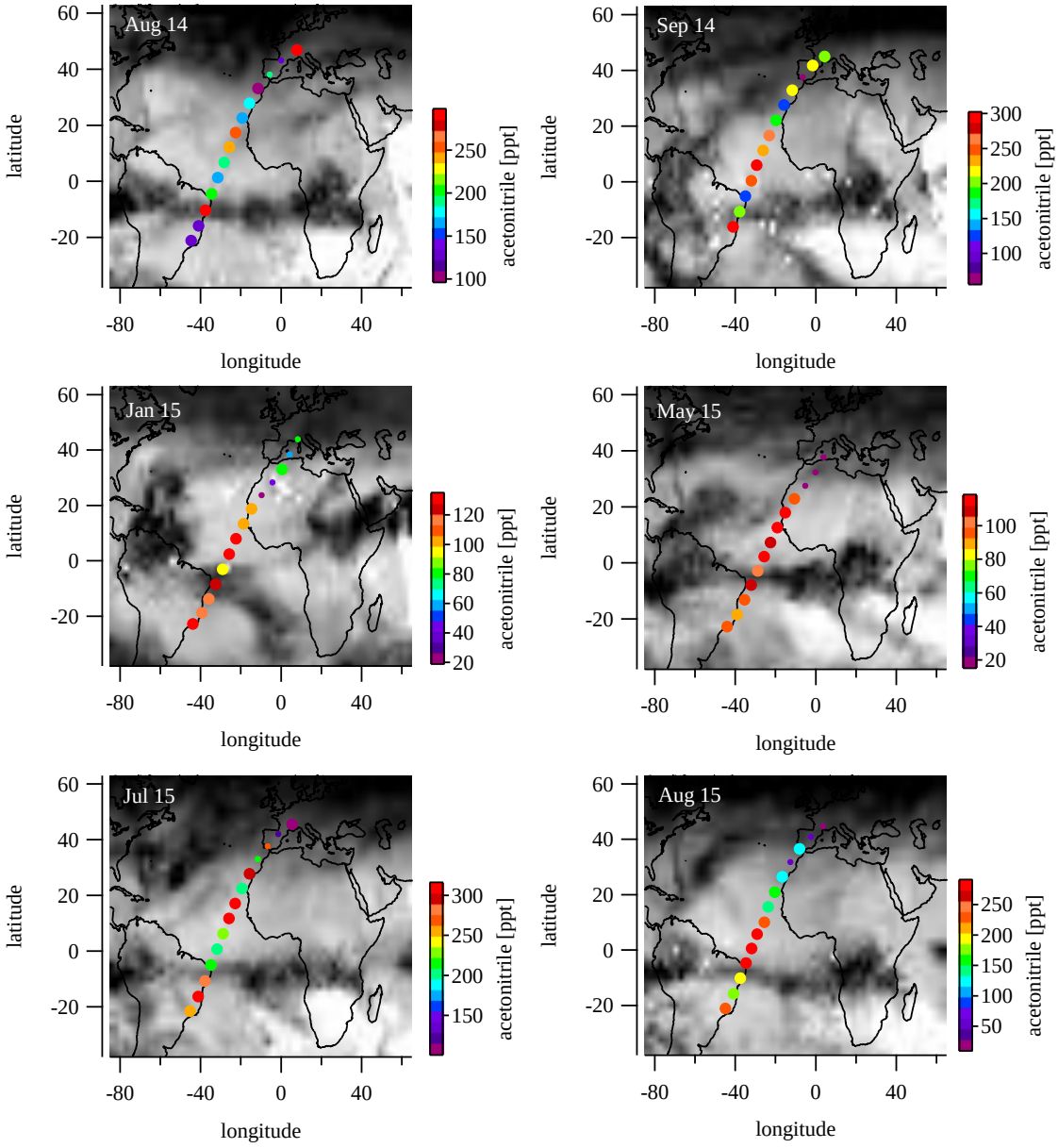

Figure 4-10: Flights between Munich and São Paulo. The color code of the sampling markers refers to acetonitrile concentration. Bigger markers represent tropospheric samples, the smaller one stratospherically influenced samples. Black and white shaded areas represent the OLR from 180 – 300 Wm^{-2}. The color coding of the acetonitrile mixing ratios is on different scales for the individual flights

During the flights to São Paulo the influence of the ITCZ on acetonitrile mixing ratios is not as clearly visible as for the flight to Cape Town discussed in chapter 4.4. The observed mixing ratios in January and May, when acetonitrile is low within the seasonal cycle, is about 40 ppt higher than the mixing ratios observed during the flight to Cape town which was in February. Also the expanse of high mixing ratios spans a higher latitudinal range. The more widespread tropical and subtropical elevated mixing ratios can be explained with the help of backwards trajectories. Whereas over Central Africa the fast and direct convective uplifting is also represented in backwards trajectories the trajectories for the flights to South America show wider distributed starting points and therefore different areas of origin and longer transport times.

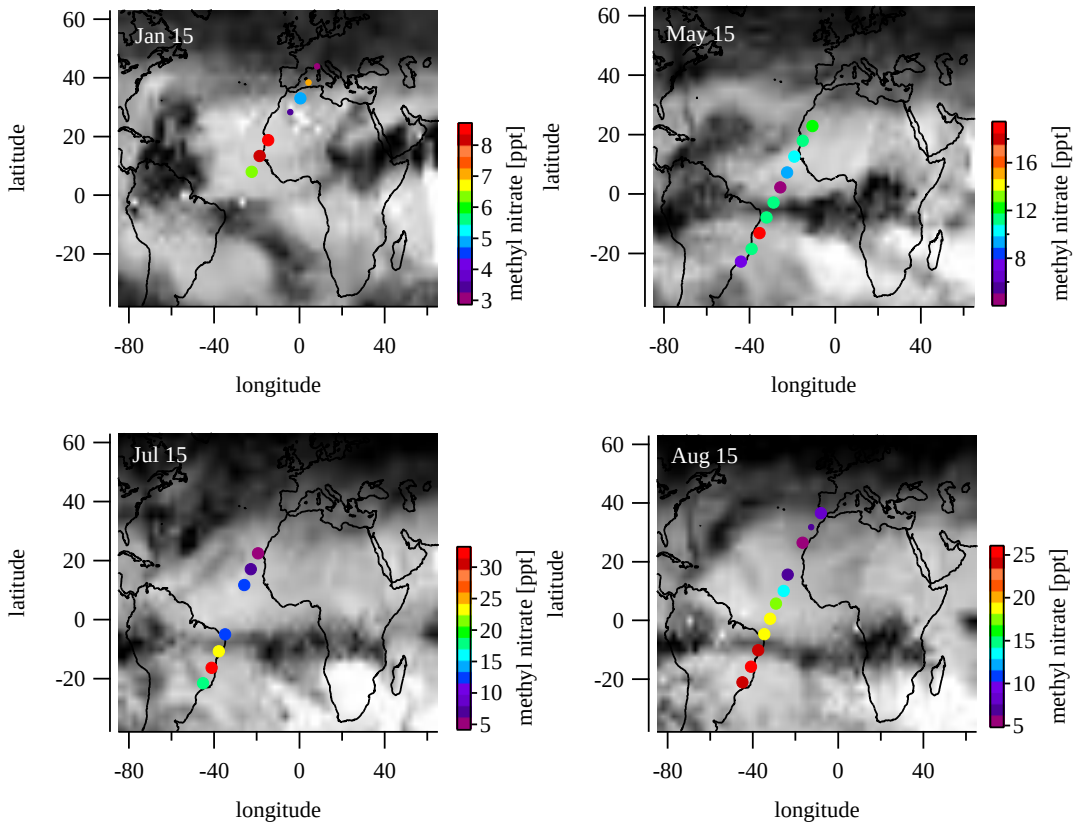

Figure 4-11: Flights between Munich and São Paulo. The color code of the sampling markers refers to methyl nitrate concentration. Bigger markers represent tropospheric samples, the smaller one stratospherically influenced samples. Black and white shaded areas represent the OLR from 180 – 300 Wm^{-2}

Due to instrumental changes (chapter 2.2) which improved the limit of detection (< 3 ppt) methyl nitrate was found in the flights from 2015 at average mixing ratios listed in Table 4-2. Methyl nitrate was only found in tropospheric samples except for four stratospherically influenced samples which show low mixing ratios of methyl ni-

trate (Figure 4-11). For acetonitrile and methyl nitrate a weak correlation was found for these flights (acetonitrile vs. methyl nitrate: y = 76.6 + 6.9 x; R^2=0.36) whereas on the route to Cape Town no correlation was found (R^2=0.007). The acetonitrile/methyl nitrate average ratios were 15 ± 9 ppt/ppt with highest values (> 20 ppt/ppt) over the Atlantic. Backwards trajectory analysis showed that the samples were characterized by the highest acetonitrile/methyl nitrate ratios originated from the African continental boundary layer which was also observed during the flight to Cape Town.

Again, higher mixing ratios in methyl nitrate could be observed when backwards trajectories showed influence from the Pacific marine boundary layer (MBL) and emphasizes that this area is an important source for methyl nitrate.

Flight to Mexico City

In April 2015 one flight took off from Mexico City to Munich. The results are shown in Figure 4-12.

The first samples were taken within the troposphere and backwards trajectories showed contact with the MBL over the Pacific the prior eight days. Average acetonitrile mixing ratios of those samples of 195 ± 28 ppt and in stratospheric samples (64 ± 52 ppt) are higher than observed mixing ratios in May on the way from São Paulo or from California. They are in the range of mixing ratios observed during summer on the São Paulo route.

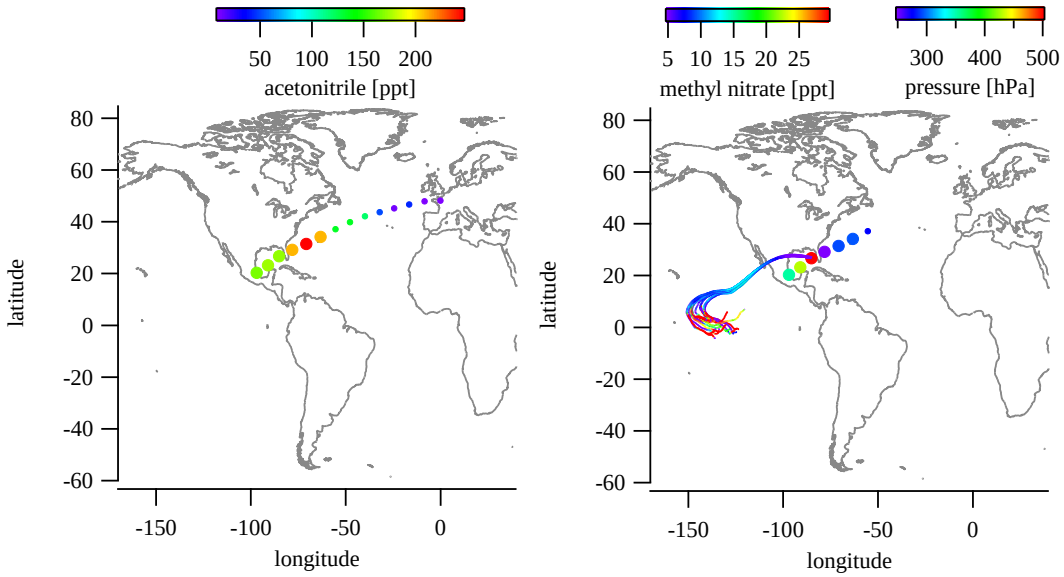

Figure 4-12: Flight between Mexico City and Munich. The color code of the sampling markers refers to acetonitrile (left panel) and methyl nitrate (right panel) concentration. Bigger markers represent tropospheric samples, the smaller one stratospherically influenced samples. In the left panel the 8-days-backwards trajectories are displayed. The color code refers to calculated pressures along the transport pathway

Methyl nitrate was also observed in these first samples which had contact to the MBL. Especially in sample 3 when backwards trajectories show an intensive influence of the tropical MBL a high concentration of 29 ppt of methyl nitrate was measured. The 8-days backwards trajectories for this sample are additionally displayed in Figure 4-12. Though, methyl nitrate is a photochemically produced, secondary pollutant, Blake et al. (2003) found the equatorial Pacific to be a major source of methyl nitrate and other C_2-C_4 alkyl nitrates.

4.6 Summary

From August 2014 until August 2015 analysis of organic nitrogen compounds was done for 22 individual flights. Acetonitrile was observed on every flight. Due to improved sensitivity after instrumental changes (pump exchange, see chapter 2.2) from January on methyl nitrate was measured above the limit of detection in 77% of the tropospheric and 12 % of the stratospheric samples.

During the flights to California the seasonal cycle of acetonitrile was observed. As a biomass burning marker, acetonitrile mixing ratios are enhanced in the summer months June-September due to enhanced biomass burning. The mixing ratios determined with GC-NCD analysis were significantly lower than PTR-MS measurements and other measurement campaigns in this region. Furthermore acetonitrile was found to be equally distributed along the flightpath with no clear longitudinal trend except some elevated mixing ratios over the continental part of the flight route.

On the flights to Beijing and Tokyo acetonitrile mixing ratios ranged from 71 ± 33 ppt to 125 ± 53 ppt with higher mixing ratios on the more southern route. Backwards trajectories showed that the northern route to Tokyo was more influenced by sources being further north and at elevated altitude, whereas the more southern route was dominated by air masses being recently influenced by more fresh emissions from North America, the Gulf of Mexico and the Atlantic. On the flight to Hong Kong the fast uplift by the Indian summer monsoon was observed by high mixing ratios of acetonitrile and methyl nitrate in the first samples after departure. Backwards trajectories of those samples showed the Indian subcontinent and an anticyclonic uplift as source of those air masses. Lelieveld et al. (2018) showed that the monsoon is a meteorological phenomenon which is very efficient in the fast uplift of anthropogenic pollutants and the oxidative capacity is intensified by enhanced OH recycling due to lightning NO_x.

On the route to Cape Town the plane was flying exclusively the troposphere. Acetonitrile and methyl nitrate were measured in all samples. The latitudinal trend of primary emitted compound acetonitrile with maximum mixing ratios around the equator showed the fast uplift by the convective systems within the ITCZ. The higher mixing ratios of

methyl nitrate observed north of the ITCZ could be traced back to the Pacific region as source.

On the flights to South America the seasonal cycle of acetonitrile which was observed on the routes between California and Munich could also be observed during these flights. The influence of the ITCZ was not as clear as on the flight to Cape Town. Backwards trajectories along those flight paths showed wider distributed source areas of the air masses which were encountered. Furthermore, backwards trajectory analysis showed that air masses with origin over the African continent were characterized by high acetonitrile/methyl nitrate ratios.

As observed in other studies the equatorial Pacific region was identified as primary source of methyl nitrate (Blake et al. 2003; Chuck et al. 2002; Neu et al. 2008). Backwards trajectory analysis showed this region as origin of air masses for samples with the highest mixing ratios of methyl nitrate which were observed on flights to Cape Town, São Paulo and Mexico City.

Chapter 5

NOTOMO 2015

NOcturnal chemistry at the Taunus Observatorium: insights into Mechanisms of Oxidation

Parts of the NOTOMO and PARADE NMHC data sets were published in:

Sobanski, N., Tang, M. J., Thieser, J., Schuster, G., Pöhler, D., Fischer, H., Song, W., Sauvage, C., Williams, J., Fachinger, J., Berkes, F., Hoor, P., Platt, U., Lelieveld, J., and Crowley, J. N.: Chemical and meteorological influences on the lifetime of NO_3 at a semi-rural mountain site during PARADE, Atmospheric Chemistry and Physics, 16, 4867-4883, doi:10.5194/acp-16-4867-2016, 2016.

Sobanski, N., Thieser, J., Schuladen, J., Sauvage, C., Song, W., Williams, J., Lelieveld, J., and Crowley, J. N.: Day and Night-Time Formation of Organic Nitrates at a Forested Mountain Site in South-West Germany, Atmospheric Chemistry and Physics, 17 (2): 4115–30, doi:10.5194/acp-17-4115-2017, 2017.

5 NOTOMO

The NOTOMO campaign (NOcturnal chemistry at the Taunus Observatorium: insights into Mechanisms of Oxidation) took place from the beginning of June to end of July 2015 at the Taunus Observatory (50.22 N, 8.45 E, 850 m above sea level) on top of the *Kleiner Feldberg* mountain.

Measurements discussed in this chapter focus on NMHC, acetonitrile and alkyl nitrates. NMHC were measured with GC-FID on the site and nitrogen compounds were analyzed with GC-NCD from canister samples as described in chapter 2.

The analyzed VOCs are discussed in context of site meteorology and inorganic pollutants such as NO_x and O_3. Furthermore the NOTOMO NMHC data set is compared to data from 2012 when the PARADE campaign was conducted in the same place and season.

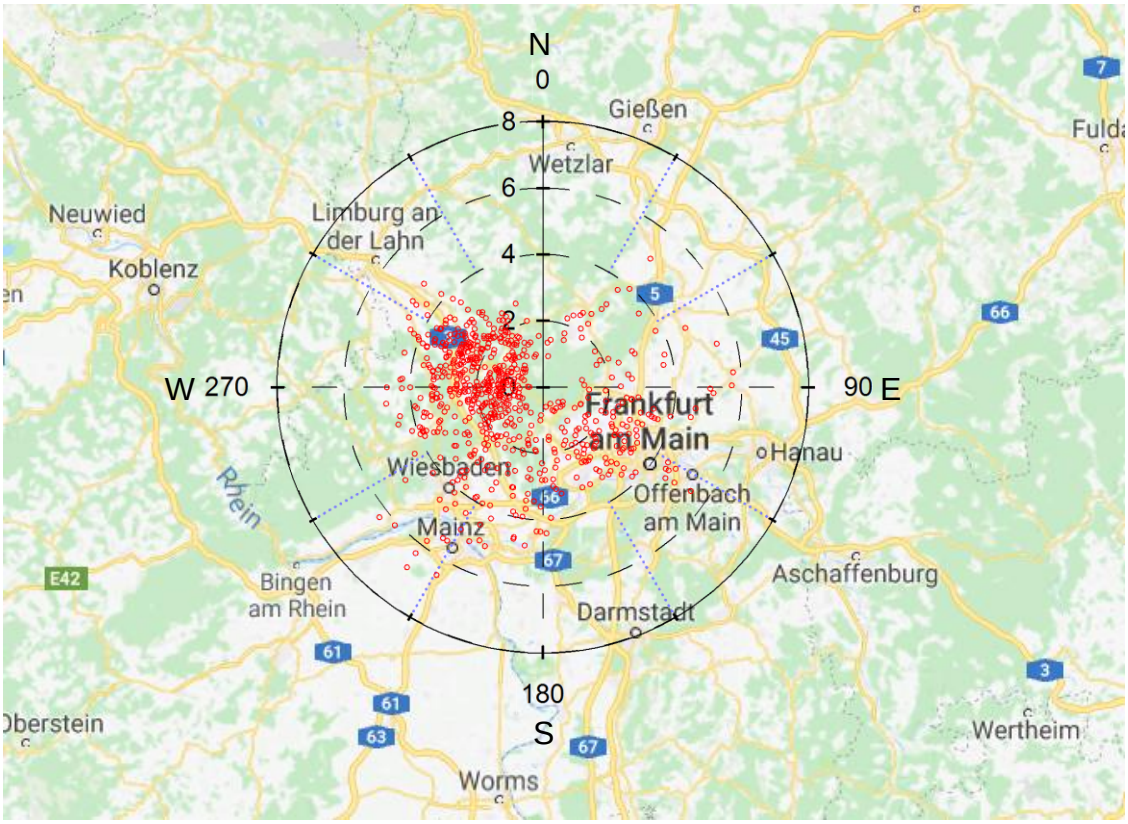

Figure 5-1: Location of Taunus Observatory in top of the *Kleiner Feldberg* with surrounding rural and urban areas. The roseplot shows wind speed versus wind direction to indicate the source areas

5.1 Site description and data overview

The observatory is surrounded by rural and forested areas in a sector SW-SE of the mountain. In contrast the sector SE-SW is dominated by highly populated and industrialized areas including the urban center of Rhine-Main and the cities of Frankfurt, Mainz and Wiesbaden with about 1.2 million inhabitants in sum. Detailed information on the area can be found in Crowley et al. 2010 and Sobanski et al. 2016.

5.1.1 Meteorology and air mass origin

During NOTOMO the weather conditions were very variable changing between wet and cold periods associated with air mass origin from the Atlantic and warm and dry periods coming from continental Europe. Meteorological data was provided by the state of Hessen environmental agency (HLNUG, Hessisches Landesamt für Naturschutz, Umwelt und Geologie). Their measurement container is also operated on top of the *Feldberg*. The data was downloaded from their homepage (www.hlnug.de on 18.09.2015).

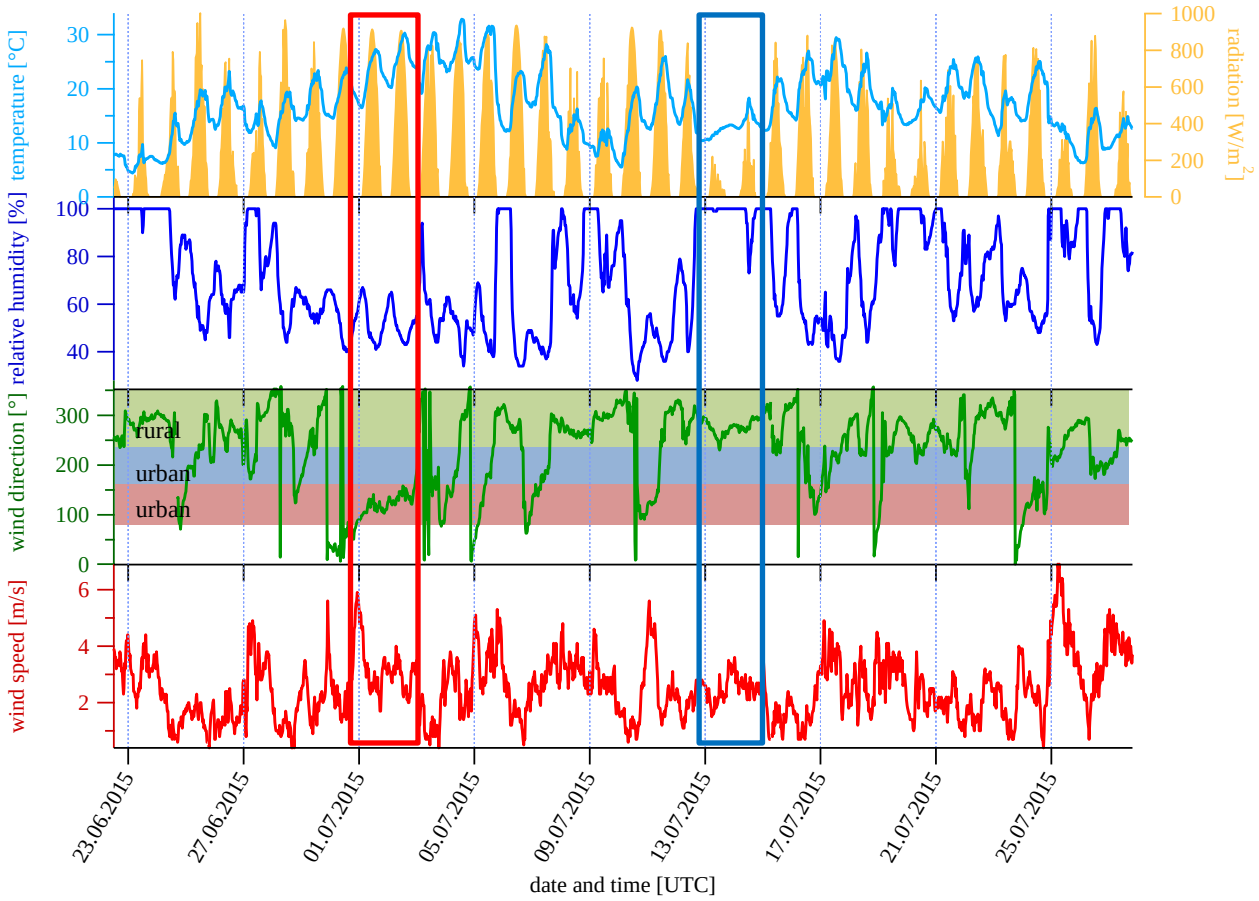

Figure 5-2: Overview of meteorological conditions during NOTOMO. Highlighted in red are days with stable, warm and dry conditions. Contrasting in blue, days with rainy and cloudy weather

Figure 5-2 shows the meteorological conditions during the campaign. Temperature ranged from 4 °C up to 33 °C with an average of 17 °C, relative humidity varied between 28% and 100% with an average of 71%. The dominating wind direction was coming from a sector between SW and NW (225° - 315°), where the surrounding is more rural. Two periods of different meteorological conditions are highlighted and will be discussed in more detail. In the red highlighted period from 1st to 2nd July the overall conditions were sunny, dry and hot. Moreover the wind was coming from Frankfurt. These conditions are required for high photochemical activity. In contrast, during the blue highlighted period from 13th to 14th July the weather was cloudy, rainy, cool and air masses were coming from more rural surroundings.

5.2 Results and discussion

During NOTOMO a data set of 10 NMHCs over a period of 37 days with a temporal resolution of one hour was generated. Gaps in the data set were caused by power failure or contamination within the analytical system. NMHCs were measured with GC-FID. The analytical technique is described in chapter 2.1. During the campaign 116 WAS (whole air samples) were collected at the site and analyzed in the laboratory with GC-NCD as explained in chapters 2.2 and 2.3. The proximity of the *Kleiner Feldberg* and Mainz allowed analysis of the canister samples usually within two days. The maximum storage time was four days. Furthermore the NOTOMO data set comprises measurement of $ClNO_2$ and SO_2 (chemical ionization mass spectrometry), NO_2, NO_3, N_2O_5, total peroxy nitrates, total alkyl nitrates (thermal dissociation cavity ring-down spectroscopy). The analytical techniques are described by Sobanski et al. 2017; Sobanski et al. 2016 and Phillips et al. 2012. All data with higher temporal resolution than NMHC measurement was averaged over GC-FID sampling time.

Figure 5-3 to Figure 5-5 show the timelines of NMHCs and the organic nitrogen compounds. In Table 5-1 the average mixing ratios are listed along with standard deviations, minimum and maximum observed mixing ratios.

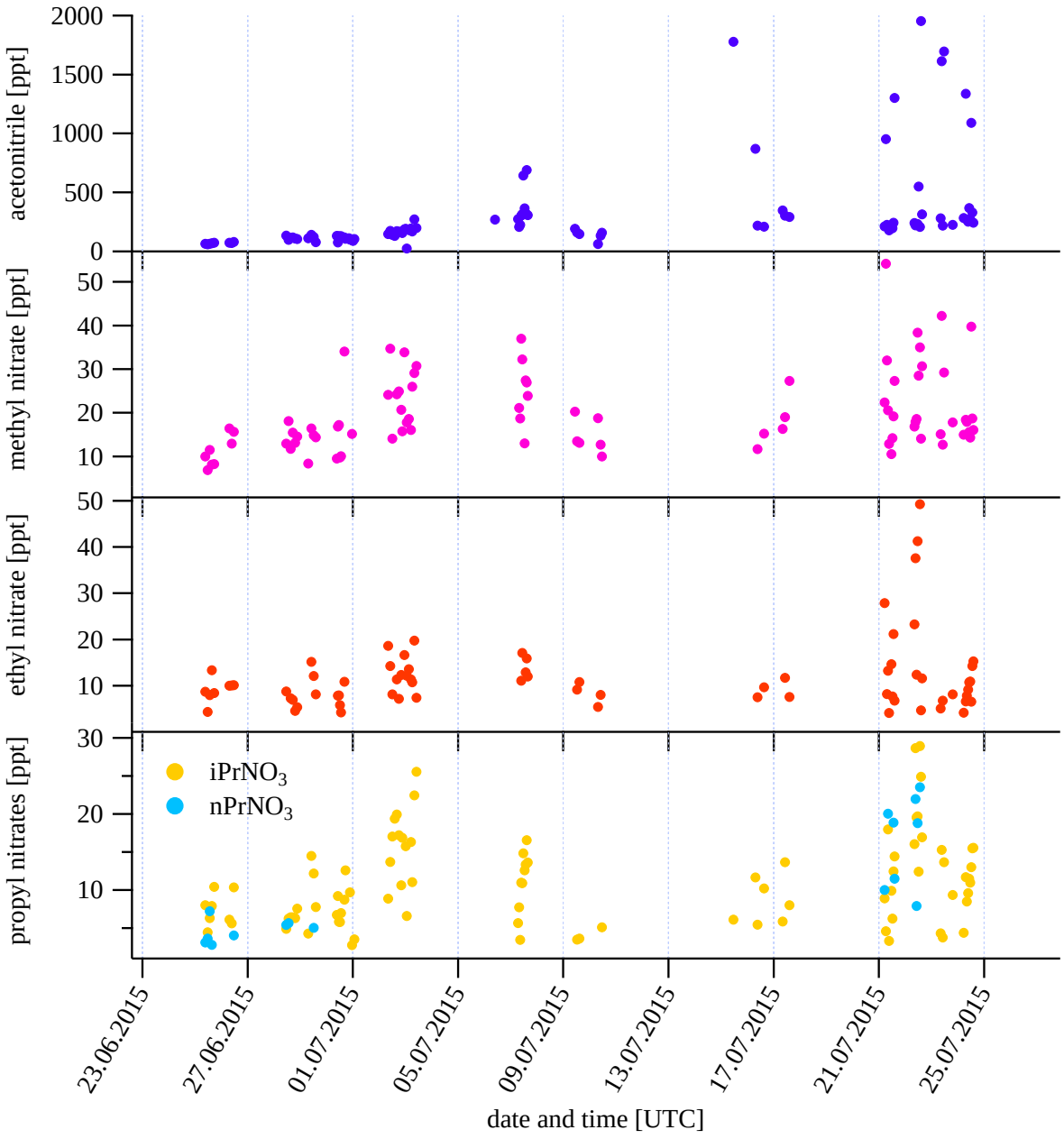

Figure 5-3: Timeline of organic nitrogen compounds from WAS

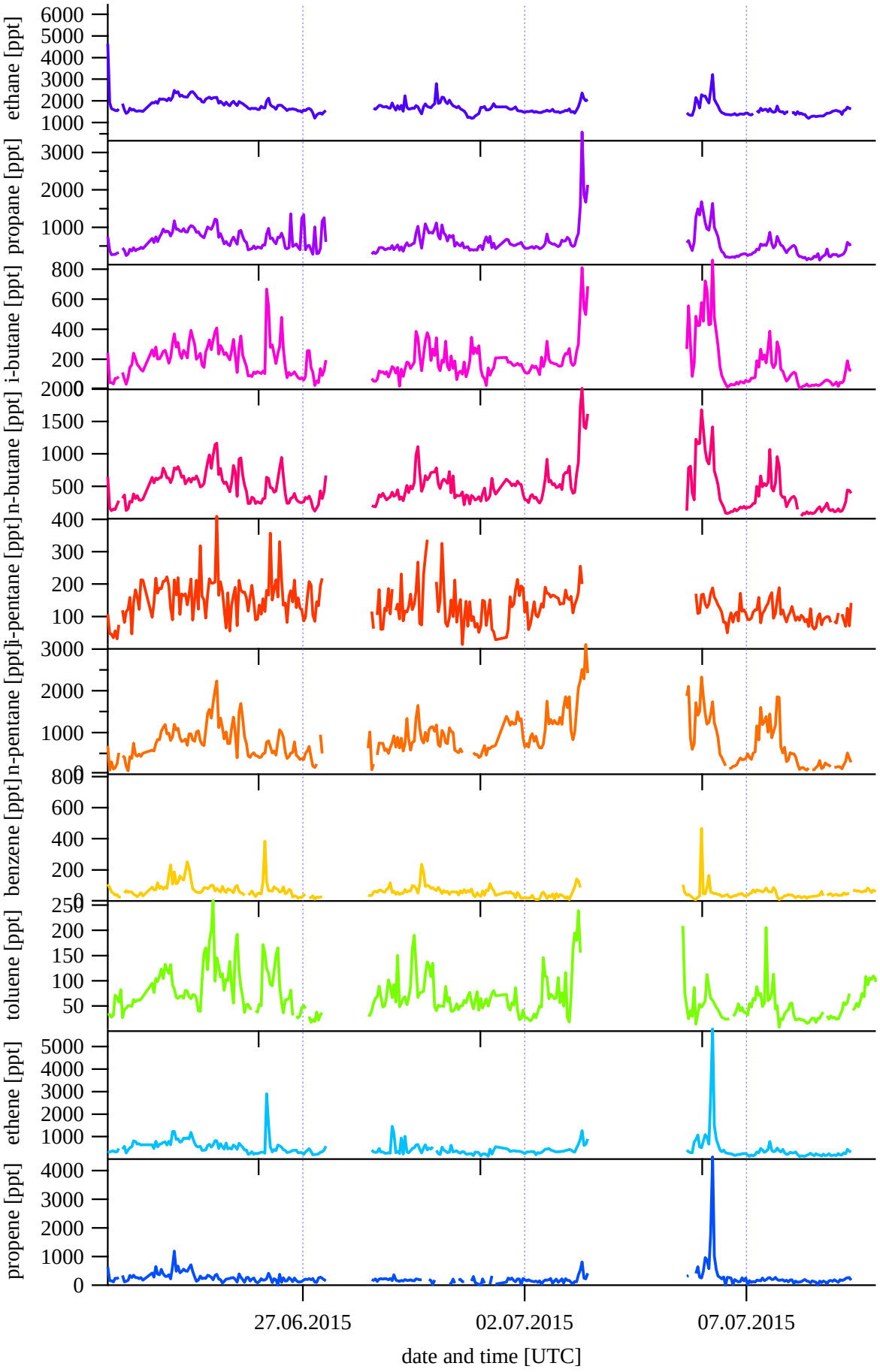

Figure 5-4: Timeline of NMHC measurements

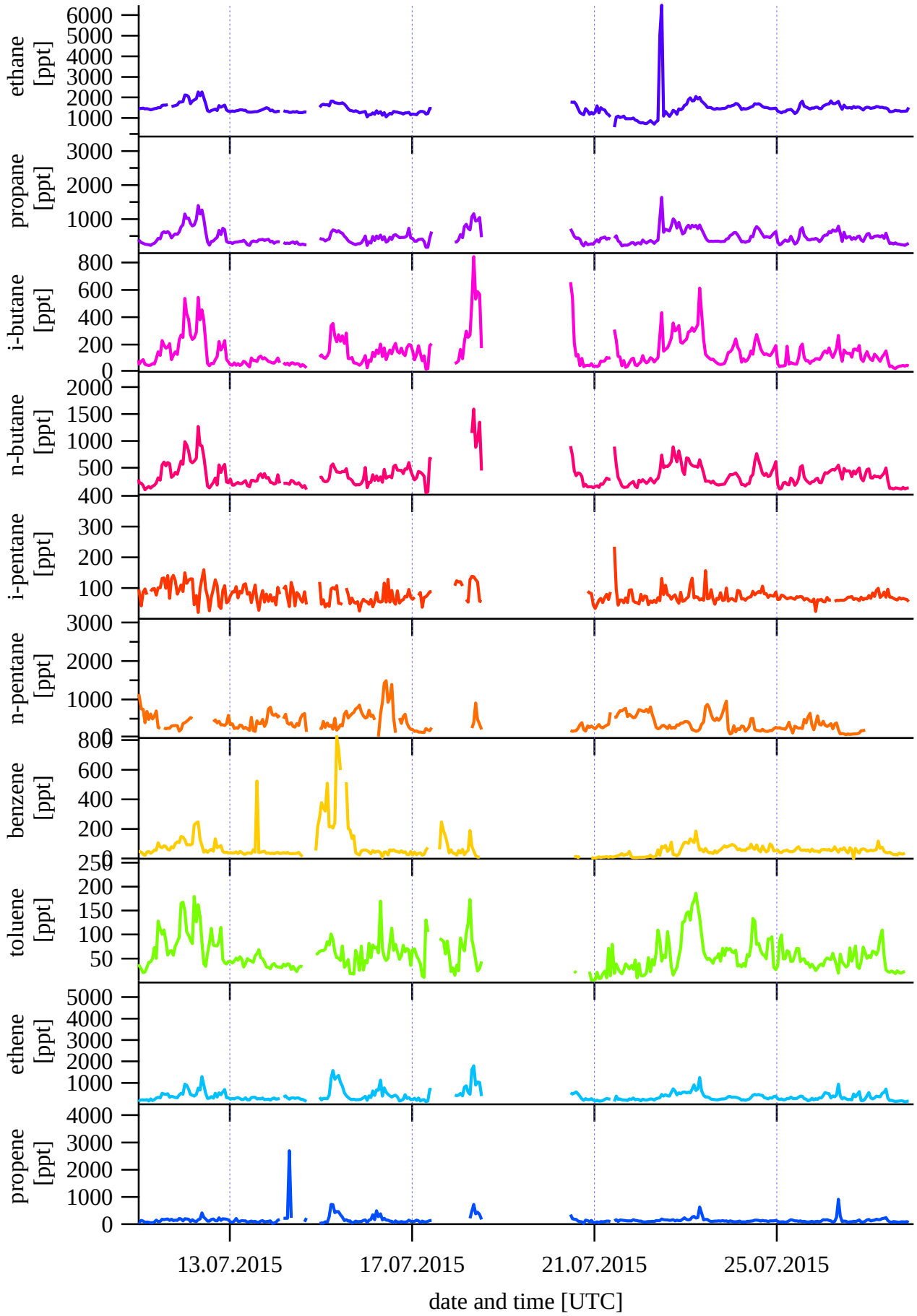

Figure 5-5: Timeline of NMHC measurements

In summer 2011 the GC-FID system was operated during the PARADE campaign which was also conducted in the same location. The average NMHC mixing ratios are shown in Table 5-1. During NOTOMO the mixing ratios of ethane, propane, *i*-butane, *n*-butane, ethene and propene were higher by factors of 1.4-2.6 compared to data from 2011. The aromatics were slightly lower during NOTOMO. Overall, this is in contrast to the results from von Schneidemesser et al. 2010 who found a decreasing trend in long-term measurements of NMHCs from the last years. However, the NOTOMO and PARADE data reflect only limited periods, which are also subject to seasonal cycles and local fluctuations.

During NOTOMO, *n*-Pentane showed unusual high mixing ratios compared to other NMHCs which are expected to decrease in atmospheric abundance with increasing chain length in processed air masses. Also compared to PARADE the mixing ratios were higher by a factor of 3.

The typical European emission ratio of *i*-butane/*n*-butane is between 0.4 and 0.6. The comparison of the two campaigns showed a lower ratio during NOTOMO (0.4; PARADE=0.56).

The reported mixing ratios of organic nitrogen compounds represent averaged values of two individual measurements of the canisters. The relative standard deviation between single measurements was between 10 and 20% and is within measurement uncertainty. No correlations with measurement conditions which could have influenced the results in any direction were found. The sample temperature during analysis was held constantly at 40 °C and the pressure decrease between single measurements was in agreement with sampling volume of the preconcentration system. Furthermore there was no regularity found for the individual measurements resulting in either the higher or the lower mixing ratio. Accordingly systematic errors are excluded to explain the discrepancy between repetitive measurements of the samples.

Methyl-, ethyl- and *i*-propyl nitrates were regularly observed in WAS. *n*-Propyl nitrate was found in 16 samples. *i*-Butyl nitrate was not included in the table and the figures because its mixing ratios were below the LOD in most samples. It was observed in 5 samples with mixing ratios ranging from 2-6 ppt.

Sobanski et al. (2017) measured total alkyl nitrates during the campaign which varied between 0-1 ppb. The light chained alkyl nitrates measured from canisters account for 2-75% of total alkyl nitrates with 22% on average.

The average mixing ratios of alkyl nitrates are in the same order of magnitude as measurement by Flocke in 1988 at *Schauinsland/ Black Forrest*, a site comparable to *Kleiner Feldberg* in southern Germany.

During NOTOMO alkyl nitrate abundancies were found to be decreasing with increasing chain length. In contrast at *Schauinsland i*-propyl nitrate showed the highest mixing ratios.

Table 5-1: Overview of the VOC results from NOTOMO and PARADE campaigns. Units are in ppt

	NOTOMO 2015			PARADE 2011		
Compound	ave ± SDEV	min	max	ave ± SDEV	min	max
Ethane	1572 ± 402	559	6482	602 ±362	303	7230
Propane	536 ± 296	123	3545	307±177	107	2442
i-Butane	162 ± 128	7	860	120±126	22	1326
n-Butane	413 ± 265	36	2012	211±146	49	1387
i-Pentane	105 ± 53	13	410	218±140	41	962
n-Pentane	613 ± 444	37	3107	182±128	28	1004
Benzene	66 ± 72	1	824	77±29	26	294
Toluene	63 ± 39	4	258	92±55	17	413
Ethene	419 ± 349	98	5780	294±369	27	4779
Propene	199 ± 2428	2	4475	169±251	31	2130
Acetonitrile	301 ± 376	25	1953			
Methyl nitrate	20 ± 9	7	54			
Ethyl nitrate	12 ± 8	4	49			
i-Propyl nitrate	11 ± 6	3	29			
n-Propyl nitrate	11 ± 7	3	24			

5.2.1 Diel cycles

The diel cycles for the entire campaign are displayed in Figure 5-6 and Figure 5-7 as box and whisker plots. The NMHC mixing ratios showed only a weak dependency on the day time. A slight increase and enhanced variability in the morning hours (5-10 UTC; UTC = local time – 2 h) was observed especially for more reactive components with shorter lifetime such as ethene and propene. This increase can be explained by the extension of the planetary boundary layer and the enhanced transport towards the hilltop after sunrise rather than rush hour traffic because a regular afternoon rush hour effect was not observed. 80% of the campaign was dominated by air masses coming from wind directions between 225° and 135° where the surrounding area is semi-rural and the direct influence of anthropogenic sources is attenuated.

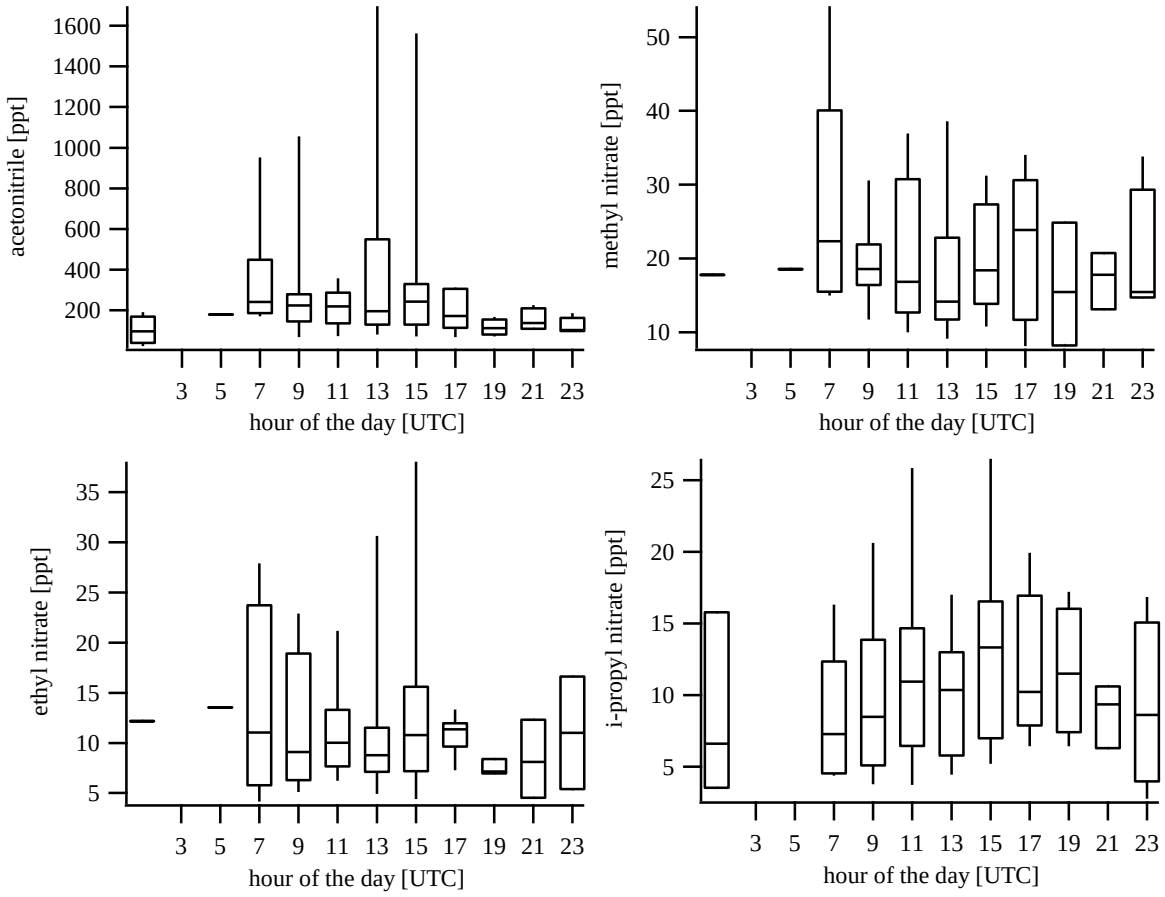

Figure 5-6: Diel variation of organic nitrogen compounds. Vertical lines within the boxes represent mean values, 25% of the data lies above the lower limit of the box, 75% below the upper limit, whiskers represent 10% and 90% of the data points. (UTC = local time – 2 h)

Median acetonitrile mixing ratios were slightly higher during daytime compared to night time. The mean values were affected by single measurements at the end of the campaign. This is indicated by extremely high whiskers which represent occasionally occurring peaks of acetonitrile.

Methyl and ethyl nitrate showed changing median mixing ratios along with high variability throughout the days rather than significant diel variation. This was in agreement with measurements of total alkyl nitrates of Sobanski (2017) and Flocke (1991).

Median *i*-propyl nitrate mixing ratios start to increase at around 9:00 in the morning with maximum values at 15:00 (local time). This clearly shows a photochemically driven daytime production of this compound.

It is in agreement with the consideration that the branching ratio of 0.05 for the production of *i*-propyl nitrate is about twice as for the production of *n*-propyl nitrate and more than a factor of 3.5 in comparison to the production of ethyl nitrate.

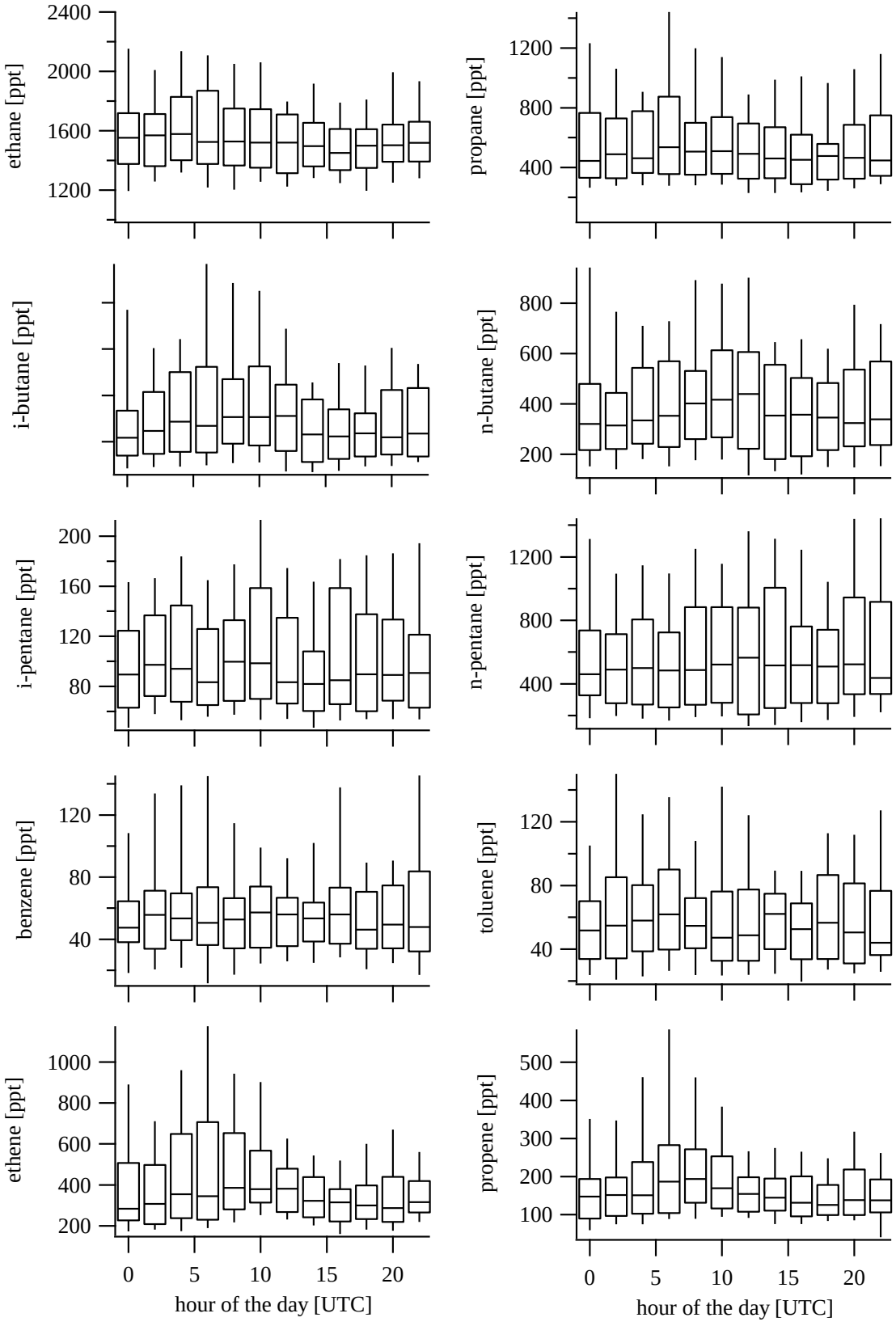

Figure 5-7: Diel cycles of NMHC. Vertical lines within the boxes represent mean values, 25% of the data lies above the lower limit of the box, 75% below the upper limit, whiskers represent 10% and 90% of the data points. (UTC = local time – 2 h)

5.2.2 Acetonitrile

Acetonitrile is a marker compound for biomass burning and anthropogenic pollution. The zoom of a wind rose (< 400 ppt) in Figure 5-8 shows the dependency of acetonitrile mixing rations on wind direction. The cities of Frankfurt Mainz and Wiesbaden are upwind of the Taunus observatory in the sector between 135° and 225°. Air masses reaching the site from this area always showed elevated mixing ratios of acetonitrile (200-400 ppt). Air masses from less urban areas (225°-315°) showed lower acetonitrile mixing ratios of 0-300 ppt. The few peaking mixing ratios (400-2000 ppt) observed at the end of the campaign (see Figure 5-3) were excluded from this plot to put emphasis on the general situation. Air masses with those high mixing ratios were associated with wind directions from both, rural and urban sectors, and were considered as exceptions. The acetonitrile mixing ratios were in the same order of magnitude as found by Hamm & Warneck 1990 who measured average mixing ratios of 340 ppt in Mainz and 147 ppt in Deuselbach, a rural location 100 km west of Mainz.

Other dependencies were not found for acetonitrile. Although its water solubility is high and one could expect wash out or wet depostition as physical removal process, no trend with humidity was found. During rain events no samples were taken.

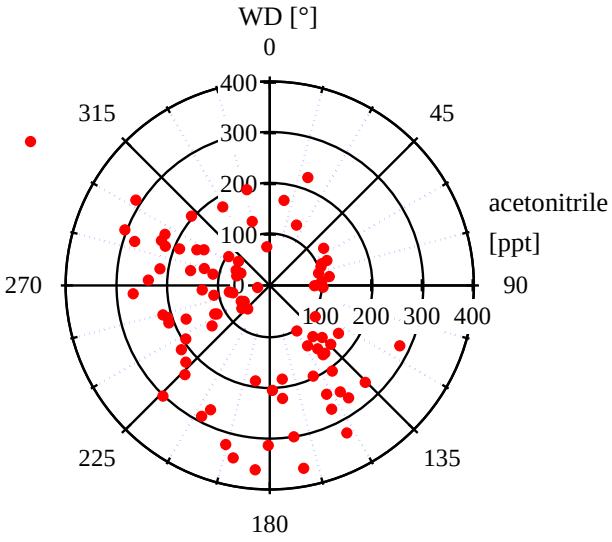

Figure 5-8: Wind rose of acetonitrile measurements

5.2.3 Photochemistry during the campaign

To compare different photochemical scenarios during the campaign two timeframes were chosen, which showed stable meteorological conditions over two days (Figure 5-2). A warm and dry period with air masses coming from a wind sector dominated by urban surrounding on the 1st and 2nd July 2015 showed generally higher mixing ratios for NMHCs and NO_2. Also ozone reached high levels of more than 95 ppb in the afternoon. In contrast, the overall meteorology from 12th and 13th July was wet, cloudy and cold. Figure 5-9 comprises different methods to have a closer look at the photochemical situation and history.

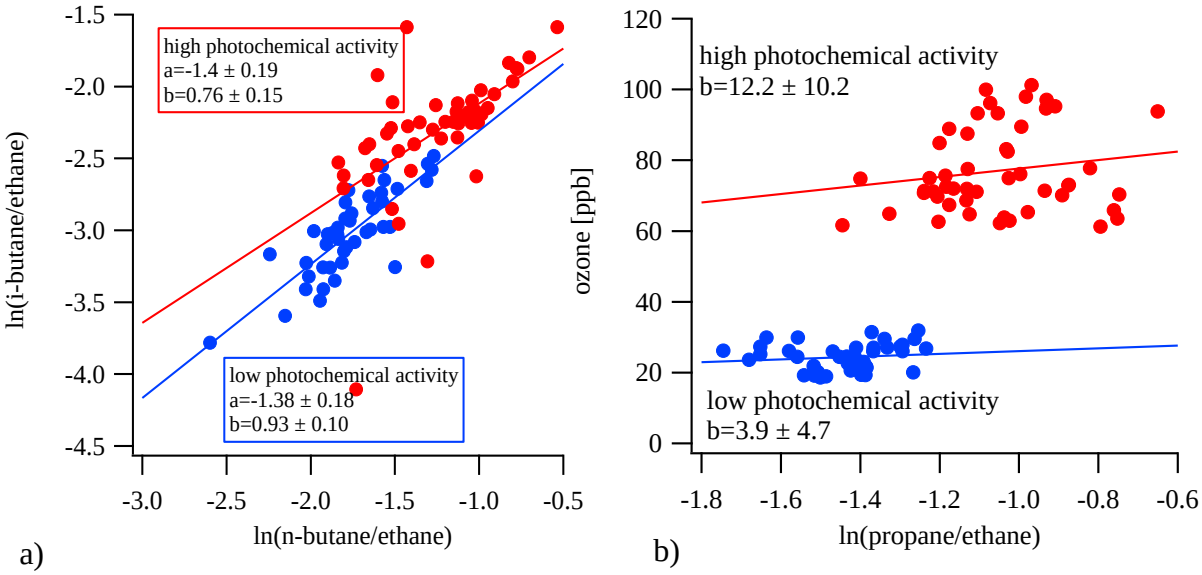

Figure 5-9: Plot of a) logarithmic ratios of ln(i-butane/ethane) vs ln(n-butane/ethane) and b) ozone vs. l(propane/ethane) separated for days with high (red) and low (blue) photochemical activity.

Plot a) shows ln(*i*-butane/ethane) vs. ln(*n*-butane/ethane). In red are the data points from the days with high photochemical activity. The data points scatter between -3 and -1.5 on the axis of ordinates and -1.5 and -0.5 on the abscissa and showed a slope of 0.76 (R^2=0.35). Lower values for the logarithmic ratios can be observed for the time frame with lower photochemical activity (ordinate: -4.0—2.5; abscissa: -2.5—1.5) with a slope of 0.93 (R^2=0.67). High tropospheric ozone mixing ratios indicated high photochemical activity from 1st to 2nd July. Nevertheless the red data shows more recently emitted and less processed air masses (red) in comparison to the data selection of the 12th and 13th July which shows more oxidized air masses. This is in agreement with the wind direction which showed that in red the air masses were coming directly from the urban center of the Rhine-Main area. Although photochemistry is low during the second time frame, the air masses are characterized by enhanced photochemical processing which is due to more rural sources and longer processing time after emission. Moreover

the values of R^2 are higher for the blue and lower for the red data selection and showed the influence of sources by high variability of emissions vs. photochemical processing. The slopes for the two different data selections are in the range of the calculated slopes for OH chemistry (0.88). NO_3 measurements showed mixing ratios up to 40 ppt (9.8×10^8 molecules cm^{-3}) during the timeframe with high photochemical activity. At these levels NO_3 radical driven chemistry of NMHC is negligible and does not have significant influence on the lifetime in comparison to OH.

Furthermore Figure 5-9 b) shows the correlation between ozone and the natural logarithm of the propane/ethane ratio which is a proxy for air mass age. As already described in chapter 3.2.3, this is a method to show if the conditions are ozone forming or depleting (Parrish et al. 2004). The lower the ln of the NMHC ratio is, the older the air mass is. The positive correlation of ozone with ln(propane/ethane) during both periods showed ozone depleting regimes. When the photochemical activity was mitigated and air masses reached the station from rural regions the slope of the correlation is 3.9 with R^2=0.02. The slope for the data selection during high photochemical activity was higher by a factor of about 4. However, source influences by nearby located urban areas were stronger masking the effect of ozone production. Another factor is the strong emission of biogenic VOCs like isoprene and other terpenes at warm and dry conditions. These compounds are depleted by ozonolysis while ozone is depleted, as well.

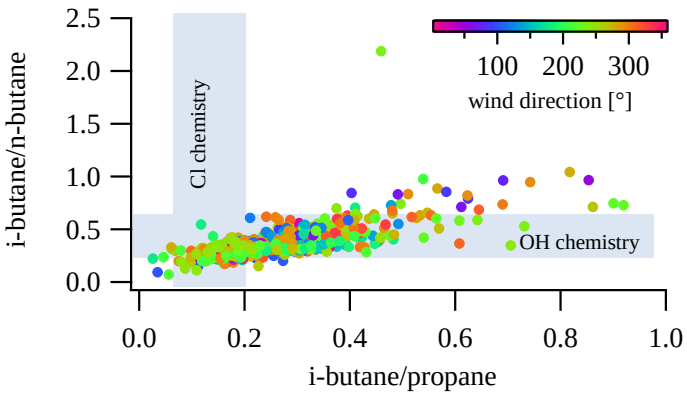

Figure 5-10: Diagram of *i*-butane/*n*-butane vs. *i*-butane/propane showed OH as dominant oxidant

Figure 5-10 shows the ratios of *i*-butane/*n*-butane vs. *i*-butane/propane for the complete campaign. *i*-Butane and *n*-butane have comparable reaction rate coefficients with OH but differ in their reaction rate coefficient with Cl radicals. During transport and photochemical processing with OH radical their ratio is expected to stay constant. The typical northern hemispheric emission ratio is 0.4-0.6. Propane and *i*-butane have comparable

reaction rate coefficient with Cl but differ in the reaction with OH, meaning their ratio stays constant during reaction with Cl but changes with OH processing.

The data throughout the campaign lay in the highlighted area for OH chemistry which is also emphasized by the slope of the logarithmic ratio. During the campaign no significant influence of other oxidizing radicals than OH was found.

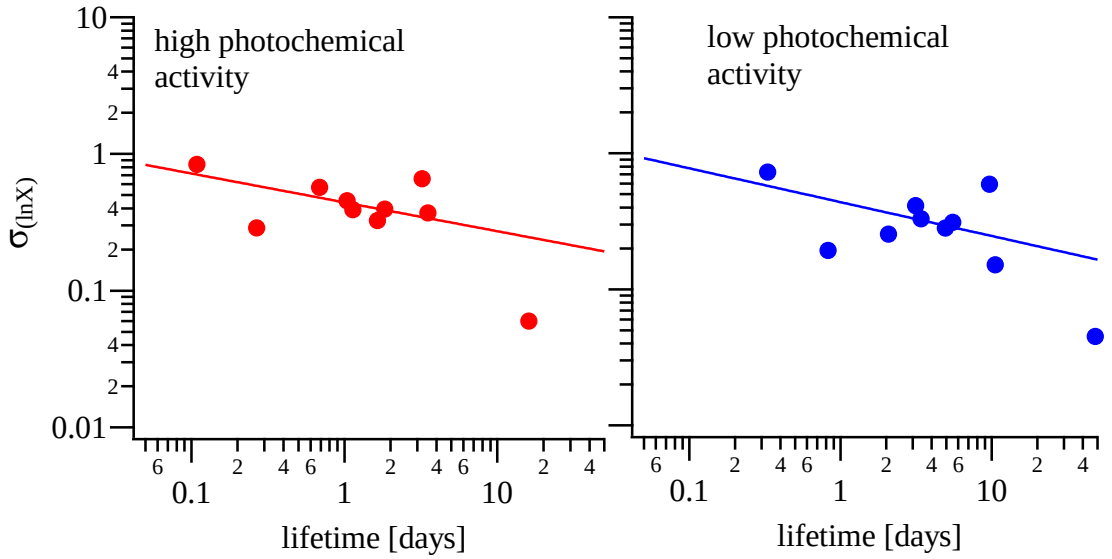

Figure 5-11: Lifetime-variability plots for NOTOMO under high and low photochemistry. Solid marker show all measured NMHC

Table 5-2: Fitting parameters for NOTOMO lifetime-variability plots

Parameters	High photochemical activity	low photochemical activity
	OH: $3x10^6$ molecules cm^{-3}	OH: 10^6 molecules cm^{-3}
	O_3: 80 ppb	O_3: 25 ppb
A	0.44	0.43
b	0.21	0.25
χ	0.254	0.255

A comparison of the lifetime-variability relationship for the two different time frames is shown in Figure 5-11. The markers show the results of all measured hydrocarbons. Lifetimes were calculated assuming OH concentrations of $3x10^6$ molecules cm^{-3} and aver-

age O_3 of 80 ppb (≈ $2x10^{12}$ molecules cm^{-3}) for high photochemical activity. For low chemical activity OH was assumed to be and the average O_3 was 25 pbb (≈ $6x10^{11}$ molecules cm^{-3}) during these days. Fitting was calculated based on $\sigma(\ln X) = A \cdot \tau^{-b}$ and the parameters are listed in Table 5-2 (detailed description can be found in chapter 1.3 and 3.2.5).

As a reminder, exponents of $b \approx 0$ show no correlation between variability and estimated lifetimes and are typical for measurement location which are highly influenced by source and emission processes. $b \approx 0.5$ are typical for rural locations (Jobson et al. 1998, chapter 1.3)

The results from lifetime-variability were in agreement with analysis from logarithmic ratios. Though the b exponents from 1st - 2nd July and 12th - 13th July are comparable the small difference is in agreement with air mass age and photochemical procession as observed with the method of logarithmic ratios. The time frame with high photochemical activity showed less processed and more source influenced air masses with b = 0.21, while the timeframe with low photochemical activity with b = 0.25 described further oxidized air masses with longer travel times. During PARADE b was around 0.3 for the entire campaign. This concludes that the pollutants were more degraded which is also mirrored in generally lower absolute mixing ratios of NMHCs in 2011 (Table 5-1).

As described in chapter 3.2.5 A behaved as a function of the PBL fraction. Applying this to the NOTOMO results would lead to the conclusion that the PBL fraction was about 30%.

χ^2 as proxy for fit quality are quite high in comparison to CYPHEX results. Nevertheless, under the assumed radical concentration these were the optimum values for χ^2 (Table 5-2). Different test calculations with different radical compositions, including Cl and NO_3 did not improve χ^2.

5.2.4 Alkyl nitrates

Alkyl nitrates are formed by photochemically induced reactions of NMHCs and NO_x. As described in Bertman et al. (1995) the ratios of alkyl nitrates and their mother hydrocarbon can give information about air mass age. If alkyl nitrate sources are exclusively from photochemical oxidation of mother alkanes, the ratios will vary depending on the competition between production and removal of organic nitrates by photolysis (reaction [X] and [XI]).

The temporal evolution of alkyl nitrates can kinetically be described by equation [25] which integrates to equation [26] giving the ratio of the nitrate and the initial hydrocarbon. The factor β comprises the branching ratio of the alkyl nitrate formation from peroxy radicals and the fraction of the position of the H abstraction during the initial reaction of the hydrocarbon with OH. Assuming no nitrates have been produced at t=0 the second term (in braces) is also zero. Therefore the ratio is independent from RH as well.

$$RH \xrightarrow{\beta k_A} RONO_2 \qquad [X]$$

$$RONO_2 \xrightarrow{k_B} \text{products} \ldots \qquad [XI]$$

$$\frac{d[RONO_2]}{dt} = \beta k_A [RH] - k_B [RONO_2] \qquad [25]$$

$$\frac{[RONO_2]}{[RH]} = \frac{\beta k_A}{k_B - k_A}\left(1 - e^{(k_A - k_B)t}\right) + \left\{\frac{[RONO_2]_0}{[RH]_0} e^{(k_A - k_B)t}\right\} \qquad [26]$$

Table 5-3: Kinetic data used for calculations based on Bertman et al. (1995)

	Ethyl	*i*-Propyl
β	0.014	0.029
k_A	0.24×10^{-12}	1.1×10^{-12}
k_B	1.11×10^{-6}	1.61×10^{-6}

The NOTOMO data set showed a broad distribution of different air mass ages. Furthermore the ethyl nitrate/ethane ratio is higher than predicted.

A closer look at the sample distribution within this figure showed that air masses coming from the wind direction between 135° and 225°, where the urban centers are located, concentrated between 0.5 and 1 day and are closer to the hypothetical line than air

masses reaching the site from the rural surrounding. Those samples are more complex and scattered over the range of air mass ages.

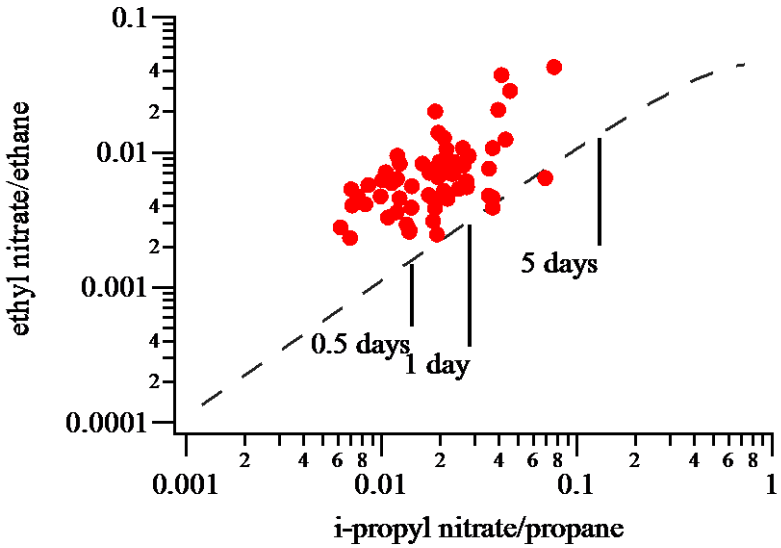

Figure 5-13: Correlation plot of ratios of nitrates with mother alkanes in comparison with calculated temporal evolution. The dashed line shows the calculated theoretical progression of the ratios of ethyl nitrate/ethane and *i*-propyl nitrate/propane. 0.5; 1 and 5 days of chemical processing are highlighted in the diagram

Due to photochemical production as common source a positive correlation of O_3 with alkyl nitrates is expected and was found in other studies (Flocke, Volz-Thomas, and Kley 1991; O'Brien et al. 1995). Figure 5-12 shows the correlation plots of ozone with methyl, ethyl and *i*-propyl nitrate for the entire campaign. Although the scattering is high, and hence, the coefficients of determination are low all alkyl nitrates showed a positive correlation with ozone. The corresponding fitting parameters are listed in Table 5-4.

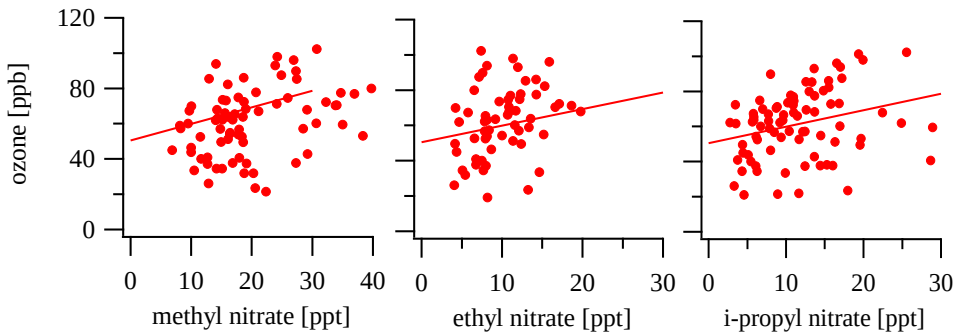

Figure 5-12: Correlation plots of ozone with methyl, ethyl and propyl nitrate

The production rates of alkyl nitrates $P(AN_i)$ of ethyl and propyl nitrate were calculated using [27] (see also chapter 3.2) with average mixing ratios of ethane (1572 ppt) and propane (536 ppt) from the entire campaign. Since no methane data was available for NOTOMO an average mixing ratio of 1.8 ppm was assumed according to PARADE data and average global mixing ratios (Sobanski et al. 2017; Khalil 2000). OH was assumed to be 10^6 molecules cm^{-3} (Spivakovsky et al. 2000). Reaction rate coefficients and branching ratios and were taken from Table 1-1 and Table 1-2.

$$P(AN_i) = \alpha_{i(OH)} k_{OH+RH_i} [OH][RH_i] \quad [27]$$

Table 5-4: Fitting parameter for the correlation plots of ozone and alkyl nitrates and calculated production rates.

	Methyl nitrate	Ethyl nitrate	*i*-Propyl nitrate
a	45.1 ± 5.0	45.2 ± 7.0	51.1 ± 4.6
b	0.81 ± 0.2	1.66 ± 0.6	0.94 ± 0.3
R^2	0.11	0.10	0.08
$P(AN_i)$ in [ppt h^{-1}]	0.022	0.019	0.11

The production rates for methyl nitrate were 0.022 ppt h^{-1}, 0.019 ppt h^{-1} for ethyl nitrate and 0.11 ppt h^{-1} for *i*-propyl nitrate. According to this the yields of methyl and ethyl nitrate from photochemical production from their mother alkanes are expected to be equal and the yields of *i*-propyl nitrate is expected to be higher by an order of magnitude. The production rate competes with the reaction rate. On the one hand, a sink for alkyl nitrates is, as for alkanes, the reaction with the OH radical. The reaction rate coefficients are comparable or smaller. Furthermore alkyl nitrates are removed from the atmosphere by photolysis. The relevant kinetic coefficients were already introduced in chapter 3.2 and displayed in Table 3-4. In general the production rates of alkyl nitrates are higher by about 8 orders of magnitude in comparison to the removal. Relatively, the production rates of methyl and ethyl nitrate are comparable. The relative reaction rates for the removal from the atmosphere show that ethyl nitrate is removed twice as fast as methyl nitrate. This goes along with the average mixing ratios observed during NOTOMO which were highest for methyl nitrate. In contrast, the slope which is observed from the ozone correlation plot is highest for ethyl nitrate. Methyl nitrate has the lowest

slope. One explanation is that the background mixing ratios of methyl nitrate are higher due to the higher atmospheric lifetime. The average mixing ratios of ethyl and *i* propyl nitrate are about the same, although the production rate of *i*-propyl nitrate is higher by a factor of about 6 and the removal is only twice in comparison to ethyl nitrate. This stronger impact of photochemistry cannot be observed in the correlation plot with ozone, but becomes visible analyzing the diel cycles shown in Figure 5-6. Furthermore the campaign average mixing ratios of the mother alkanes differed by a factor of 3.

A general view on the importance of short chained alkyl nitrates gives the fraction of total alkyl nitrates (f_{AN}). Figure 5-14 shows f_{AN} from WAS (methyl + ethyl + *i*-propyl nitrate) of total alkyl nitrates (∑AN)from Sobanski et al. 2017.

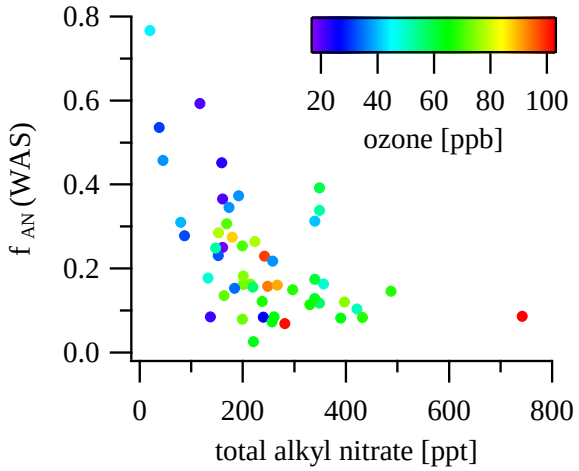

Figure 5-14: fraction of methyl, ethyl and propyl nitrate of total alkyl nitrates

f_{AN} of light chained alkyl nitrates increased with decreasing ∑AN. The data points are color coded for O_3 as marker for photochemical activity. It can be seen that lower ∑AN with corresponding high f_{AN} was observed predominantly at conditions of lower photochemical activity. With increasing O_3 and thus increasing photochemical activity, especially at warm and dry days, ∑AN increased with decreasing relevance of methyl, ethyl and *i*-propyl nitrate. This is due to enhanced BVOC emission at these conditions. The branching ratio for typical plant emitted hydrocarbons like isoprene, pinenes, limonene or myrcene are higher (α = 0.07 - 0.23) as the ones of saturated, short chained mother alkanes (Perring et al. 2013). During NOTOMO no BVOCs were measured. However, from data from the PARADE campaign in 2011 it is known that BVOCs can account for up to 80% of the noon time ∑AN production (Sobanski et al. 2017).

5.3 Plant cuvette experiments

Since the NOTOMO campaign was conducted in a rural environment and was influenced by air masses coming from less populated areas and which are rich in vegetation, a plant cuvette experiment was made at the laboratory to investigate the emissions of organic nitrogen containing compounds. The experimental set up was introduced in chapter 2.4.

In Figure 5-15 and Figure 5-16 the results of the different measurements are displayed. From all observed peaks acetonitrile was the only one which was identified on the GC-NCD system. All other peaks had not been observed before and could not be identified during the experiment. In reference to the retention times determined previously, it can be ruled out that these were alkyl nitrates. They were labelled by their retention time. Furthermore the expected TMA was only observed during the measurement of mountain ash. For the chenopodia all compounds decreased with time following introduction into the cuvette. Higher mixing ratios (MR) during the first run were due to mixing with lab air after opening the cuvette or contact between foil and plant during the exchange. Only the peak at RT 3.35 min is lower in the beginning and increasing with measurement time. This compound was the dominating one emitted by all plants which have been part of the experiment. The typical mixing ratio was between 10 and 20 ppt based on the calibration of acetonitrile. The comparison of different fertilizer concentrations for the chenopodia showed slightly higher mixing ratios for higher fertilizer concentrations. Acetonitrile mixing ratios typically ranged between 2 and 5 ppt.

Hawthorn and pear showed comparable behavior. The measurement of mountain ash showed an increased variety of compounds and also different dominating peaks.

A peak at RT 4.45 was observed for the first time and higher than the most of the compounds. Especially high mixing ratios up to 130 ppt were observed at RT 4.62 (right axis in Figure 5-16). The increasing MR during the measurement showed that these compounds are emitted by the plants as well as RT 3.35. The decline in the end of the experiment lead to the assumption that a diel cycle is possible or reservoirs of those compounds ran out.

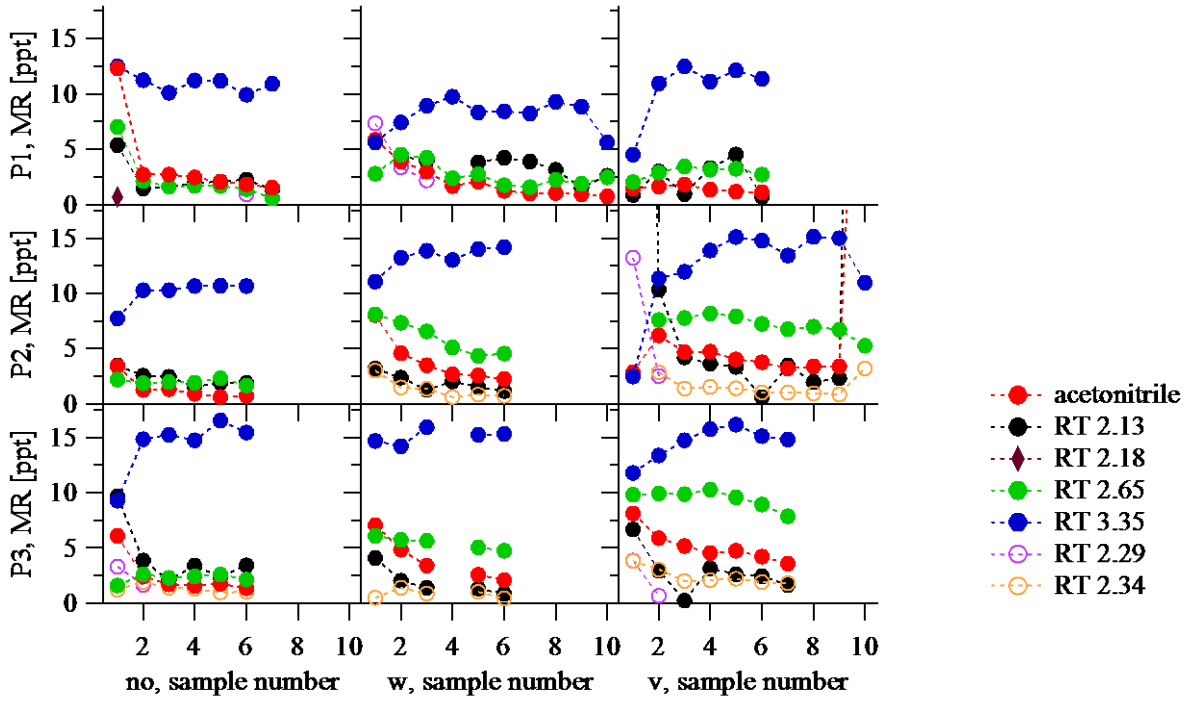

Figure 5-15: Results from the measurements of individually treated *chenopodia*.

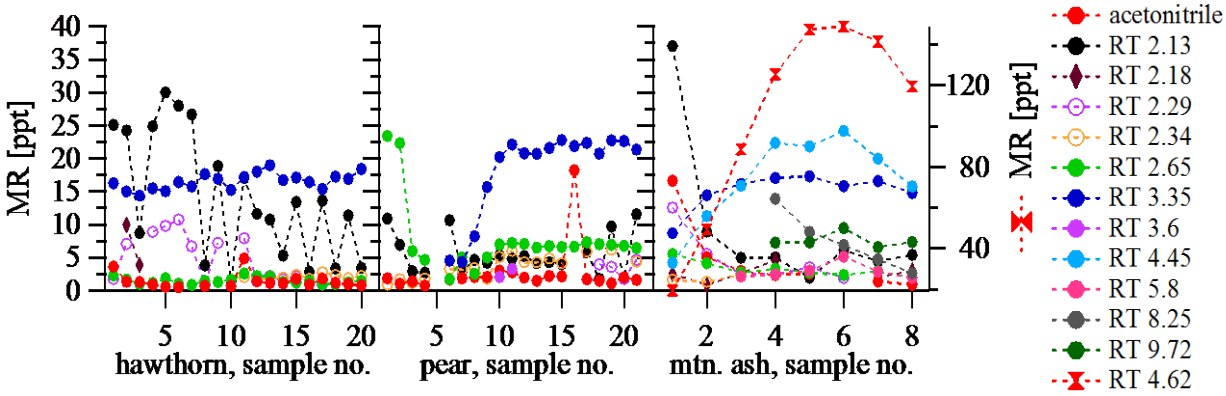

Figure 5-16:Results from the measurements of *hawthorne*, *pear* and *mtn. ash*

Conclusions

The experiment showed that plants are sources for a variety of organic nitrogen containing compounds. But the alkyl nitrates which are part of the analysis of this doctoral thesis were not found to be emitted from the plants. Therefore we assumed that the alkyl nitrates measured during the NOTOMO campaign were products from the photochemi-

cal depletion of NMHCs and direct emissions which could have had influence on the results can be excluded.

Although, the results from the cuvette measurements are not exact according to mixing ratios and no identification of the measured peaks was possible, the results amongst the individual plants showed consistency.

This laboratory experiment showed that the GC-NCD system coupled with a preconcentration system is able to measure a diversity if nitrogen containing compounds at a sufficient chromatographic resolution.

It can run several hours performing quasi-online measurements. The limiting factor was the consumption of liquid nitrogen for cryogenic enrichment and focusing. A 50 l tank last about 25-30 runs.

5.4 Summary

In summer 2015 the NOTOMO campaign was performed at the *Taunus Observatory* at the *Kleiner Feldberg*, Tanus in Germany. This location is surrounded by semi-rural environment in the northwestern-norther area and the area from south-east to southwest is dominated by the urban and highly populated Rhine-Main center. GC-FID measurements provided a four-week data set of NMHCs and WAS were analyzed for nitrogen-containing organic compounds.

On average NMHCs were found to be enhanced in comparison to the PARADE campaign measurements in 2011 not reflecting the downward trend from long term NMHC measurements.

Two timeframes with stable meteorological conditions were analyzed in more detail concerning photochemistry and air mass age.

At the 1st and 2nd July the weather was dry and warm giving the conditions for high photochemical activity. During these days the air masses were characterized by more recent emission of NMHCs from the urban center. On the 12th and 13th July the conditions were cloudy and wet and less photochemical activity was expected. During this time the air masses were characterized by a more aged NMHC composition. Analysis showed ozone depleting regimes for both times frames. Nevertheless, for the high photochemical activity there might have been a masking effect by enhanced variability by direct source influences. No evidence of chlorine chemistry was found during NOTOMO.

Alkyl nitrate and acetonitrile measurements showed good agreement with other studies in this area or comparable locations. Alkyl nitrate data showed air mass ages of 0.5 to 5 days and the fraction of methyl-, ethyl, and *i*-propyl nitrate from total alkyl nitrate

showed a dependency on photochemical activity. The magnitude of the fraction increased with lower photochemical activity, because during these days biogenic emission became more important. The alkyl nitrate production from these compounds exceeded those of the lower alkanes.

6 Summary

The aim of this work was to establish and evaluate an analysis system for the determination of organic nitrogen containing trace gases in the atmosphere. This system was assembled from an ENtech preconcentrator, a gas chromatograph and a nitrogen chemiluminescence detector. It is able to measure acetonitrile, alkyl nitrates and organic amines at low ppt levels (1.5-3 ppt) from measurements of WAS and quasi-online with a temporal resolution of 30 min. We also found out the expected equimolar response and equal sensitivity of the chemiluminescence detector was not achieved because of different trapping efficiencies of the measured compounds. Therefore each component had to be calibrated separately.

In addition a GC-FID system was operated giving information on NMHCs. The combination of the NMHC and organic nitrogen compounds are explored.

The results of three different measurement campaigns and projects are reported in this thesis. The general characteristics of the air analyzed were as diverse as they could be.

During CYPHEX highly photochemically processed air masses were measured and the contrast between the two distinct flow regimes from Western and Eastern Europe were examined and compared to European emission inventories. NMHC analysis showed that transport times varied from 48 up to 120 h and the chemical composition of these strongly aged air masses is to some extent comparable to measurements at high altitudes, where only chemical processes play a role and source effects are negligible.

As far as we know this thesis reports the first measurements of short chained alkyl nitrates ($< C_5$) from the Mediterranean area.

The GC-NCD system was operated for measurements of WAS from the CARIBIC projects. One year of global measurements in the UT/LS region showed that the important biomass burning marker acetonitrile has a decreasing trend going from the troposphere to the stratosphere. Its annual cycle showed a maximum during northern hemispheric summertime due to enhanced biomass burning and forest fires. The strong convective uplift by the ITCZ over Africa and the influence of the Asian summer monsoon were shown within the data set. The Pacific ocean was identified as an important source of methyl nitrate.

During NOTOMO the comparative analysis during two different timeframes the measurements of NMHC and alkyl nitrates showed the contrast between source influenced and processed air masses at transport times of 0.5 to 5 days. The fraction of C_1-C_3 alkyl nitrates of total alkyl nitrates ranged from 3-80% depending on meteorological and photochemical conditions. A plant cuvette experiment showed that plants are emitters of

organic nitrogen containing compounds. Nevertheless, the examined alkyl nitrates were not found amongst the observed compounds and an influence of the results by direct emissions can be excluded.

Bibliography

Akagi, S. K., Yokelson, R. J. , Wiedinmyer, C., Alvarado, M. J., Reid, J. S., Karl, T., Crounse, J. D.,Wennberg, P. O.: Emission Factors for Open and Domestic Biomass Burning for Use in Atmospheric Models, Atmospheric Chemistry and Physics 11 (9): 4039–72. doi:10.5194/acp-11-4039-2011, 2011.

Anderson, R. S., Huang, L., Iannone, R., and Rudolph, J.: Measurements of the $^{12}C/^{13}C$ Kinetic Isotope Effects in the Gas-Phase Reactions of Light Alkanes with Chlorine Atoms, The Journal of Physical Chemistry A 111 (3): 495–504. doi:10.1021/jp064634p, 2007.

Anderson, R. S., Huang, L., Iannone, R., Thompson, A. E., and Rudolph, J.: Carbon Kinetic Isotope Effects in the Gas Phase Reactions of Light Alkanes and Ethene with the OH Radical at 296 ± 4 K, Journal of Physical Chemistry A. doi:10.1021/jp0472008, 2004.

Andreae, M. O., and Merlet, P.: Emission of Trace Gases and Aerosols from Biomass Burning, Global Biogeochemical Cycles 15 (4): 955–66, 2001

Arsene, C.. Bougiatioti, A, Kanakidou, M., Bonsang, B., and Mihalopoulos, N., Tropospheric OH and Cl Levels Deduced from Non-Methane Hydrocarbon Measurements in a Marine Site, Atmospheric Chemistry and Physics Discussions 7 (3): 6329–56. doi:10.5194/acpd-7-6329-2007, 2007.

Assonov, S. S., Brenninkmeijer, C. A. M., Schuck, T., and Umezawa, T.: N_2O as a Tracer of Mixing Stratospheric and Tropospheric Air Based on CARIBIC Data with Applications for CO2, Atmospheric Environment 79, Elsevier Ltd: 769–79, doi:10.1016/j.atmosenv.2013.07.035, 2013.

Atkinson, R., Baulch, D. L., Cox, R. A., Crowley, J. N., Hampson, R. F., Hynes, R. G., Jenkin, M. E., Rossi, M. J., and Troe, J.: Evaluated Kinetic and Photochemical Data for Atmospheric Chemistry: Volume II -- Gas Phase Reactions of Organic Species, Atmospheric Chemistry and Physics, doi:10.5194/acp-6-3625-2006, 2006.

Atkinson, R.: Kinetics and Mechanisms of the Gas-Phase Reactions of the NO3 Radical with Organic Compounds, The Journal of Physical and Chemical Reference Data. doi:10.1063/1.555887, 1991.

Atkinson, R.: Gas-Phase Tropospheric Chemistry of Volatile Organic Compounds: 1. Alkanes and Alkenes, Journal of Physical and Chemical Reference Data 26 (2), 215–90, doi:10.1063/1.556012, 1997.

Atkinson, R., Aschmann, S. M., Carter, W. P. L., Winer, A. M., and Pitts, J. N.: Alkyl Nitrate Formation from the NO_x-Air Photooxidations of C_2-C_8 *n*-Alkanes, Journal of Physical Chemistry, 86 (20): 4563–69, 1982.

Atkinson, R., and Carter, W. P. L.: Kinetics and Mechanisms of the Gas-Phase Reactions of Ozone with Organic Compounds under Atmospheric Conditions, Chemical Reviews 84: 437–70, doi:10.1021/cr00063a002, 1984.

Atkinson, R., Carter, W. P. L., and Winer, A. M.: Effects of Temperature and Pressure on Alkyl Nitrate Yields in the Nitrogen Oxide (NO_x) Photooxidations of *n*-Pentane and *n*-Heptane, The Journal of Physical Chemistry, doi:10.1021/j100234a034, 1983.

Atkinson, R., Perry, R. A., and Pitts, J. N.: Kinetics of the Reaction of OH Radical with CO and N2O, Chemical Physics Letters 44 (2): 0–4, 1976.

Atlas, E., Pollock, W., Greenberg, J., Heidt, L., and Thompson, A. M.: Alkyl Nitrates, Nonmethane Hydrocarbons, and Halocarbon Gases over the Equatorial Pacific Ocean during SAGA 3, Journal of Geophysical Research 98 (D9): 16933, doi:10.1029/93JD01005, 1993.

Atlas, E.: Evidence for $\geq C_3$ Alkyl Nitrates in Rural and Remote Atmospheres, Nature 331 (6155): 426–28, doi:10.1038/331426a0, 1988.

Baker, A. K., Schuck, T. J., Brenninkmeijer, C. A. M., Rauthe-Schöch, A., F. Slemr, F., van Velthoven, P. F. J., and Lelieveld, J.: Estimating the Contribution of Monsoon-Related Biogenic Production to Methane Emissions from South Asia Using CARIBIC Observations, Geophysical Research Letters 39 (10),doi:10.1029/2012GL051756, 2012.

Baker, A. K., Schuck, T. J., Slemr, F., van Velthoven, P. F. J., Zahn, A., and Brenninkmeijer,: Characterization of Non-Methane Hydrocarbons in Asian Summer Monsoon Outflow Observed by the CARIBIC Aircraft, Atmospheric Chemistry and Physics 11 (2): 503–18, doi:10.5194/acp-11-503-2011, 2011.

Baker, A. K., Slemr, F., and Brenninkmeijer, C. A. M.: Analysis of Non-Methane Hydrocarbons in Air Samples Collected Aboard the CARIBIC Passenger Aircraft, Atmospheric Measurement Techniques Discussions 2 (December 2008): 2377–2401, doi:10.5194/amtd-2-2377-2009, 2009.

Baker, A. K., Traud, S., Brenninkmeijer, C. A. M., Hoor, P., Neumaier, M, Oram, D. E., Rauthe-Schöch, A., Sprung, D., Schloegl, S., Slemr, F., van Velthoven, P. F. J., Werni, H., Zahn, A., Ziereis, H.: Pollution Patterns in the Upper Troposphere over Europe and Asia Observed by CARIBIC, Atmospheric Environment 96: 245–56, doi:10.1016/j.atmosenv.2014.06.010, 2014.

Becker, H. G. O., and Berger, W.: Organikum, Angewandte Chemie. doi:10.1002/ange.19650772420, 2009.

Bertman, S. B., Roberts, J. M., Parrish, D. D., Buhr, M. P., Goldan, P. D., Kuster, W. C., Fehsenfeld, F. C., Montzka, S. A., and Westberg, H.: Evolution of Alkyl Nitrates with Air Mass Age, Journal of Geophysical Research 100 (D11): 22805, doi:10.1029/95JD02030, 1995.

Blake, D. R., and Rowland, F. S.: Urban Leakage of Liquefied Petroleum Gas and Its Impact on Mexico City Air Quality, Science (New York, N.Y.) 269 (5226): 953–56, doi:10.1126/science.269.5226.953, 1995.

Blake, N. J., Blake, D. R., and Swanson A. L.: Latitudinal, Vertical, and Seasonal Variations of C_1-C_4 Alkyl Nitrates in the Troposphere over the Pacific Ocean during PEM-Tropics A and B: Oceanic and Continental Sources, Journal of Geophysical Research 108 (D2): 8242, doi:10.1029/2001JD001444, 2003.

Blake, N. J., Blake, D. R., Wingenter, O. W., Sive, B. C., Kang, C. H., Thornton, D. C., Bandy, A. R., Atlas, E., Flocke, F., Harris, J. M., Rowland, R.: Aircraft Measurements of the Latitudinal, Vertical, and Seasonal Variations of NMHCs, Methyl Nitrate, Methyl Halides, and DMS during the First Aerosol Characterization, Journal of Geophysical Research 104: 21803, doi:10.1029/1999JD900238, 1999.

Bonn, B., von Schneidemesser, E., Andrich, D., Quedenau, J., Gerwig, H., Lüdecke, A, Kura, J., Pietsch, A., Ehlers, C., Klemp, D., Kofahl, C., Nothard, R., Kerschbaumer, A., Jinkermann, W., Grote, R., Pohl, T., Weber, K., Lode, B., Schönberger, P., Churkina, G., Butler, T. M., Lawrence, M. G.: BAERLIN2014 - The Influence of Land Surface Types on and the Horizontal Heterogeneity of Air Pollutant Levels in Berlin, Atmospheric Chemistry and Physics 1–62, doi:10.5194/acp-2016-57, 2016.

Borbon, A., Gilman, J. B., Kuster, W. C., Grand, N., Chevaillier, S., A. Colomb, A., Dolgorouky, C.Gros, V., Lopez, M., Sarda-Esteve, R., Holloway, J., Stutz, J., Petetin, H., McKeen, S., Beckmann, M., Warneke, C., Parrish, D. D., de Gouw, J. A.:Emission Ratios of Anthropogenic Volatile Organic Compounds in Northern Mid-Latitude Megacities: Observations versus Emission Inventories in Los Angeles and Paris, Journal of Geophysical Research Atmospheres 118 (4): 2041–57, doi:10.1002/jgrd.50059, 2013.

Brenninkmeijer, C. A. M., Crutzen, P., Boumard, F., Dauer, T., Dix, B., Ebinghaus, R., D. Filippi, D., Fischer, H., Franke, H., Frieß, U., Heintzenberg, J., Helleis, F., Hermann, M., Kock, H. H., Koeppel, C., Lelieveld, J., Leuenberger, M., Martinsson, B. G., Miemczyk, S., Moret, H. P., Nguyen, H., N., Nyfeler, P., Oram, D., O'Sullivan, D., Penkett, S., Platt, U., Pupek, M., Ramonet, M., Randa, B., Reichelt, M., Rhee, T. S., Rohwer, J., Rosenfeld, K., Scharffe, D., Schlager, H., Schumann, U., Slemr, F., Sprung, D., Stock, P., Thaler, R., Valentino, F., van Velthoven, P., Waibel, A., Wandel, A., Waschitschek, K., Wiedensohler, A., Xueref-Remy, I., Zahn, A., Zech, U., Ziereis, H.: Civil Aircraft for the Regular Investigation of the Atmosphere Based on an Instrumented Container: The New CARIBIC System, Atmospheric Chemistry and Physics Discussions 7 (2): 5277–5339. doi:10.5194/acpd-7-5277-2007, 2007.

Carpenter, L. J., Liss, P. S., and Penkett, S. A.: Marine Organohalogens in the Atmosphere over the Atlantic and Southern Oceans, Journal of Geophysical Research: Atmospheres. doi:10.1029/2002JD002769, 2003.

Chuck, A. L., Turner, S. M., and Liss, P. S.: Direct Evidence for a Marine Source of C_1 and C_2 Alkyl Nitrates, Science 297 (August): 1151–54, 2002.

Clemitshaw, K. C., Williams, J., Rattigan, O. V., Shallcross, D. E., Law, K. S., and Cox, R. A.: Gas-Phase Ultraviolet Absorption Cross-Sections and Atmospheric Lifetimes of Several C_2-C_5 Alkyl Nitrate, Journal of Photochemistry and Photobiology A Chemistry 102 (2–3): 117–26, doi:10.1016/S1010-6030(96)04458-9, 1997.

Cremer, S., Sledge, M. F., and Heinze, J.: Chemical Mimicry: Male Ants Disguised by the Queen's Bouquet, Nature doi:10.1038/419897a, 2002.

Cromwell, B. T.: The Micro-Estimation and Origin of Trimethylamine an Chenopodium Vulvaria L, Biochemical Journal 46 (5): 578–82, 1950.

Crowley, J. N., Schuster, G., Pouvesle, N., Parchatka, U., Fischer, H., Bonn, B., Bingemer, H., and Lelieveld, J.: Nocturnal Nitrogen Oxides at a Rural Mountain-Site in South-Western Germany, Atmospheric Chemistry and Physics,10,2795-2812, 2010.

Darnall, K., Carter, W., Winer, A., Lloyd, A., and Pitts, J: Importance of RO_2 + Nitric Oxide in Alkyl Nitrate Formation from C_4-C_6 Alkane Photooxidations under Simulated Atmospheric Conditions, Journal of Physical Chemistry, 80,17, 1976.

de Gouw, J. A., Warneke, C., Scheeren, H. A., van der Veen, C., Bolder, M., Scheele, M. P., Williams, J., Wong, S., Lange, L., Fischer, H., Lelieveld, J., Overview of the

trace gas measurements on board the Citation aircraft during the intensive field phase of INDOEX, Journal of Geophysical Research 106 (D22): 28453, 10.1029/2000JD900810, 2001.

DeMore, W. B., Sander, S. P., Golden, D. M., Hampson, R. F., Kurylo, M. J., Howard, C. J. , Ravishankara, A. R., Kolb, C. E., and Molina, M. J.: Chemical Kinetics and Photochemical Data for Use in Stratospheric Modeling, JPL Publication 97–4 (12): 278. doi:10.1002/kin.550171010, 1997.

Derstroff, B., Hüser, I., Bourtsoukidis, E., Crowley, J. N., Fischer, H., Gromov, S., Harder, H., Janssen, R. H. H., Kesselmeier, J., Lelieveld, J., Mallik, C., Martinez, M., Novelli, A., Parchatka, U., Phillips, G. J., Sander, R., Sauvage, C., Schuladen, J., Stönner, C., Tomsche, L., and Williams, J.: Volatile organic compounds (VOCs) in photochemically aged air from the eastern and western Mediterranean, Atmospheric Chemistry and Physics, 17, 9547-9566, https://doi.org/10.5194/acp-17-9547-2017, 2017.

Doche, C., Dufour, G., Foret, G., Eremenko, M., Cuesta, J., Beekmann, M., and Kalabokas, P.: Summertime tropospheric-ozone variability over the Mediterranean basin observed with IASI, Atmospheric Chemistry and Physics, 14, 10589-10600, https://doi.org/10.5194/acp-14-10589-2014, 2014.

Ehhalt, D H, Rohrer, F., Wahner, A., Prather, M. J., and Blake, D. R.: On the Use of Hydrocarbons for the Determination of Tropospheric OH Concentrations, Journal of Geophysical Research-Atmospheres 103 (D15): 18981–97, doi:10.1029/98JD01106, 1998.

Fall, P. L.: Modern Vegetation, Pollen and Climate Relationships on the Mediterranean Island of Cyprus, Review of Palaeobotany and Palynology 185. Elsevier B.V.: 79–92, doi:10.1016/j.revpalbo.2012.08.002, 2012.

Finlayson-Pitts, B. J., and Pitts, J. N.: Chemistry of the Upper and Lower Atmosphere: Theory, Experiments, and Applications. Chemistry of the Upper and Lower Atmosphere. doi:10.1016/B978-0-12-257060-5.50027-7, 1999.

Flocke, F., Volz-Thomas, A., and Kley, D.: Measurements of Alkyl Nitrates in Rural and Polluted Air Masses, Atmospheric Environment. Part A. General Topics 25 (9): 1951–60, doi:10.1016/0960-1686(91)90276-D, 1991.

Gettelman, A, Hoor, P., Pan, L. L., Randel, W. J., Hegglin, M. I., and Birner, T.: The extratropical upper troposphere and lower stratosphere, Rev. Geophys., 49, RG3003 doi:10.1029/2011RG000355, 2001.

Gibbs, A G, and Slinn, W. G. N.: 1973: Fluctuations in Trace Gas Concentrations in the Troposphere, Journal of Geophysical Research 78 (3): 574–76, http://dx.doi.org/10.1029/JC078i003p00574; doi:10.1029/JC078i003p00574, 1973.

Glavas, S., and Moschonas, N.: Determination of PAN, PPN, PnBN and Selected Pentyl Nitrates in Athens, Greece, Atmospheric Environment 35 (32): 5467–75, doi:10.1016/S1352-2310(01)00283-7, 2001.

Granier, C., Bessagnet, B., Bond, T., D'Angiola, A., Denier van der Gon, H., Frost, G. J., Heil, A., Kaiser, J. W., Kinne, S., Klimont, Z., Kloster, S., Lamarque, J.-F., Liousse, C., Maui, T., Meleux, F., Mieville, A., Ohara, T., Raut, J.-C., Riahi, K., Schultz, M. G., Smith, S. J., Thompson, A., van Aardenne, J., van der Werf, G. R., van Vuuren, D. P.: Evolution of Anthropogenic and Biomass Burning Emissions of

Air Pollutants at Global and Regional Scales during the 1980-2010 Period, Climatic Change 109 (1): 163–90, doi:10.1007/s10584-011-0154-1, 2011.

Greene, M. J., and Gordon, D. M.: Cuticular Hydrocarbons Inform Task Decisions, Nature. doi:10.1038/423032a, 2003.

Gros, V., Williams, J., van Aardenne, J. A., Salisbury, G., Hofmann, R., Lawrence, M. G., von Kuhlmann, R., Lelieveld, J., Krol, M., Berresheim, H., Lobert, J. M., and Atlas, E.: Origin of anthropogenic hydrocarbons and halocarbons measured in the summertime european outflow (on Crete in 2001), Atmospheric Chemistry and Physics, 3, 1223-1235, https://doi.org/10.5194/acp-3-1223-2003, 2003.

Guenther, A, Karl, T., Harley, P., Wiedinmyer, C., Palmer, P. I., and Geron, C.: Estimates of Global Terrestrial Isoprene Emissions Using MEGAN (Model of Emissions of Gases and Aerosols from Nature), Atmospheric Chemistry and Physics 6 (11): 3181–3210, 2006.

Haagen-Smit, A. J.:Chemistry and Physiology of Los Angeles Smog, Industrial & Engineering Chemistry. doi:10.1021/ie50510a045, 1952.

Hamm, S., and Warneck, P.: The Interhemispheric Distribution and the Budget of Acetonitrile in the Troposphere, Journal of Geophysical Research: Atmospheres. doi:10.1029/JD095iD12p20593, 1990.

Hamrud, M.: Residence Time and Spatial Variability for Gases in the Atmosphere, Tellus 35B (486): 295–303, 1983.

Herron, J T, and Huie, R. E.. "Rate Constants for the Reaction of Ozone with Ethene and Propene, from 235.0 to 362.0 K, Journal of Physical Chemistry, 78 (21): 2085–88, doi:10.1021/j100614a004, 1974.

Hoerger, C. C., Claude, A., Plass-Duelmer, C., Reimann, S., Eckart, E., Steinbrecher, R., Aalto, J., Arduini, J., Bonnaire, N., Cape, J. N., Colomb, A., Connolly, R., Diskova, J., Dumitrean, P., Ehlers, C., Gros, V., Hakola, H., Hill, M., Hopkins, J. M., Jaeger, J., Junek, R., Kajos, M. K., Klemp, D., Leuchner, M., Lewis, A. C., Locogne, N., Maione, M, Martin, D., Michl, K., Nemitz, E., O'Doherty, S., Ballesta, P. P., Ruuskanen, T. M., Sauvage, S., Schmidbauer, N., Spain, T. G., Straube, E., Vana, M., Vollmer, M. K., Wegener, R., and Wegener, A.: ACTRIS Non-Methane Hydrocarbon Intercomparison Experiment in Europe to Support WMO GAW and EMEP Observation Networks, Atmospheric Measurement Techniques 8 (7): 2715–36. doi:10.5194/amt-8-2715-2015, 2015.

Holzinger, R., Warneke, C., Hansel, A., Jordan, A., Lindinger, W., Scharffe, D. H., Schade, G., and Crutzen, P. J.: Biomass Burning as a Source of Formaldehyde, Acetaldehyde, Methanol, Acetone, Acetonitrile, and Hydrogen Cyanide, Geophysical Research Letters 26 (8): 1161–64, doi:10.1029/1999GL900156, 1999.

Jacobson, M. Z.: Fundamentals of Atmospheric Modeling Second Edition. Fundamentals of Atmospheric Modeling Second Edition, doi:10.1017/CBO9781139165389, 2005.

Jaenicke, R.: Chemistry of the Unpolluted and Polluted Tropsphere. Edited by Georgii, H. W., and W. Jaeschke, W., Vol. 1. Norwell, Mass.: D. Reidel, doi:10.1017/CBO9781107415324.004, 1982.

Jobson, B. T., McKeen, S. A., Parrish, D. D., Fehsenfeld, F. C., Blake, D. R., Goldstein, A. H., Schauffler, S. M., and Elkins, J.W.: Trace Gas Mixing Ratio Variability versus Lifetime in the Troposphere and Stratosphere: Observations, Journal of Geophysical Research 104 (D13): 16091, doi:10.1029/1999JD900126, 1999.

Jobson, B. T., Niki, H., Yokouchi, Y., Bottenheim, J., Hopper, F., and Leaitch, R.: Measurements of C_2-C_6 Hydrocarbons during the Polar Sunrise 1992 Experiment: Evidence for Cl Atom and Br Atom Chemistry, Journal of Geophysical Research-Atmospheres 99 (D12): 25355–68. doi:10.1029/94JD01243, 1994.

Jobson, B. T., Parrish, D. D., Goldan, P., Kuster, W. C., Fehsenfeld, F. C., Blake, D. R., Blake, N. J., and Niki, H.: Spatial and Temporal Variability of Nonmethane Hydrocarbon Mixing Ratios and Their Relation to Photochemical Lifetime, Journal of Geophysical Research 103 (97): 13557–67, doi:10.1029/97JD01715, 1998.

Junge, C E.: Studies of Global Exchange Processes in the Atmosphere by Natural and Artificial Tracers Low Latitudes, Journal of Geophysical Research 68 (13): 3849–56,1963.

Junge, C. E.: Residence Time and Variability of Tropospheric Trace Gases, Tellus 26 (4): 477–88, doi:10.1111/j.2153-3490, 1974.

Talukdar, R. K., Herndon, S. C., Burkholder, J. B., Roberts, J. M., and Ravishankara, A. R.: Atmospheric Fate of Several Alkyl Nitrates Part 1 - Rate Coefficients of the Reactions of Alkyl Nitrates with Isotopically Labelled Hydroxyl Radicals, Journal of the Chemical Society, Faraday Transactions 93 (16): 2787, doi:10.1039/a701780d, 1997.

Kalabokas, P. D., Cammas, J. P., Thouret, V., Volz-Thomas, A., Boulanger, D., and Repapis, C. C.: Examination of the Atmospheric Conditions Associated with High and Low Summer Ozone Levels in the Lower Troposphere over the Eastern Mediterranean, Atmospheric Chemistry and Physics 13 (20): 10339–52. doi:10.5194/acp-13-10339-2013, 2013.

Kalabokas, P. D., Mihalopoulos, N., Ellul, R., Kleanthous, S., and Repapis, C. C.: An Investigation of the Meteorological and Photochemical Factors Influencing the Background Rural and Marine Surface Ozone Levels in the Central and Eastern Mediterranean, Atmospheric Environment 42 (34). Elsevier Ltd: 7894–7906, doi:10.1016/j.atmosenv.2008.07.009, 2008.

Kalabokas, P. D., Volz-Thomas, A., Brioude, J., Thouret, V., Cammas, J.-P., and Repapis, C. C.: Vertical Ozone Measurements in the Troposphere over the Eastern Mediterranean and Comparison with Central Europe, Atmospheric Chemistry and Physics Discussions 7 (1): 2249–74, doi:10.5194/acpd-7-2249-2007, 2007.

Karl, T., Apel, E., Hodzic, A., Riemer, D., Blake, D., and Wiedinmyer, C.: Emissions of Volatile Organic Compounds Inferred from Airborne Flux Measurements over a Megacity, Atmospheric Chemistry and Physics Discussions 8 (4): 14273–309. doi:10.5194/acpd-8-14273-2008, 2008.

Kessler, A., and Baldwin, I. T.: Defensive Function of Herbivore-Induced Plant Volatile Emissions in Nature." Science, doi:10.1126/science.291.5511.2141, 2001.

Khalil, M. A. K.: Atmospheric Methane : Its Role in the Global Environment. Edited by Khalil, M. A. K., Springer-Verlag Berlin Heidelberg GmbH, doi:10.1007/978-3-662-04145-1, 2000.

Kleanthous, S., Vrekoussis, M., Mihalopoulos, N., Kalabokas, P., and Jos Lelieveld: On the Temporal and Spatial Variation of Ozone in Cyprus, The Science of the Total Environment 476–477 (April): 677–87, doi:10.1016/j.scitotenv.2013.12.101, 2014.

Koppmann, R.: Chemistry of Volatile Organic Compounds in the Atmosphere, In Handbook of Hydrocarbon and Lipid Microbiology, doi:10.1007/978-3-540-77587-4, 2010

Kourtidis, K., Zerefos, C., Rapsomanikis, S., Simeonov, V., Balis, D., Perros, P. E., Thompson, A. M., Witte, J., Calpini, B., Sharobiem, W. M., Papayannis, A., Mihalopoulos, N., Drakou, R.: Regional Levels of Ozone in the Troposphere over Eastern Mediterranean Journal of Geophysical Research Atmospheres 107 (18): 1–13, doi:10.1029/2000JD000140, 2002.

Kouvarakis, G., Vrekoussis, M., Mihalopoulos, N., Kourtidis, K., Rappenglueck,B., Gerasopoulos, E., Zerefos, C.: Spatial and temporal variability of tropospheric ozone (O_3) in the boundary layer above the Aegean Sea (eastern Mediterranean), Journal of Geophysical Research 107: 1–14, doi:10.1029/2000JD000081, 2002.

Krieger, J., and Heinz Breer, H.: Olfactory Reception in Invertebrates, Science, doi:10.1126/science.286.5440.720, 1999.

Kurokawa, J., Ohara, T., Morikawa, T., Hanayama, S., Janssens-Maenhout, G., Fukui, T., Kawashima, K., and Akimoto, H.: Emissions of Air Pollutants and Greenhouse Gases over Asian Regions during 2000-2008: Regional Emission Inventory in ASia (REAS) Version 2, Atmospheric Chemistry and Physics, doi:10.5194/acp-13-11019-2013, 2013.

Lamarque, J.-F., Bond, T. C., Eyring, V., Granier, C., Heil, A., Klimont, Z., Lee, D., Liousse, C., Mieville, A., Owen, B., Schultz, M. G., Shindell, D., Smith, S. J., Stehfest, E., Van Aardenne, J., Cooper, O. R., Kainuma, M., Mahowald, N., McConnell, J. R., Naik, V., Riahi, K., and van Vuuren, D. P.: Historical (1850–2000) gridded anthropogenic and biomass burning emissions of reactive gases and aerosols: methodology and application, Atmospheric Chemistry and Physics, 10, 7017-7039, https://doi.org/10.5194/acp-10-7017-2010, 2010.

Lei, W., de Foy, B., Zavala, M., Volkamer, R., and Molina, L. T.:Characterizing Ozone Production in the Mexico City Metropolitan Area: A Case Study Using a Chemical Transport Model, Atmospheric Chemistry and Physics 7, 1347–66, doi:10.5194/acp-7-1347-2007, 2007.

Lelieveld, J., Bourtsoukidis, E., Brühl, C., Fischer, H., Fuchs, H., Harder, H., Hofzumahaus, A., Holland, F., Marno, D., Neumaier, M., Pozzer, A., Schlager, H., Williams, J., Zahn, A., Ziereis, H.: The South Asian Monsoon — Pollution Pump and Purifier, Science 2501 (June): 1–9, doi:10.1126/science.aar2501, 2018.

Liakakou, E., Bonsang, B., Williams, J., Kalivitis, N., Kanakidou, M., and Mihalopoulos, N.: C_2-C_8 NMHCs over the Eastern Mediterranean: Seasonal Variation and Impact on Regional Oxidation Chemistry, Atmospheric Environment 43 (35). Elsevier Ltd: 5611–21, doi:10.1016/j.atmosenv.2009.07.067, 2009.

Lightfoot, P. D., Cox, R. A., Crowley, J. N., Destriau, M., Hayman, G. D., Jenkin, M. E., Moortgat, G. K., and Zabel, F.: Organic Peroxy Radicals: Kinetics, Spectroscopy and Tropospheric Chemistry, Atmospheric Environment Part A, General Topics, doi:10.1016/0960-1686(92)90423-I, 1992.

Livesey, N. J., Fromm, M. D., Waters, J. W., Manney, G. L., Santee, M. L., and Read, W. G.: Enhancements in Lower Stratospheric CH_3CN Observed by the Upper Atmosphere Research Satellite Microwave Limb Sounder Following Boreal Forest Fires, Journal of Geophysical Research: Atmospheres 109 (D6), doi:10.1029/2003JD004055, 2004.

Lobert, J. M., Scharffe, D. H., Hao, W. M., and Crutzen, P. J.: Importance of Biomass Burning in the Atmospheric Budgets of Nitrogen-Containing Gases, Nature 346 (6284): 552–54, doi:10.1038/346552a0, 1990.

Mayrsohn, H., and Crabtree, J.H.: Source Reconciliation of Atmospheric Hydrocarbons, Atmospheric Environment 10: 137–43, 1996.

Molina, M. J., and Rowland, F. S.: Stratospheric Sink for Chlorofluoromethanes: Chlorine Atom-catalysed Destruction of Ozone, Nature, doi:10.1038/249810a0, 1974.

Moschonas, N., Glavas, S., and Kouimtzis, T.: C_3 to C_9 Hydrocarbon Measurements in the Two Largest Cities of Greece, Athens and Thessaloniki. Calculation of Hydrocarbon Emissions by Species. Derivation of Hydroxyl Radical Concentrations, Science of the Total Environment 271 (1–3): 117–33, doi: 10.1016/S0048-9697(00)00838-X, 2001.

Moschonas, N., and Glavas, S.: Non-Methane Hydrocarbons at a High-Altitude Rural Site in the Mediterranean (Greece), Atmospheric Environment 34 (6): 973–84, doi:10.1016/S1352-2310(99)00205-8, 2000.

Nelson, P. F., and Quigley, S. M.: The m,p-Xylenes:Ethylbenzene Ratio. A Technique for Estimating Hydrocarbon Age in Ambient Atmospheres, Atmospheric Environment 17 (3): 659–62, doi:10.1016/0004-6981(83)90141-5, 1983.

Neu, J. L., Lawler, M. J., Prather, M. J., and Saltzman, E. S.: Oceanic Alkyl Nitrates as a Natural Source of Tropospheric Ozone, Geophysical Research Letters 35 (13), doi: 10.1029/2008GL034189, 2008.

O'Brien, J. M., Shepson, P. B., Muthuramu, K., Hao, C., Niki, H., Hastie, D. R., Taylor, R., and Roussel, P. B.: Measurements of Alkyl and Multifunctional Organic Nitrates at a Rural Site in Ontario, Journal of Geophysical Research, 100, Dll, doi: 22 795-22 804, doi: 10.1029/94JD03247, 1995.

O'Dowd, C. D., Aalto, P., Hmeri, K., Kulmala, M., and Hoffmann, T.: Atmospheric Particles from Organic Vapours, Nature 416 (6880): 497–98, doi:10.1038/416497a, 2002

Ohara, T., Akimoto, H., Kurokawa, J., Horii, N., Yamaji, K., Yan, X., and Hayasaka, T.: An Asian Emission Inventory of Anthropogenic Emission Sources for the Period 1980-2020, Atmospheric Chemistry and Physics, doi:10.5194/acp-7-4419-2007, 2007.

Özel, M. Z., Hamilton, J. F., and Lewis, A. C.: New Sensitive and Quantitative Analysis Method for Organic Nitrogen Compounds in Urban Aerosol Samples, Environmental Science & Technology 45 (4): 1497–1505, doi:10.1021/es102528g, 2011.

Parrish, D. D., Dunlea, E. J., Atlas, E. L., Schauffler, S., Donnelly, S., Stroud, V., Goldstein, A. H., Millet, D. B., McKay, M., Jaffe, D. A., Price, H. U., Hess, P. G., Flocke, F., Roberts, J. M., Changes in the Photochemical Environment of the Temperate

North Pacific Troposphere in Response to Increased Asian Emissions, Journal of Geophysical Research : Atmospheres 109 (23): 1–16, doi:10.1029/2004JD004978, 2004.

Parrish, D. D., Hahn, C., Williams, R., Norton, F., Fehsenfeld, H., Singh, J., Shetter, B., Gandrud, B., and Ridley, B.: Indications of Photochemical Histories of Pacific Air Masses from Measurements of Atmospheric Trace Species at Pt. Arena, California, Journal of Geophysical Research-Atmospheres 97 (D14): 15883–902, doi:10.1029/92JD01242, 1992.

Parrish, D. D., Kuster, W. C., Shao, M., Yokouchi, Y., Kondo, Y., Goldan P. D., de Gouw, J. A., Koike, M., and Shirai, T.: Comparison of Air Pollutant Emissions among Mega-Cities, Atmospheric Environment 43 (40). Elsevier Ltd: 6435–41, doi:10.1016/j.atmosenv.2009.06.024, 2009.

Parrish, D. D., Stohl, A., Forster, C., Atlas, E. L., Blake, D. R., Goldan, P. D., Kuster, W. C., and de Gouw, J. A.: Effects of Mixing on Evolution of Hydrocarbon Ratios in the Troposphere, Journal of Geophysical Research: Atmospheres 112 (10): 1–17, doi:10.1029/2006JD007583, 2007.

Penkett, S. A., Burgess, R. A., Coe, H., Coll, I., Hov, O., Lindskog, A., Schmidbauer, N., Solberg, S. M., Roemer, M., Thijsse, T., Beck, J., Reeves, C. E., Evidence for Large Average Concentrations of the Nitrate Radical (NO_3) in Western Europe from the HANSA Hydrocarbon Database, Atmospheric Environment 41 (16): 3465–78, doi:10.1016/j.atmosenv.2006.11.055, 2007.

Perring, A. E., Pusede, S. E., and Cohen, R. C.: An Observational Perspective on the Atmospheric Impacts of Alkyl and Multifunctional Nitrates on Ozone and Secondary Organic Aerosol, Chemical Reviews 113 (8): 5848–70 doi:10.1021/cr300520, 2013.

Phillips, G J, Tang, M. J., Thieser, J., Brickwedde, B., Schuster, G., Bohn, B., Lelieveld, J., and Crowley, J. N.: Significant Concentrations of Nitryl Chloride Observed in Rural Continental Europe Associated with the Influence of Sea Salt Chloride and Anthropogenic Emissions, Geophysical Research Letters, 39, 10, 1–5, doi:10.1029/2012GL051912, 2012.

Prinn, R. G., Weiss, R. F., Miller, B. R., Huang, J., Alyea, F. N., Cunnold, D. M., Fraser, P. J., Hartley, D. E., and Simmonds, P. G.: Atmospheric Trends and Lifetime of CH_3CCI_3 and Global OH Concentrations, Science 269 (5221): 187–92, doi:10.1126/science.269.5221.187, 1995.

Rudolph, J., Ramacher, B., Plass-Dülmer, C., Müller, K. P., and Koppmann, R.: The Indirect Determination of Chlorine Atom Concentration in the Troposphere from Changes in the Patterns of Non-Methane Hydrocarbons, Tellus, 49 B, 592 – 601, doi:10.3402/tellusb.v49i5.16016, 1997.

Rudolph, J, and Johnen, F. J.: Measurements of Light Atmopsheric Hydrocarbons over the Atlantic in Regions of Low Biological Activity Journal of Geophysical Research 95 (89), 20583–91, doi:10.1029/JD095iD12p20583, 1990.

Salisbury, G., Williams, J., Holzinger, R., Gros, V., Mihalopoulos, N., Vrekoussis, M., Sarda-Estève, R., Berresheim, H., von Kuhlmann, R., Lawrence, M., and Lelieveld, J.: Ground-based PTR-MS measurements of reactive organic compounds during the MINOS campaign in Crete, July–August 2001, Atmospheric Chemistry and Physics, 3, 925-940, doi.org/10.5194/acp-3-925-2003, 2003.

Scheeren, H. A., Lelieveld, J., Roelofs, G. J., Williams, J., Fischer, H., de Reus, M., de Gouw, J. A., Warneke, C., Holzinger, R., Schlager, H., Klüpfel, T., Bolder, M., van der Veen, C., and Lawrence, M.: The impact of monsoon outflow from India and Southeast Asia in the upper troposphere over the eastern Mediterranean, Atmospheric Chemistry and Physics, 3, 1589-1608, https://doi.org/10.5194/acp-3-1589-2003, 2003.

Schuck, T. J., Brenninkmeijer, C. A. M., Slemr, F., Xueref-Remy, I., and Zahn, A.: Greenhouse Gas Analysis of Air Samples Collected Onboard the CARIBIC Passenger Aircraft, Atmospheric Measurement Techniques 2 (2): 449–64. doi:10.5194/amt-2-449-2009, 2009.

Simpson, I. J., Akagi, S. K., Barletta, B., Blake, N. J., Choi, Y., Diskin, G. S., Fried, A., et al. 2011. "Boreal Forest Fire Emissions in Fresh Canadian Smoke Plumes: C1-C10 Volatile Organic Compounds (VOCs), CO2, CO, NO2, NO, HCN and CH3CN." Atmospheric Chemistry and Physics 11 (13): 6445–63. doi:10.5194/acp-11-6445-2011, 2011.

Simpson, I. J., Akagi, S. K., Barletta, B., Blake, N. J., Choi, Y., Diskin, G. S., Fried, A., Fuelberg, H. E., Meinardi, S., Rowland, F. S., Vay, S. A., Weinheimer, A. J., Wennberg, P. O., Wiebring, P., Wisthaler, A., Yang, M., Yokelson, R. J., and Blake, D. R.: Boreal forest fire emissions in fresh Canadian smoke plumes: C_1-C_{10} volatile organic compounds (VOCs), CO_2, CO, NO_2, NO, HCN and CH_3CN, Atmospheric Chemistry and Physics, 11, 6445-6463, https://doi.org/10.5194/acp-11-6445-2011, 2011.

Simpson, I. J., Blake, N. J., Blake, D. R., Atlas, E. L., Flocke, F., Crawford, K. H., Fuelberg, Henry E., Kiley, C. M., Meinardi, S., and Rowland, F. S., Photochemical Production and Evolution of Selected C_2–C_5 Alkyl Nitrates in Tropospheric Air Influenced by Asian Outflow, Journal of Geophysical Research 108 (D20): 8808, doi:10.1029/2002JD002830, 2003.

Sindelarova, K., Granier, C., Bouarar, I., Guenther, A., Tilmes, S., Stavrakou, T., Müller, J. F., Kuhn, U., Stefani, P., and Knorr, W., Global Data Set of Biogenic VOC Emissions Calculated by the MEGAN Model over the Last 30 Years, Atmospheric Chemistry and Physics 14 (17): 9317–41, doi:10.5194/acp-14-9317-2014, 2014.

Singh, H. B., Salas, L., Herlth, D., Kolyer, R, Czech, E., Viezee, W, Li, Q., Jacob, D. J., Blake, D., Sachse, G., Harward, C. N., Fuelberg, H., Kiley, C. M., Zhao, Y., Kondo, Y.: In Situ Measurements of HCN and CH_3CN over the Pacific Ocean: Sources, Sinks, and Budgets, Journal of Geophysical Research, 108 (D20): 8795, doi:10.1029/2002jd003006, 2003.

Slinn, W. G. N.: A Simple Model for Junge's Relationship between Concentration Fluctuations and Residence Times for Tropospheric Trace Gases, Tellus 40B: 229–32, doi:10.3402/tellusb.v40i3.15909, 1988.

Sobanski, N., Tang, M. J., Thieser, J., Schuster, G., Pöhler, D., Fischer, H., Song, W., Sauvage, C., Williams, J., Fachinger, J., Berkes, F., Hoor, P., Platt, U., Lelieveld, J., and Crowley, J. N.: Chemical and meteorological influences on the lifetime of NO_3 at a semi-rural mountain site during PARADE, Atmospheric Chemistry and Physics, 16, 4867-4883, doi:10.5194/acp-16-4867-2016, 2016.

Sobanski, N., Thieser, J., Schuladen, J., Sauvage, C., Song, W., Williams, J., Lelieveld, J., and Crowley, J. N.: Day and Night-Time Formation of Organic Nitrates at a For-

ested Mountain Site in South-West Germany, Atmospheric Chemistry and Physics, 17 (2): 4115–30, doi:10.5194/acp-17-4115-2017, 2017.

Spivakovsky, C. M., Logan, J. A., Montzka, S. A., Balkanski, Y. J., Foreman-Fowler, M., Jones, D. B. A., Horowitz, L. W., Fusco, A. C., Brenninkmeijer, C. A. M.,Prather, M. J., Wofsy, S. C., and McElroy, M. B.: Three-Dimensional Climatological Distribution of Tropospheric OH: Update and Evaluation, Journal of Geophysical Research: Atmospheres, 105, (D7), doi: 10.1029/1999JD901006, 2000.

Stephens, E. R., and Burleson, F. R.: Analysis of the Atmosphere for Light Hydrocarbons, Journal of the Air Pollution Control Association 17 (3): 147–53, doi:10.1080/00022470.1967.10468960, 1976.

Stephens, E. R., and Burleson, F. R.: Distribution of Light Hydrocarbons in Ambient Air." Journal of the Air Pollution Control Association 19 (12): 929–936, doi:10.1080/00022470.1969.10469359, 1969.

Sun, S., Moravek, A., von der Heyden, L., Held, A., Sörgel, M., and Kesselmeier, J.: Twin-cuvette measurement technique for investigation of dry deposition of O_3 and PAN to plant leaves under controlled humidity conditions,Atmospheric Measurement Techniques, 9, 599-617, https://doi.org/10.5194/amt-9-599-2016, 2016.

Talbot, R. W., Dibb, J. E., E. M. Scheuer, E. M., Bradshaw, J. D., Sandholm, S. T., Singh, H. B., Blake, D. R., Blake, N. J., Atlas, E., and Flock, F.: Tropospheric Reactive Odd Nitrogen over the South Pacific in Austral Springtime, Journal of Geophysical Research Atmospheres 105 (D5): 6681–94, doi:10.1029/1999JD901114, 2000.

Thorenz, U. R., Baker, A. K., Leedham Elvidge, E. C., Sauvage, C., Riede, H., van Velthoven, P. F. J., Hermann, M., Weigelt, A., Oram, D. E., Brenninkmeijer, C. A. M., Zahn, A., Williams, J.: Investigating African Trace Gas Sources , Vertical Transport , and Oxidation Using IAGOS-CARIBIC Measurements between Germany and South Africa between 2009 and 2011, Atmospheric Environment, 158. Elsevier Ltd: 11–26, doi:10.1016/j.atmosenv.2017.03.021, 2017.

Treacy, J., El Hag, M., O'Farrell, D., and Sidebottom, H.: Reactions of Ozone with Unsaturated Organic Compounds, Berichte der Bunsengesellschaft für Physikalische Chemie 96 (3): 422–27, doi:10.1002/bbpc.19920960337, 1992.

van der Werf, G. R., Randerson, J. T., Giglio, L., Collatz, G. J., Kasibhatla, P. S., and Arellano Jr., A. F.: Interannual variability in global biomass burning emissions from 1997 to 2004, Atmospheric Chemistry and Physics, 6, 3423-3441, doi:10.5194/acp-6-3423-2006, 2006.

von Schneidemesser, E., Monks, P. S., and Plass-Dülmer, C.: Global Comparison of VOC and CO Observations in Urban Areas, Atmospheric Environment 44 (39). Elsevier Ltd: 5053–64, doi:10.1016/j.atmosenv.2010.09.010, 2010.

Vrekoussis, M, Kanakidou, M., Mihalopoulos, N, Crutzen, P. J., Lelieveld, J., Perner, D., Berresheim, H., and Baboukas, E.. 2004.: Role of the NO_3 Radicals in Oxidation Processes in the Eastern Mediterranean Troposphere during the MINOS Campaign, Atmospheric Chemistry and Physics 4 (3): 169–82, doi:10.5194/acp-4-169-2004, 2004

Waliser, D. E., Graham, N. E., and Gautier, C.: Comparison of the Highly Reflective Cloud and Outgoing Longwave Radiation Datasets for Use in Estimating Tropical

Deep Convection, Journal of Climate, doi:10.1175/1520-0442(1993)006<0331:COTHRC>2.0.CO;2, 1993.

Warneck, P., and Williams, J.: Gas-Phase Photochemistry, in The Atmospheric Chemist's Companion: Numerical Data for Use in the Atmospheric Sciences, Springer Dordrecht Heidelberg, London, New York, doi:10.1007/978-94-007-2275-0, 2012.

Warneke, C., S. A. McKeen, S. A., de Gouw, J. A., Goldan, P. D., Kuster, W. C., Holloway, J. S., Williams, E. J., Lerner, B.M., Parrish, D. D., Trainer, M., Fehsenfeld, F. C., Kato, S., Atlas, E. L., Baker, A., Blake, D. R.: Determination of Urban Volatile Organic Compound Emission Ratios and Comparison with an Emissions Database, Journal of Geophysical Research: Atmospheres 112 (10), doi:10.1029/2006JD007930, 2007.

Wicke, W.: Beobachtungen an Chenoopodium Vulvaria: Über Die Ausscheidung von Trimethylamin, European Journal of Organic Chemistry 124 (2): 338–40, 1862.

Williams, J., Fischer, H., Harris, G. W., Crutzen, P. J., Hoor, P., Hansel, A., Holzingcr, R., and Lindinger, W.: Variability-Lifetime Relationship for Organic Trace Gases: A Novel Aid to Compound Identification and Estimation of HO Concentrations, Journal of Geophysical Research 105: 20473–86, doi: 10.1029/2000JD900203, 2002

Williams, J., Gros, V., Bonsang, B., and V. Kazan, V.: HO Cycle in 1997 and 1998 over the Southern Indian Ocean Derived from CO, Radon, and Hydrocarbon Measurements Made at Amsterdam Island, Journal of Geophysical Research: Atmospheres 106 (D12): 12719–25, doi:10.1029/2001JD900116, 2001.

Zhang, Q., Streets, D. G., Carmichael, G. R., He, K. B., Huo, H., Kannari, A., Klimont, Z., Park, I. S., Reddy, S., Fu, J. S., Chen, D., Duan, L., Lei, Y., Wang, L. T., and Yao, Z. L.: Asian emissions in 2006 for the NASA INTEX-B mission, Atmospheric Chemistry and Physics, 9, 5131-5153, doi:10.5194/acp-9-5131-2009, 2009.

Deutscher Verband Flüssiggas e.V.; Annual Report 2014, on 12.02.2019, 13:14.

http://dvfg.de/fileadmin/user_upload/Verband_-_Markt_-_etc/DVFG-Jahresbericht-2014.pdf

List of figures

List of tables

Abbrevation Index

ACTRIS	Aerosols, Clouds, and Trace gases Research Infrastructure Network
AN	Alkyl nitrates
CARBIC	Civil Aircraft for the Regular Investigation of the atmosphere Based on an instrumented Container
CFC	Chloro Flouro Carbons
CPC	Condensational Particle Counter
CRM	Comparative Reactivity Method
CYPHEX	CYprus PHotochemistry EXperiment
DOAS	DifferentialOptical Absorption Spectroscopy
FID	Flame Ionisation Detector
Flexpart	FLEXible PARTicle dispersion model
GC	Gas Chromatograph
HIRES	HIgh REsolution Sampler
HR	Hydrocarbon Ratio
ITCZ	Intertropical Convergence Zone
LOD	Limit Of Detection
LPG	Liquid Petroleum Gas
MR	Mixing Ratio
NCD	Nitrogen Chemiluminescence Detector
NDIR	Non-Dispersive Infrared
NIR	Near Infra Red
NMHC	Non-Methane HydroCarbons
NOTOMO	NOcturnal chemistry at the Taunus Observatorium: insights into Mechanisms of Oxidation
OLR	Outgoing Longwave Radiation
OPC	Optical Particle Counter
OVOC	Oxygenated Volatile Organic Compounds
PBL	Planetary Boundary Layer
PTR-ToF-MS	Proton Transfer Reaction- Time of Flight-Mass Spectrometer
PV	Potential Vorticity
SP2	Soot Particle Detector
STE	Stratosphere-Troposphere Exchange
TRAC	Triggered Retrospective Air Collector
UT/LS	Upper troposphere/lower Stratosphere
UV	Ultra Violett
VOC	Volatile Organic Compounds
WAS	Whole Air Sample

Symbols

α	Branching ratio
a	Axis intercept from linear regression
A	Factor from exponential regression (lifetime-variability)
b	Slope from linear regression / exponent from exponential regression (life-time-variability)
C	Constant from lifetime-variability considerations
f	Fraction
k	Reaction rate coefficient
M_{tot}	Average concentration (lifetime-variability)
n	number of data points
P	Production rate
Q_{tot}	Total source strength
R	Coefficient of determination
t	Time
X	Radical concentration/ component concentration
σ	Standard deviation
τ	Lifetime